*Ahmad Aswad Mahaidin*,*
*Mohd. Asri Selamat,*
*Samsiah Abdul Manaf*
*and Talib Ria Jaafar*

*Structural Material Program, Advanced Materials Research Centre (AMREC) SIRIM Berhad,*
*Lot 34, Jalan Hi-Tech 2/3, Kulim Hi-Tech Park,*
*09000, Kulim, Kedah,*
*Malaysia*

***(aswad@sirim.my)***

## EFFECT OF CARBON ADDITION ON THE DENSIFICATION AND PROPERTIES OF SINTERED CEMENTED CARBIDE (WC-Co)

***RINGKASAN:*** *Logam keras merupakan bahan yang terkenal dalam bidang pemotongan logam dan aplikasi-aplikasi yang melibatkan hakisan. Semen karbida (WC-Co) digunakan secara meluas dalam aplikasi-aplikasi tersebut. Penambahan karbon ke dalam WC-Co meningkatkan proses densifikasi. Oleh itu, kajian dilakukan untuk mengkaji kesan penambahan karbon ke atas densifikasi dan sifat-sifat WC-Co yang telah disinter. Sampel dihasilkan menggunakan teknik kaji logam (metalurgi) serbuk, di mana serbuk WC-Co dimampat pada tekanan 625 MPa, tekanan isostatik sejuk pada 200 MPa dan disinter pada suhu antara 1350 °C hingga 1450 °C di dalam medium asas berunsurkan nitrogen. Sifat fizikal dan mekanikal sampel dianalisa. Hasil kajian menunjukkan penambahan 0.8 % karbon dan ke atas akan mengurangkan ketumpatan sampel WC-Co yang telah disinter.*

**ABSTRACT:** Hardmetal is a well known material in metal cutting and wear related applications. Cemented carbide (WC-Co) is the most widely used for this application, in which addition of carbon to the WC-Co improves densification process. This study investigates the effect of carbon addition on the densification and properties of sintered WC-Co. The samples are fabricated using powder metallurgy technique, in which the powders are compacted at 625 MPa, cold-isostatic pressed at 200 MPa and sintered at temperatures between 1350 °C and 1450 °C under nitrogen-based atmosphere. The physical and mechanical properties of the samples were analyzed. The study reveals that addition of 0.8 % of carbon and above will greatly reduce the density of the WC-Co sintered powders.

Keywords: WC-Co, powder metallurgy, carbon addition.

## INTRODUCTION

Hardmetal is a well known material in metal cutting and wear related applications due to its superior mechanical properties and has been used extensively in metal cutting technology and wear related applications. Hard metal containing 95 % cemented carbide has been used as cutting tool. Formation of a complex shape from hard metal is difficult through machining process. In addition, the properties of tungsten alloys are sensitive to processing and can be degraded by residual porosity. Hence, powder metallurgy technique is introduced in this work.

WC-Co conventional powder is usually sintered at relatively high temperature where liquid phase formation occurs due to cobalt melting. This is important as to provide extensive wetting during densification process. Cobalt acts as the metal binder because of its capillary action during liquid phase sintering that enhances densification. The wetting ability of cobalt enables the WC-Co composite to achieve high density and form a rigid skeletal structure.

Complete densification plays an important role in determining the mechanical properties of the composite. Even small proportion of porosity could lead to catastrophic failure. Cha *et al.*, (2003) reported that densification can be enhanced by adding free carbon. Addition of small amount of uncombined carbon also could inhibit grain growth during liquid phase sintering (Yao *et al.*, 1998).

Another important aspect of WC-Co fabrication is the grain growth of WC grains. Since submicron or finer particle size was used during the consolidation process, the large specific surface area of the powders increases the possibility of microstructural engrossment due to high reactivity (Gonzalez *et al.*, 2004). It is a current trend for hardmetal industry to control the grain size of WC particles in order to increase hardness while maintaining a reasonable toughness. Although addition of free carbon is reported to inhibit grain growth, high carbon content will result in abnormal grain growth. Therefore, it is critical to study the limitation of the free carbon percentage added to the formulation.

There is a lack of published work and detailed explanation on the effect of carbon percentage on densification and properties of sintered powders. This paper studies on how the carbon percentage affects physical and mechanical properties of WC-Co sintered powders.

## MATERIALS AND METHOD

WC-Co powders were mixed in Turbula Mixer for three hours based on the composition in Table 1. The wet mixing process includes tungsten balls with 3:1 ball to powder ratio, paraffin wax and heptanes. Paraffin wax was added for lubrication during compaction process while heptanes were added to convert the powders into suspension as a preparation for wet mixing. The mixed powders were dried and formed granules after wet mixing was completed.

**Table 1.** Composition for WC-Co consolidation.

| Composition | Tungsten carbide, WC (wt%) | Cobalt, Co (wt%) | Carbon, C (wt%) |
|---|---|---|---|
| 0.2%C | 93.8 | 6.0 | 0.2 |
| 0.4%C | 93.6 | 6.0 | 0.4 |
| 0.6%C | 93.4 | 6.0 | 0.6 |
| 0.8%C | 93.2 | 6.0 | 0.8 |
| 1.0%C | 93.0 | 6.0 | 1.0 |

Then the powders were compacted at 625 MPa using uniaxial pressing. Cold-isostatic pressing (CIP) was introduced to WC-Co green body at 200 MPa to reduce porosity and to obtain a uniform green density distribution. The green samples were sintered for 1 hour at 1350-1450 °C using 450-1450 °C and 450-1320-1450 °C heating schedule (Figure 1 and Figure 2). The sintering process took place in tube furnace under nitrogen-based atmosphere.

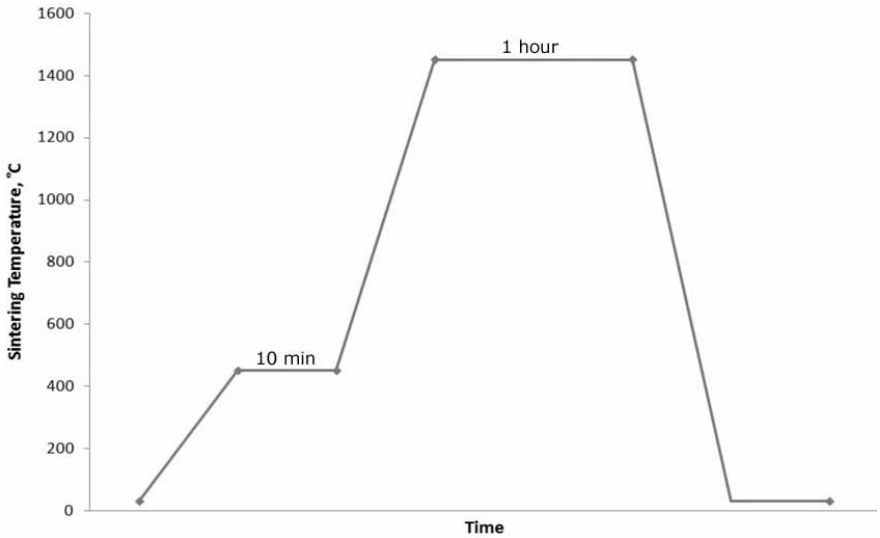


***Figure 1.*** *Direct heating schedule.*

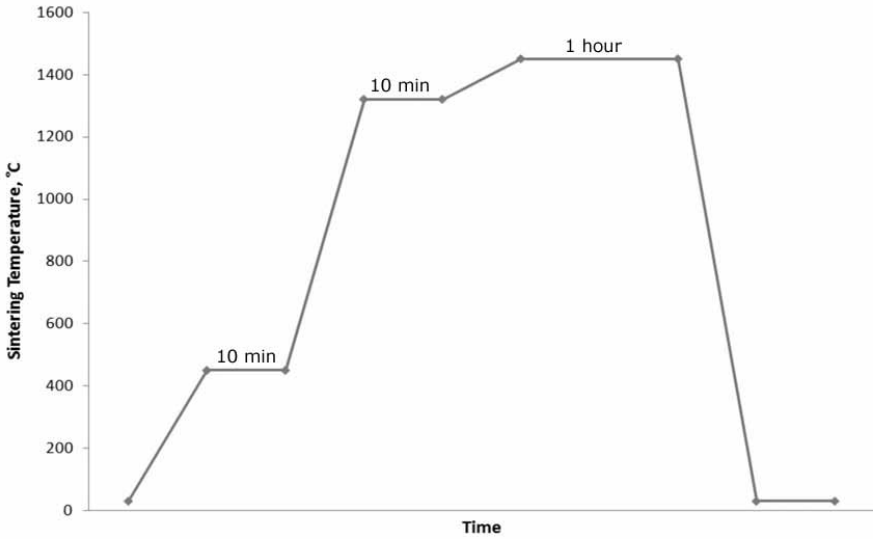


***Figure 2.*** *Heating schedule with holding step at 1320 °C.*

The shrinkage of the sintered WC-Co-C powders was calculated. The density and hardness of the samples were determined using density meter and Vicker's hardness tester, respectively. The strength of the sintered powders was tested using Transverse Rupture Strength (TRS).

## RESULTS AND DISCUSSION

The WC-Co-C sintered in liquid phase environment showed the effects of carbon addition in terms of physical and mechanical properties.

Table 2 showed that the percent of shrinkage for WC-Co samples relatively increase with increasing carbon content at fixed sintering temperature. However, the shrinkage drops after more than 0.8 % of carbon was added into the formulation. It is reported that high carbon content leads to high shrinkage rates and resulted in a fully dense materials (Petersson, 2004).

**Table 2.** Percent of shrinkage of WC-Co sintered powders with different percentage of carbon addition.

| Percent of carbon (%) | Shrinkage rate (%) | | |
|---|---|---|---|
| | 1350°C | 1400°C | 1450°C |
| 0.2 | 12.541 | 17.086 | 17.409 |
| 0.4 | 17.444 | 18.189 | 18.514 |
| 0.6 | 17.452 | 18.147 | 18.197 |
| 0.8 | 17.226 | 17.083 | 17.545 |
| 1 | 16.851 | 16.629 | 17.167 |

Since submicron WC powders are used, shrinkage may start at a lower temperature (Cha *et al.*, 2003). The finer particle size increase the contact points where the initial bonding takes place, thus enhance the diffusion rate between the particles. This was supported by Silva *et al.*, (2001) whom reported a significant shrinkage takes place during solid state instead of liquid state, in which pores are depleted due to the diffusion between WC and Co particles as well as WC grain growth.

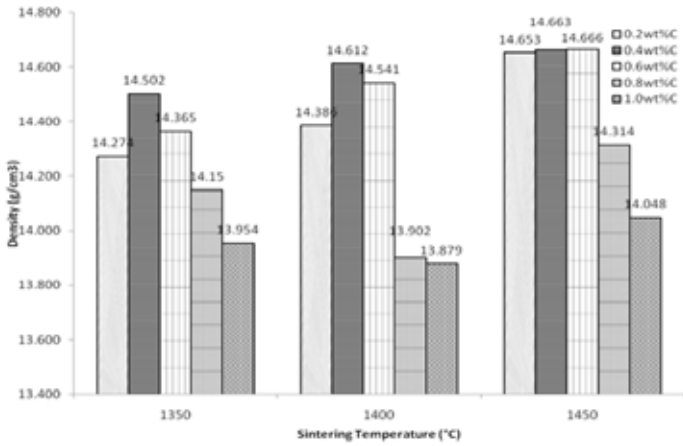


***Figure 3.*** *Relationship between percentage of carbon addition and density of WC-Co at 1350-1450 °C.*

Figure 3 shows that with addition of 0.2 – 0.6 %C, the sintered density increases as sintering temperature increases. Meanwhile the addition of 0.8 %C and 1.0 %C shows fluctuation after the density drops at 1400 °C before increases at 1450 °C. This is probably due to the pores that reemerged during the sintering process at 1400 °C and closed back once again at 1450 °C when the cobalt liquid distribute

through out the sample. However, these samples possessed lower density compared to the other three probably because it is over-sintered. At 1350 °C, almost all samples have already achieved 14.00 g/cm$^3$.

Based on Figure 4, WC-Co with the addition of 0.2 – 0.6 %C has a relatively high hardness at 1350 °C and 1400 °C than 0.8 %C and 1.0 %C. It is due to the fact that 0.2 – 0.6 %C are denser compared to 0.8 %C and 1.0 %C. However, the hardness is almost similar for the sample sintered at 1450 °C when the samples are fully sintered. Among all the sintered powders, WC-Co-0.2 %C sintered at 1400 °C has the highest hardness, which is 1937.0 HV.

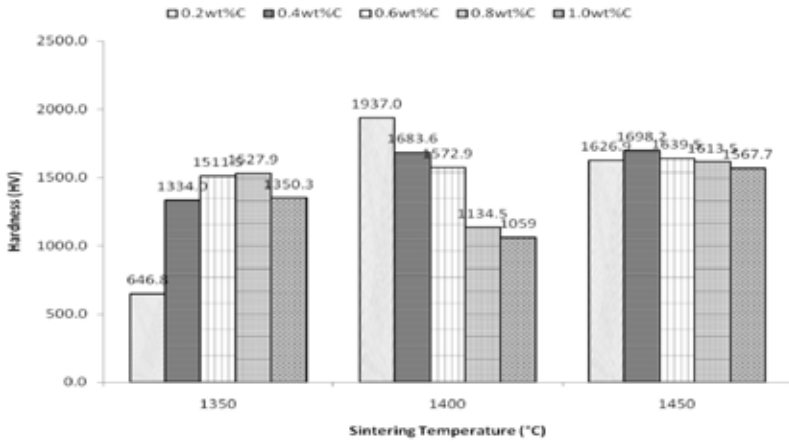


***Figure 4.*** *Hardness of WC-Co with the addition of 0.2 – 1.0%C at sintering temperature of 1350-1450 °C.*

However, if the direct-heated 0.2 %C is compared with 0.2 %C sintered with holding step, it appeared that direct-heated WC-Co possessed lower strength than the sintered sample using heating schedule with holding step as shown in Table 3. Although the hardness is much higher, its strength may not be sufficient to be used in cutting tool applications.

**Table 3.** The comparison between WC-Co-0.2%C at 1400°C using direct heating schedule and WC-Co-0.2%C with holding step.

| Properties | 450-1450°C (direct sinter) | 450-1320-1450°C (holding steps) | Commercial Insert |
|---|---|---|---|
| Density (g/cm$^3$) | 14.4 | 14.5 | 14.7 |
| Hardness (HV) | 1937.0 | 1793.0 | 1575.0 |
| Transverse Rupture Strength (MPa) | 812.3 | 1357.5 | 1700.0 |

Based on these results, it shows that the holding step at 1320 °C is necessary to improve the properties of the WC-Co-C sintered powders. This is because the holding step promote melting and homogeneous distribution of cobalt (Lee *et al.*, 2006). The melting and distribution of cobalt throughout the sintered powders is very important for densification process that will determine its physical and mechanical properties.

## CONCLUSION

The addition of carbon affects the physical and mechanical properties of WC-Co sintered powders. It is clearly shown that by adding 0.8 % of carbon and above, the density of the WC-Co samples is reduced. Small addition of free carbon proved to inhibit grain growth when compared to the conventional WC-Co sintered powders. The study also reveals that introducing holding step at temperature of 1320 °C improved the strength of WC-Co composite.

## REFERENCES

Cha, S. I. and Hang, S. H. (2003). Microstructures of binderless tungsten carbides sintered by spark plasma sintering process. *Materials Science and Engineering*. **A356** : pp 381-389.

Da Silva, A. G. P., Schubert, W. D. and Lux, B. (2001). The role of the binder phase in the WC-Co sintering. *Materials Research*. **4** : pp 59-62.

Gonzalez, R., Ordonez, A. and Sanchez, J. M. (2004). HIP after sintering of ultrafine WC-Co. *International Journal of Refractory and Hard Materials*. **23 (3)** : pp 193-198.

Lee, G. –H. and Kang, S. (2006). Sintering of nanosized WC-Co powders produced by a gas reduction-carburization process. *Journal of Alloy Compounds*. **419 (1-2)** : pp 281-289.

Petersson, A. (2004). Sintering shrinkage of WC-Co and WC-(Ti, W)C-Co materials with different carbon contents. *International Journal of Refractory Metals and Hard Materials*. **22 (4-5)** : pp 211-217.

Yao, Z., Stiglich, J. J. and Sudarshan, T. S. (1998). Nanosized WC-Co holds promise for the future. *Metal Powder Report*. **53 (3)** : pp 26-33.

*Muhammad Jabir Suleiman[1], Mohamad Azmirruddin Ahmad[1], Nurzilla Mohamed[1], Yusli Mohamad Junus[1], Rosdi Ibrahim[1], Mazlan Mohamad[1], Mohammed Rafiq Abdul Kadir[2], Noor Hayaty Abu Kassim[3], Roila Awang[4] and Shamsul Muhammad[5]*

*[1] Advanced Materials Research Centre (AMREC), SIRIM Berhad Lot 34, Jalan Hi-Tech 2/3, Kulim Hi-Tech Park, 09000 Kulim, Kedah, Malaysia.*

*[2] Faculty of Mechanical, University of Technology Malaysia (UTM) 81310 Skudai, Johor, Malaysia.*

*[3] Faculty of Dentistry, University of Malaya (UM), 50603 Kuala Lumpur, Malaysia.*

*[4] Engineering and Process Division, Malaysian Palm Oil Board (MPOB) No. 6, Persiaran Institusi Bandar Baru Bangi, 43000 Kajang, Selangor, Malaysia.*

*[5] Herbal Medicine Research Centre (HMRC), Institute of Medical Research (IMR) Jalan Pahang, 50588 Kuala Lumpur, Malaysia.*

***(jabir@sirim.my)***

## EFFECT OF ATMOSPHERE ON THE SINTERED TITANIUM ALLOY PRODUCED BY METAL INJECTION MOLDING (MIM) TECHNIQUE

***RINGKASAN:*** *Titanium aloi implan telah dihasilkan bagi aplikasi kraniofasial melalui teknik "Metal Injection Molding" (MIM). MIM adalah satu kaedah yang cekap untuk menghasilkan komponen berbentuk kompleks pada kadar pengeluaran tinggi. Dalam atmosfera normal, implan akan bertindak balas dengan elemen pemanas grafit pada suhu yang tinggi untuk membentuk karbida titanium (TiC) yang juga disebabkan oleh tindak balas dengan sistem pengikat. Justeru itu, pengaruh atmosfera kepada implan yang melalui proses pensinteran pada suhu yang tinggi telah diselidiki, supaya dapat meningkatkan sifat-sifat gabungan titanium aloi implan yang disinter. Tindakbalas ini dapat dielakkan dengan cara memasukkan gas argon atau dijalankan dalam keadaan vakum ketika proses pembakaran. Implan yang mengandungi serbuk titanium aloi dan sistem pengikat berdasarkan stearin sawit dan polietilena, dicampur melalui mesin pencampuran z-blade. Sistem pengikat kemudian dikeluarkan melalui proses penyahikatan dan dibakar dalam argon dan keadaan vakum pada suhu 1250 °C selama 4 jam. Keputusan kajian menunjukkan bahawa implan yang di sinter di dalam gas argon pada suhu 1250 °C, mengalami peningkatan kepadatan 4.525 g/cm$^3$, serta kekerasan, 458 HV dibandingkan dengan implan disinter dalam keadaan vakum yang sedikit lebih rendah dengan kepadatan dan kekerasan 4.512 g/cm$^3$ dan 426 HV. Penumpatan tinggi implan dalam gas lengai; argon, telah dicapai kerana pergabungan zarah logam. Ini sebagai hasil pencegahan titanium aloi dari tindak balas dengan suasana normal, seterusnya memperbaiki penghabluran pertumbuhan bijian yang kecil berbanding implan dalam keadaan vakum. Pola XRD (X-ray Diffraction) juga menunjukkan bahawa dengan penambahan gas argon dalam proses pensinteran, pembentukan TiC dapat dikurangkan secara berkesan.*

**ABSTRACT:** Titanium alloy produced as an implant for craniofacial application was prepared through Metal Injection Molding (MIM) technique. The MIM is an efficient method for the high volume production of complex shaped components. In normal atmosphere, the implants will react with graphite heating element at high temperature to form titanium carbide (TiC) which was also due to its reactions with binder system. Therefore the influence of the atmosphere during sintering of implants at high temperature was investigated in order to improve the properties of sintered titanium alloy implant. This reaction can be avoided by introducing argon gases or in vacuum atmosphere during the sintering process. The implant which contained titanium alloy powder and binder system based on palm stearin (PS) and polyethylene (PE), are mixed using the z-blade mixer. The binder system was then removed through the debinding process and sintered in either argon or vacuum atmosphere at 1250 °C for 4 hours. The result showed that the implants sintered in argon at 1250 °C, experienced an increased in density of 4.525 g/cm$^3$, as well as hardness, 458 HV compared to the implants sintered in vacuum atmosphere; which is slightly lower with density of 4.512 g/cm$^3$ and hardness of 426 HV. The high densification of implant in argon was achieved due to the each individual particles powder which became more interconnected to each other. As opposed to the normal atmosphere which produced TiC, sintering in argon results in improved crystallinity of the grain growth which is smaller compared with the vacuum atmosphere. The XRD (X-ray Diffraction) pattern also reveals that addition of argon gas in the sintering process, effectively reduce the formation of TiC.

Keywords: implant, palm stearin, titanium alloy, argon and vacuum atmosphere

## INTRODUCTION

Titanium alloy (Ti6Al4V) has been widely used in medical, craniofacial and dental implants, aircraft structural components, hand tools, and many various applications that require high density, strength and hardness. Metal Injection Molding (MIM) is an efficient method that has the capability in processing of complex and near-net shape components from metal powders (German *et al.*, 1997 and Ibrahim *et al.*, 2010). In the present work, titanium alloy which is produced as an implant for craniofacial application, was prepared through MIM process. Sintering is a thermal treatment for bonding the particles into a coherent, solid mass once the binder is extracted. Pores are eliminated as part of particle bonding during high temperature sintering (German *et al.*, 1997). This process is critical for determining the final quality of the parts because high sintered density is imperative for good mechanical properties such as hardness. Achieving full or near-full density has been the major objective for sintering processes (Mariappan *et al.*, 2009).

There are some justifications for using argon atmosphere instead of a vacuum medium during sintering. Vacuum sintering is used to maintain a clean, reproducible and controlled nonreactive atmosphere. Sintering under vacuum cleans a surface from oxide contaminations. A low partial pressure of oxygen leads to oxide reduction for many metals (German, 1994). Graphite and ultra porous carbon materials which constitute the internal parts of some furnaces are considered to be incompatible with high vacuum demands (Frage *et al.*, 2004). Sintering by using inert gas is the heating process that runs in a nonreactive atmosphere where there is less chemical reactions among the substances. The inert gas can avoid ordinarily non-reactive substances from becoming reactive, based on its noble gas nature which is resistant to bonding with other elements. In this case, an argon atmosphere is used in graphite electric furnaces to prevent the graphite heating element from burning. A carbon residue can be disastrous to the mechanical and physical properties of materials such as titanium alloy. Thus sintering without a residue is important in controlling the final chemistry.

The purpose of this study is to optimize the density and hardness properties of titanium alloy implant under two different sintering atmospheres of argon and vacuum at high temperatures. In normal atmosphere, the implants will react with graphite heating element at high temperature and also the reaction with the vapor of the binder materials to form titanium carbide (TiC) which seems to present a problem of brittleness on the sintered implants. These reactions can be avoided by introducing argon gases during the sintering process and also conducted in vacuum condition in order to provide clean, non-reactive and controlled conditions.

## MATERIALS AND METHODS

Titanium alloy (Ti6Al4V) spherical shape powder (TLS Technik Gmbh & Co. Spezialpulzer Kg) was used as a starting material with 25 µm of particle size and tap density of 2.50 g/cm$^3$, apparent density of 2.00 g/cm$^3$ and pycnometer density of 4.50 g/cm$^3$. In the beginning, the feedstock which contained titanium alloy powder and the binder system of palm stearin and polyethylene are mixed homogeneously at a ratio of 66/34 using z-blade mixer. The feedstock were then injected into a desired shape mould, using a vertical injection molding at the temperature of 180 to 200 °C with injection pressure of 6 to 9 bar. The debinding process is implemented through two steps i.e. solvent extraction to remove the PS binder and thermal pyrolysis for the remaining binders.

**Table 1.** Melting and evaporation temperature of each component binder system.

| Binder Material | Melting temperature (°C) | Evaporation temperature (°C) |
|---|---|---|
| Polyethylene (PE) | 125.9 | 488.0 |
| Palm Stearin (PS) | 54.2 | 436.5 |

Table 1 shows the melting and evaporation temperature of PE and PS which were measured using Simultaneous Thermal Analysis (STA). The melting and evaporation temperature is then used as an indicator for designing the cycle for removal of the binder system. During solvent extraction process, the implants were immersed in heptane at 60 °C for 6 hours. As for the thermal pyrolysis process, the implants were heated at 440 °C and soaked for an hour for removal of PS and partly of PE. Table 2 indicates the sintering process using High Temperature Control Atmosphere Furnace (HTCAF) from 30 °C until it reaches 770 °C for 1 hour of soaking time selected based on the α modification at the temperature below than 882 °C. The alpha (α) to beta (β) allotropic transformation cycle continues until 1250 °C with heating rate of 10 °C/min based on the high temperature β that is stable between 882 °C and its melting point of 1668 °C. The weight percentage of element was analyzed and measured using an XRD-D8 Advanced instrument (Bruker, Germany) with a Cu Kα radiation source at 40 KV and 40 mA. Implants were scanned at a speed of 0.04 °/sec, ranging from $2\theta = 10°$ to 90°.

**Table 2.** Sintering condition of titanium alloy implants.

| Sintering Condition | Sintering temperature (1250 °C) | |
|---|---|---|
| | Argon | Vacuum |
| Implant | A | B |

## RESULTS AND DISCUSSION

Carbon control is a pervasive problem and excess of this element needs to be eliminated in the final stage of debinding and early stage of sintering. An improper sintering atmosphere is a primary cause of carbon residue problems and furthermore, if the impurities are carried over to high temperature, they can react to form volatile species (German *et al.*, 1997). The sintered properties can be increased or decreased due to the removal of binder system during pre-sintering conditions. Because the final stage of debinding is via decomposition of the polymer binder, there is a concern for the relative burnout of the remaining backbone polymer. Thus, complete binder removal without a residue is important in controlling the final chemistry. At this stage, the binder burnout occurs from

within the particle and it flows to the compact surface. The surface then dries by evaporation of near-surface pendular bonds.

Rapid evaporative debinding is aided by a high temperature and agitated atmosphere that is constantly being replenished with inert argon gas. Argon molecule diffuse within the particles, flow with the vapor binder and leaves only the particles. There will be no chemical reaction or contamination caused by the binder, as it was removed or prevented by the argon molecules. It also helps to reduce the size of pores among the particles left by the binder evaporation and improved the densification of Ti6Al4V compact. Vacuum state is able to remove air or vapor binder on the compact surface. However it has limitations if the binder is trapped among the particles when the temperature is raised thus affecting the particle interconnection and produced more pores in the samples.

It is stated that almost 80 % of the binder is removed by solvent extraction and the remaining 20 % forms a gaseous product during thermal pyrolysis, as the binder evaporates and leaves the pores among the particles. Implant A showed an improved density due to the use of inert gas which does not undergo chemical reactions and do not react with any substances, thus avoiding unwanted chemical reactions which can reduce the quality of the implant. These undesirable chemical reactions are often oxidation and hydrolysis reactions with oxygen and moisture in air. PS melted completely during solvent extraction and is totally removed after heated at 436.5 °C due to its evaporation temperature.

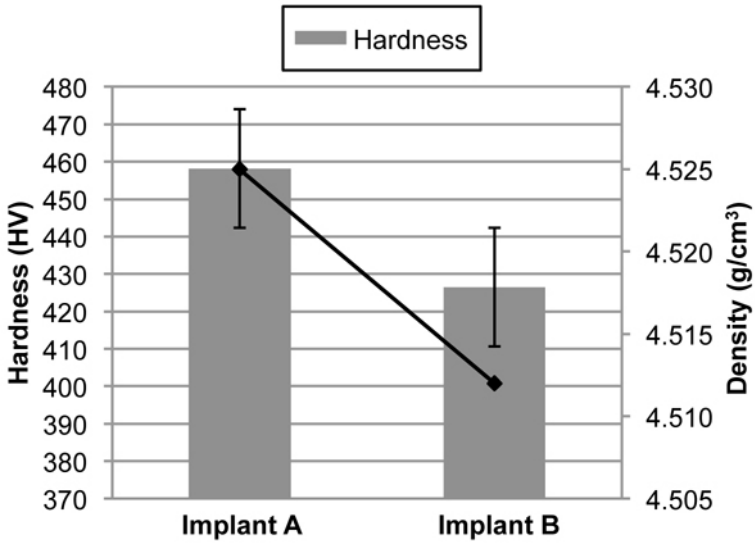


***Figure 1.*** *Hardness and density properties of titanium alloy sintered implants.*

**Table 3.** Hardness and density properties of titanium alloy sintered implants.

| Physical and Mechanical Properties | Implant A | Implant B |
|---|---|---|
| Density (g/cm$^3$) | 4.525 | 4.512 |
| Hardness (HV) | 458 | 427 |

Pure metallic components were obtained after sintering with 15 to 20 % shrinkage. During sintering, the debound part is heated, thus allowing densification of the powder into a dense solid with elimination of pores. The density of the sintered part was measured using a Shimadzu SGM-330H-A Specific Gravity Meter. In Figure 1, Implant A experienced an increased in density of 4.525 g/cm$^3$ compared to Implant B; sintered in vacuum condition which was slightly lower in density of 4.512 g/cm$^3$ showing a difference of 0.013 g/cm$^3$. During sintering process, pores were observed on the sintered part of both implants during binder removal, and this situation allows the particle to pack densely and fulfil the voids left by the binder. Uniform packing of the particles reflected the shrinkage of the implants based on constant removal of binder system among the Ti6Al4V particle. The hardness test which was carried out on a Zwick Roell ZHV10 tester shows that Implant A reached a hardness value of 458 HV, whilst Implant B was 426 HV. This shows that due to the high particle packing of Implant A, the hardness reached 458 HV.

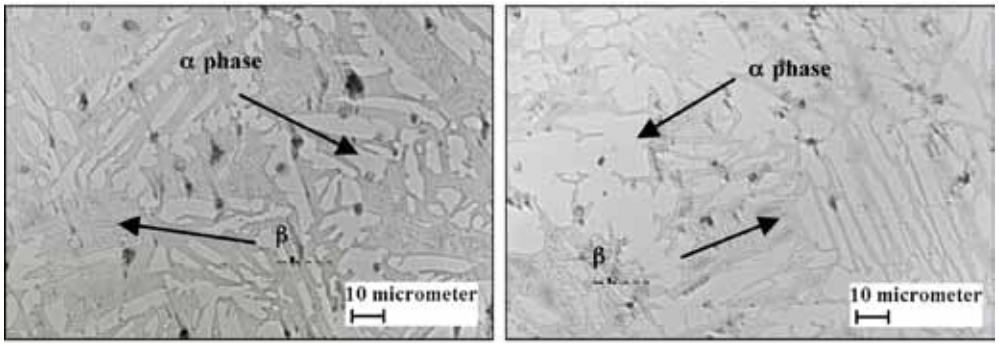


(a) (b)

***Figure 2.*** *Microstructure of titanium alloy sintered implants (a) implant A, and (b) implant B.*

Figure 2 reveals the optical microstructure of the sintered implants. Titanium exists in two allotropic modifications; β having a body-centered cubic structure with high temperature that is stable between 882 °C and its melting point of 1668 °C, and α which has a closely packed hexagonal structure modification of titanium that exists at temperatures below 882 °C. Various elements forming solid solution with titanium are classified on the basis of their effect on the solubility of α and β phases. Elements stabilizing α phase are known as α stabilizers (Aluminium (Al), Gallium (Ga), Oxygen (O), Nitrogen (N), Carbon (C)), and elements stabilizing β

phase are known as β stabilizers (Vanadium (V), Molybdenum (Mo), Niobium (Nb), Iron (Fe), Chromium (Cr), Nickel (Ni), etc.). Ti6Al4V belongs to a class of α+β alloys as these alloys contain larger amounts of beta stabilizers (4 to 6%). A central point in the evolution of microstructure in titanium alloys is the α→β transformation temperature, generally referred to as the β transus temperature, since it separates the single-phase β field from the two-phase α+β filled (Joshi, 2006).

Titanium alloys, when heat-treated above the β transus temperature, β will result in β transformation to various equilibrium or nonequilibrium phases, depending upon the cooling rate and alloying content (Joshi, 2006). Observations over a range of magnifications (100 – 500 magnification) reveal that the orientation of the microstructure for both implants is slightly different as it shows the transformed β (dark) microstructure with prior β boundaries. A thin continuous α (light) phase is present at the grain boundaries for Implant A and primary α phase for Implant B, where the grains of the α phase were well distributed in the matrix of the β phase. The large α grains were predominantly non-uniform in size and shape. Lamellar microstructures, originating from cooling out of the β phase field, and equiaxed microstructures, as a result of a recrystallization process, can either individually have a fine or coarse distribution or can both be present in a bimodal microstructure (Leyens *et al.*, 2003). Implant A reveals the improved crystallinity of grain growth where the α phase is becoming smaller in size with fine distributions compared to the Implant B.

**Table 4.** Weight percentage of elements in Ti6Al4V sintered implants.

| Elements (wt.%) | Implant A | Implant B |
|---|---|---|
| Titanium Carbide (TiC) | 66.77 | 70.47 |

The high densification of implants in argon was achieved due to the particles which became interconnected signifying that the densification was achieved due to the non-reactive properties of inert gases that prevent undesirable chemical reactions from taking place and improved the properties (Ye, *et al.*, 2008) compared to vacuum atmosphere which only prevents the chemical reaction on the surface of the sintered implants. Figure 3 shows the XRD pattern of Ti6Al4V sintered implants which reveals TiC peaks. Table 4 shows that implants in vacuum atmosphere exhibit dominant peaks of TiC until 70.47 wt.% compared to argon atmosphere with 66.77 wt.% of TiC. It is clear that the formation of TiC can be reduced through the addition of argon gas in sintering atmosphere.

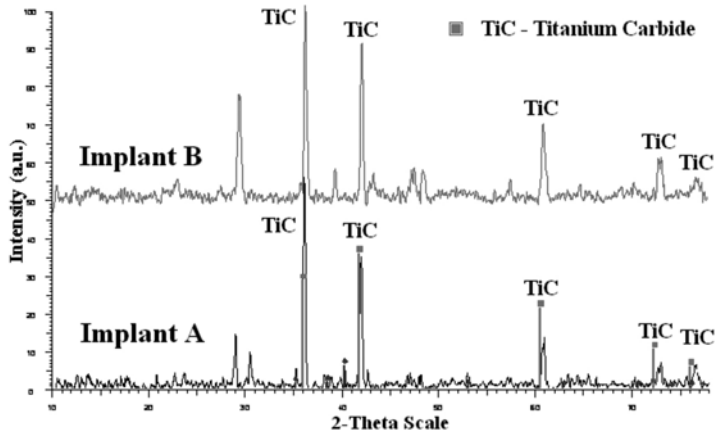


***Figure 3.*** *XRD pattern of titanium alloy sintered implants.*

## CONCLUSION

The use of argon gas in the sintering atmosphere appears to prevent reaction from the graphite heating element on the implant structure during sintering at high temperature. This prevention has improved the densification and hardness properties, compared to implants in vacuum atmosphere. The mechanical properties of Implant A have achieved the minimum requirement for sintered MIM parts as compared with the Standard Metal Powder Industries Federation (MPIF) 35 for titanium alloy. The improved cystallinity structure of titanium alloy sintered in argon was shown clearly on the micrograph. This study has proven that the formation of TiC can be reduced effectively through argon atmospheres.

## ACKNOWLEDGEMENTS

This work partly was funded by Techno Fund (TF0206D124) of Ministry of Science, Technology and Innovation (MOSTI).

## REFERENCES

Frage, N., Levin, L., and Dariel, M. P. (2004). The effect of sintering atmosphere on the densification of B4C ceramics. *Journal of Solid State Chemistry.* **177** : pp 410-414.

German, R. M. and Bose, A. (1997). *Injection Molding of Metals and Ceramics.* Metal Powder Industries Federation, Princeton, NJ, USA, pp 219-254.

German, R. M. (1994). *Powder Metallurgy Science.* Metal Powder Industries Federation, Princeton, NJ, USA, pp 282-287.

German, R. M. (1996). *Sintering Theory and Practice.* John Wiley & Sons Inc., 605 Third Avenue, NY, USA, pp 423-426.

Ibrahim, R., Azmirruddin, M., Jabir, M., Ismail, M. R., Mohamad, M., Awang, R., and Muhamad, S. (2010). Injection Molding Of Titanium Alloy Implant For Biomedical Application Using Novel Binder System Based On Palm Oil Derivatives. *American Journal of Applied Sciences* **7(6)** : pp 811-814.

Joshi, V. A. (2006). *Titanium Alloy: An Atlas of Structures and Fracture Features.* Taylor & Francis Group, Boca Raton, FL, pp 9-95.

Leyens, C. and Peters, M. (2003). *Titanium and Titanium Alloys. Fundamentals and Applications.* WILEY-VCH Verlag GmbH & Co. KGaA, Weinheim : pp 4-16.

Mariappan, R. and Kumaran, S. (2009). Effect of sintering atmosphere on structure and properties of austen-ferritic stainless steel. *Materials Science and Engineering*. **A 517 :** pp 328-333.

Ye, H., Liu, X. Y. and Hong, H. (2008). Sintering of 17-4PH stainless steel feedstock for metal injection molding. *Materials Letters*. 62 : pp 3334-3336.

*M. M. Rahman**
*T. J. Saktisahdan &*
*H. Y. Rahman*

*Department of Mechanical Engineering, Universiti Tenaga Nasional, Jalan IKRAM-UNITEN, 43000 Kajang, Selangor, Malaysia*

***(mujibur@uniten.edu.my)***

## SINTERING OF WARM FORMED COMPONENTS IN INERT GAS FIRED FURNACE

***RINGKASAN:*** *Kertas kerja ini membentangkan hasil kajian ujikaji pensinteran komponen logam yang dibentuk pada keadaan hangat menggunakan kaedah ekapaksi. Bahan suapan disediakan dengan cara mencampurkan serbuk besi ASC 100.29 dengan 0.4 wt% dan 0.8 wt% zink stearat untuk 30 minit. Bahan campuran berkenaan lalu dibentuk pada suhu 120 °C dan 180 °C. Mampatan hijau yang baik telah disinter dalam ketuhar gas argon pada jadual pensinteran yang berbeza-beza. Kadar pemanasan yang digunakan adalah 5 °C/minit dan 10 °C/minit di mana kadar penyejukan adalah kebalikan daripada kadar pemanasan. Kesemua sampel disinter pada suhu malar iaitu 1000 °C dengan membiarkan sampel pada suhu berkenaan untuk masa yang berbeza-beza iaitu 30 minit dan 60 minit. Produk yang telah disinter telah diciri melalui ujian mekanikal dan pemeriksaan mikrostruktur. Hasil kajian menunjukkan bahawa parameter pembentukan dan pensinteran memberikan kesan yang signifikan ke atas kualiti produk akhir.*

**ABSTRACT:** This paper presents the results of an experimental investigation of the sintering of metallic components formed at above ambient temperature. The feedstock was prepared through mechanically mixing of iron powder ASC 100.29 with 0.4 wt% and 0.8 wt% zinc stearate for 30 minutes. The powder mass was then shaped at 120 °C and 180 °C through uniaxial compaction method. The defect-free green compacts were then sintered at argon gas fired sintering furnace at different sintering schedules. The heating rates were 5 °C/minute and 10 °C/minute where the cooling rates were the reverse of the heating rates. The holding times were 30 minutes and 60 minutes whereas the sintering temperature was fixed at 1000 °C. The sintered products were characterized through mechanical testing and microstructure examination. The results revealed that both forming and sintering parameters significantly affect the final quality of products.

Keywords: Warm forming, sintering, mechanical properties, microstructure

## INTRODUCTION

The study of near-net-shape manufacturing through powder route has become essential since there is a need in cost reduction and improvement in mechanical properties such as higher density, strength, etc. Hence, the optimization between these two aspects, i.e., economics and mechanical properties has to be considered simultaneously. A major advance in this technology has been the warm forming process, which utilizes traditional powder forming equipment.

Warm forming is defined as compaction of metal powder at elevated but below its re-crystallization temperature (Höganäs, 1998). Sintering plays an important role in a full cycle of warm forming process in producing defect-free final products with excellent mechanical properties and microstructures. Sintering is a heat treatment process for bonding particles together into a coherent, predominantly solid structure via mass transport events. Such bonding improves the strength and other engineering properties of powder compacts. The standard way of performing the sintering operation is to subject the parts to a high temperature in a controlled atmosphere using a sintering furnace (German, 1996). The process is known as free sintering since no mechanical stress is applied on the parts. The effect of sintering is the change of inter-particle contact, which begins with rapid growth between particles because of the cold welding taken place in the green compact. At this stage, the void volume is reduced and finally as the surface tension and diffusion continue, the spheroidization of isolated pores occurs and it results in a relatively homogenous component (Simchi, 2003). Correct sintering is of paramount importance to the powder metallurgy process to ensure not only the development of the strength needed for the part to fulfill its intended role as an engineering component, but also that the dimensions of the part are correct (Xiao *et al.*, 2009).

The metal powder is generally mixed with a polymeric lubricant prior to the generation of defect-free yet high density green compacts to be sintered. During sintering, the lubricant is burnt out due to its low melting temperature which causes uneven density distribution and dimensional distortion if the sintering is not conducted through proper schedule (Nor *et al.*, 2008; Rahman & Nor, 2009). Powder forming at above ambient temperature is relatively new hence no information on the sintering characteristics of iron powder formed at different forming parameters is available in the literature. Therefore, the aim of this paper is to present the outcome of the investigation of sintering characteristics of iron powder compacts formed at above ambient temperature.

## MATERIALS AND METHOD

Main powder constituent was iron powder ASC 100.29 which has the particle size range of 20-180 μm. The powder manufactured by Höganäs AB Company has the composition of 1.5 % Cu, 0.5 % Mo, and 4 % Ni balanced with Fe. Zinc stearate ($C_{36}H_{70}O_4Z_n$) powder has been used as an admixed lubricant. The overall experiment consists of (i) feedstock preparation, (ii) green body generation, (iii) sintering, and (iv) sample characterization.

### Feedstock Preparation

In order to prepare a homogenous blend of feedstock, iron powder was mixed mechanically with 0.4 wt% and 0.8 wt% zinc stearate for 30 minutes (Rahman & Nor, 2007).

### Green Body Generation

The compaction experiment has been conducted using previous published experimental procedure (Rahman *et al.*, 2011). It consists of powder filling inside the die, powder and the die assembly heating, powder forming, and the ejection. The powder mass was shaped at two different temperatures, i.e., 120 °C, and 180 °C. The powder mass with the die assembly were heated to the required temperature and hold for 30 minutes in order to get the uniform temperature distribution (Ariffin *et al.*, 2001). The compaction load was fixed to 130 kN, which is considered suitable to generate green samples of adequate strength (Rahman *et al.*, 2010). The warm compaction rig is shown in Figure 1.

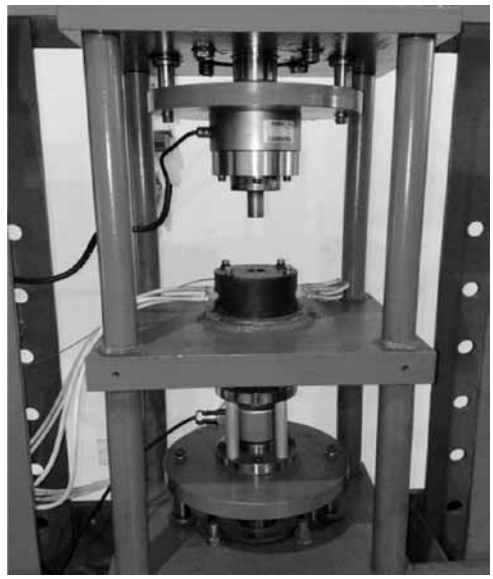

***Figure 1.*** *Warm compaction rig sintering.*

The green compacts were sintered in an argon gas fired sintering furnace by varying the sintering time (30 and 60 minutes), and heating rate (5 °C/minute and 10 °C/minute). However, the sintering temperature was kept at constant value, i.e., 1000 °C.

**Product Characterization**

The final products were characterized for their relative densities and strengths. The microstructure of the sintered products was analyzed using Scanning Electron Microscope.

## RESULTS AND DISCUSSION

Figures 2 and 3 show the density variation against heating/cooling rate at different holding time for the green compacts with different lubricant content. It can be observed that as heating rate increases, the density decreases. This is caused by the higher volume reduction when the samples were sintered at 5 °C/minute compared to 10 °C/minute. Lower heating rate promotes grain growth, thus eliminates pores that leads to density increment better than higher heating rate. It is also evident that the density of sample formed at 120 °C with 0.8 wt% of zinc stearate tends to have better density. As the melting temperature of zinc stearate is 130 °C, the effective medium of lubrication is around 120 °C compared to 180 °C. Therefore, 120 °C forming temperature has given higher relative density during compaction process and as the samples are sintered at the same schedule, higher relative density of final product is achieved at a higher density sample. Furthermore, due to the addition of higher weight percent of lubricant, i.e., 0.8 wt%, some zinc stearate is trapped inside the powder mass, which reduced the inter particle friction and eased the motion of powder particles, as a consequence, the volume became smaller hence the density became higher compared to the addition 0.4 wt% lubricant.

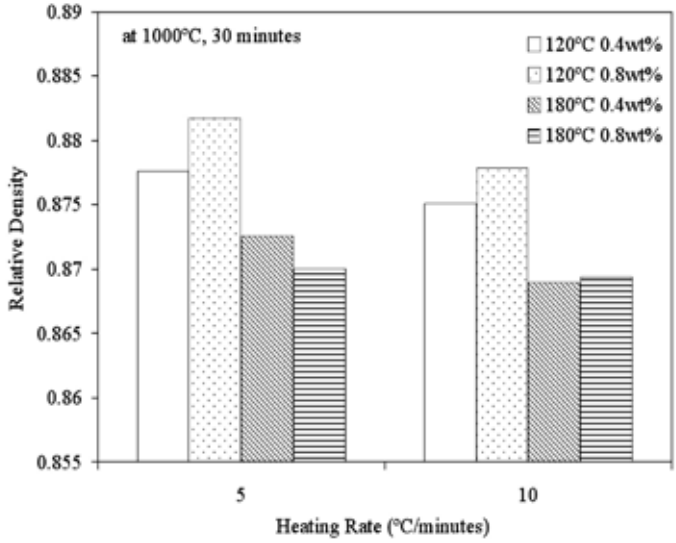


***Figure 2.*** *Sintered densities at different heating rate, 30 minutes holding time.*

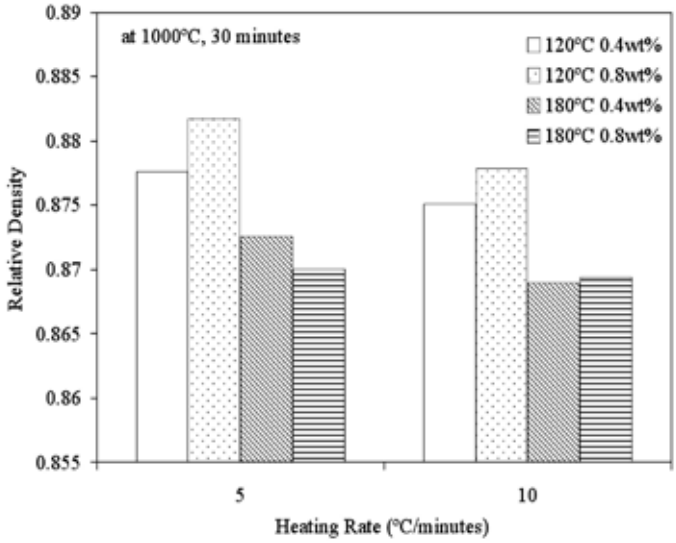


***Figure 3.*** *Sintered densities at different heating rate, 60 minutes holding time.*

In powder metallurgy, the strength of the product is the most vital factor to be considered. The higher the strength indicates the high quality of the product. Therefore, it is necessary to produce product with higher strength. Figures 4 and 5 show the variations of strength against heating/cooling rate. It can be observed that the strength increases as the heating rate increases. The reason is that at high heating rate i.e., 10 °C/minute, grain growth is inhibited, thus higher strength is achieved (Rittidech & Tunkasiri, 2009).

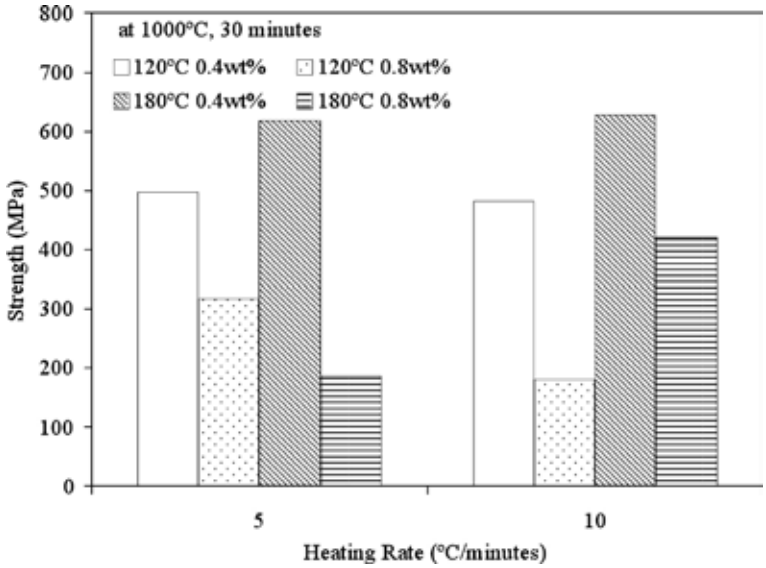


***Figure 4.*** *Sintered strengths at different heating/cooling rate, 30 minutes holding time.*

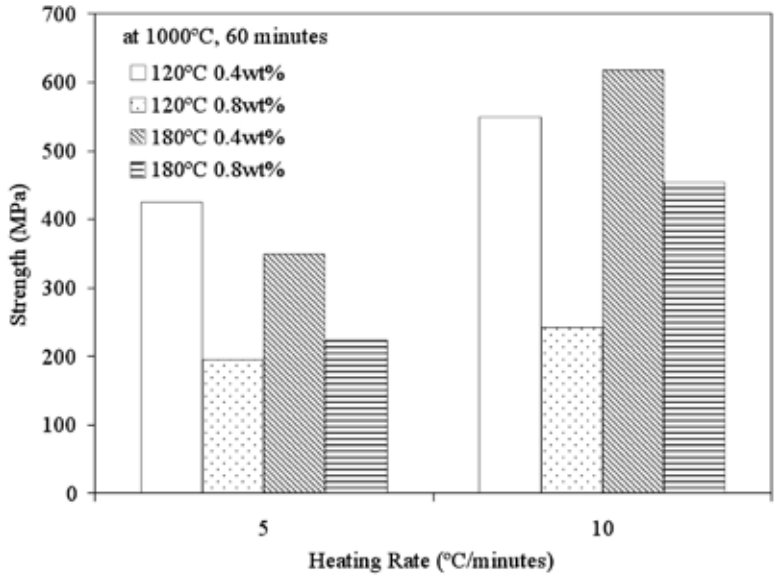


***Figure 5.*** *Sintered strengths at different heating/cooling rate, 60 minutes holding time.*

Results of microstructure analyses (Figure 6) revealed that at a certain sintering schedule, forming parameters influenced the microstructures of the final products. At higher forming temperature, i.e. 180 °C, smaller grains were observed compared to forming at lower temperature, i.e. 120 °C. This finding correlates with the argument reported earlier (Rahman *et al.*, 2010). At higher lubricant content,

more void or pores were observed. The interconnected pores are also observed at the green compacts with higher lubricant content.

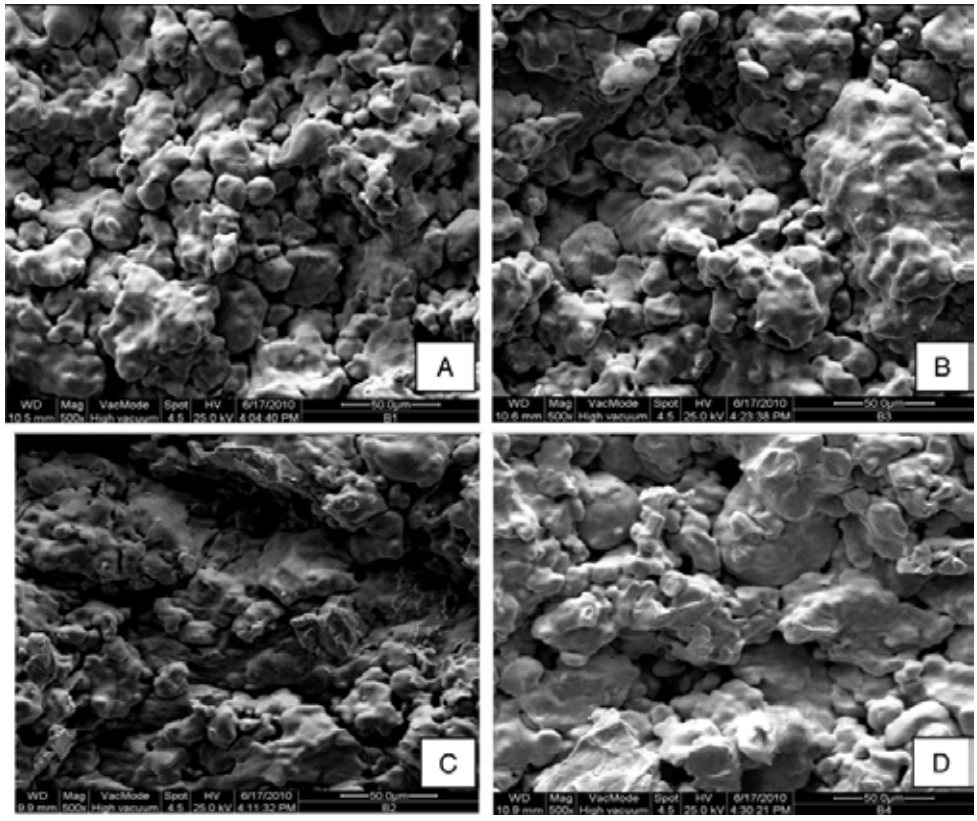


***Figure 6.*** *Microstructures of sintered products formed at different compaction parameters (A) 120°C; 0.4wt%, (B) 180°C; 0.4wt%, (C) 120°C; 0.8wt%, and (D) 180°C; 0.8wt%.*

## CONCLUSION

This study reported the investigation on the effects of sintering parameters to the final characteristics of iron based components formed through warm forming route. It can be concluded that the powder forming parameters and sintering schedules have close relationship to the mechanical properties and microstructures of the sintered products. Compaction at higher temperature is found to produce lighter yet high strength components.

## REFERENCES

Ariffin, A.K., Jumahat, A. and Rahman, M.M. (2001), The simulation of die movement in designing P/M parts. *National Design Seminar*. Johor Bahru-Malaysia. 15th January, pp 129-134.

German, R.M. (1996). Sintering theory and practice, New York: John Wiley & Sons, Inc. Höganäs (1998). *Handbook for warm compaction*. Sweden: Höganäs AB, pp 7-12.

Nor, S.S.M., Rahman, M.M., Tarlochan, F., Begum, S. and Ariffin, A.K. (2008). The effect of lubrication in reducing net friction in warm powder compaction process, *Journal of Materials Processing Technology*. **207**: pp 118-124.

Rahman, M.M. and Nor, S.S.M. (2007). An experimental investigation of T-shape component forming through warm powder compaction route, *Malaysian Symposium on Advances in Powder Metallurgy and Particulate Materials 2007*, UiTM Shah Alam, 21-22 August, pp 1-10.

Rahman, M.M. and Nor, S.S.M. (2009). An experimental investigation of metal powder compaction at elevated temperature. *Mechanics of Materials*. **41**: pp 553-560.

Rahman, M.M., Nor, S.S.M. and Rahman, H.Y. (2011). Investigation on the effect of lubrication and forming parameters to the green compact generated from iron powder through warm forming route. *Materials and Design*, **32** : pp 447-452.

Rahman, M.M., Nor, S.S.M., Rahman, A.T.A., Ariffin, A.K. and Rahman, H.Y.(2010). On the effects of warm compaction parameters to the mechanical properties and microstructures of sintered parts, *The International Conference on Experimental Mechanics 2010* (ICEM 2010), Kuala Lumpur, Malaysia, 29 November - 1 December, pp 153-159.

Rahman, M.M., Rahman, A.T.A., Nor, S.S.M. Saktisahdan, T.J. Ramesh, S. and Rahman, H.Y. (2010). Sintering characteristics of mechanical components formed from iron powder at above ambient temperature, *Malaysian Metallurgy Conference (MMC 2010) & 4th Malaysian Powder Metallurgy Symposium* (4th MPSM), Batu Feringgi-Penang, 23 & 24 November. pp 207-215.

Rittidech, A. and Tunkasiri, T. (2009). Influence of heat treatment in sintering process on characteristics of $Al_2O_3$-$ZrO_2$ Ceramics Systems, *American Journal of Applied Sciences*. **2**: pp 309-312.

Simchi, A. (2003). Effects of lubrication procedure on the consolidation, sintering and microstructural features of powder compacts, *Materials and Design*. **24**: pp 585-594.

Xiao, Z.Y., Ke, M.Y., Fang, L., Shao, M. and Li, Y.Y. (2009). Die wall lubricated warm compacting and sintering behaviors of pre-mixed Fe-Ni-Cu-Mo-C powders, *Journal of Materials Processing Technology*. **209**: pp 4527-4530.

*Mahrukh Bukhari[1], S.J. Iqbal[1], M Iqbal[2], M S Rafique[2]*

*[1] COMSATS Institute of Information Technology, Lahore, Pakistan*

*[2] University of Engineering & Technology Lahore, Pakistan*

***(sparkingstar@live.com)***

## STUDY OF SOFT X-RAY EMISSON FROM LASER PRODUCED PLASMA OF DIFFERENT MATERIAL

***RINGKASAN:*** *Pemancaran sinar-X yang lembut dari laser plasma yang dihasilkan dari bahan-bahan yang berbeza telah dikaji. Laser Nd:YAG (1.06 µm) bertenaga 10 mJ, dan FWHM 12-ns telah digunakan untuk menghasilkan plasma daripada bahan sasaran yang berbeza. Sinar-X yang dijana daripada plum plasma adalah disebabkan interaksi antara laser. Eksperimen dilakukan di bawah vakum dalam lingkungan 1 mTorr dalam bekas keluli tahan karat yang mempunyai 8 port. Tungsten, perak, aluminium dan tembaga telah digunakan sebagai bahan sasaran untuk kajian. Sinar-X yang lembut dikesan oleh 10 mikron Al PIN fotodiod (BPX 65). Semua pancaran sinar-X disimpan pada storan osiloskop digital 200 MHz osiloskop digital. Adalah didapati bahawa tungsten adalah sumber yang tidak sesuai untuk penjanaan sinar-X lembut berbanding dengan perak, aluminium dan tembaga.*

**ABSTRACT:** The soft X-ray emission from laser produced plasma of different materials has been investigated. We used Nd:YAG (1.06 µm) laser, of energy 10 mJ, and FWHM 12 ns to produce plasma from different target materials where X-rays were generated from the plasma plume due to laser matter interaction. The experiments were performed under vacuum of approximately 1 mTorr in a stainless steel chamber, consisting of eight ports. Tungsten, silver, aluminum and copper were used as the target materials for the investigation. The soft X-rays were detected by 10 micron Al filtered PIN photodiode (BPX 65) where all the X-rays signals were stored in the 200 MHz digital storage oscilloscope. It was found that tungsten is a poor source of soft X-rays as compared with the silver, aluminum and copper.

Keywords: Laser Produced Plasma, soft X-Rays, plasma.

## INTRODUCTION

The present project was aimed to inspect the soft X-ray emission from plasma, generated by a 12 ns Nd:YAG (1.06 μm) laser when metal targets were irradiated. Various techniques are commonly used for X-rays analysis including Charged Couple Device (CCD), semiconductor PIN photodiodes with appropriate filters and Photo Multiplier Tubes (PMT). Among all these techniques, semiconductors PIN photodiode detectors are the simplest and most economical tool for X-ray detection (Dutta *et al.*, 2012). Laser-produced plasmas have attracted strong interest for its potential use as an X-ray source with their high brightness and small source size (Kodama *et al.*, 1987). Plasma formed due to high power laser matter interaction is presented as ultra-bright source of X-ray radiation (Giulietti, 1998). A number of experiments have been conducted to characterize the emission of soft (Ditmire *et al.*, 1995) (Parra *et al.*, 2000) and hard X-rays (McPherson *et al.*, 1994) from Laser Plasma (LP) (Liu *et al.*, 2009). The specific spectral range emitted depends largely on the target material (Spencer *et al.*, 2005).

X-rays are created by radiative interaction of electrons with matter and collisional interactions of electrons with matter (Bushberg *et al.*, 2012). In radiative interaction of electrons with matter, an electron (which is negatively charged) approaches the nucleus (which is positively charged), can be deflected from its original direction by the attractive force of the nucleus. The change of direction causes deceleration in forward direction of the electron or a loss of its kinetic energy. The energy lost by the electron is given as an X-ray photon. The radiation produced by this type of interaction is called bremsstrahlung (in German, literally means 'braking radiation' or 'deceleration radiation') or continuous X-rays. X-rays are also generated when electrons interact with the firmly bound orbital electrons of a solid surface. This is referred as collisional interaction of an electron with matter. This type of interaction produces characteristic or line radiation.

X-rays can also be produced from laser matter interaction (Alaterre *et al.*, 1986). When intense laser pulse is irradiated on a target material, a small quantity of the material is vaporized. Through further absorption of photons, the vaporized material is heated up until it ionizes and expands from the surface of material as a plasma cloud (Kompitsas *et al.*, 2000). This laser-induced plasma acts like a micro-source of light. This can be analyzed by the detection of spectrally and temporally resolved characteristic emissions through a spectrometer (Carranza *et al.*, 2002). For temperatures of hundreds of electron volts (which is many million degree Kelvin, 1ev = 1.6 x 10-23 Joule = kT, where k is Boltzmann's constant and T is temperature in Kelvin), a very broad spectrum is emitted. This spectrum has a range from infrared to X-ray region.

## MATERIALS AND METHODS

In this experiment, PIN Photodiodes BPX 65 was used to detect the soft X-rays emitted from the Laser Produced Plasma of the target metals whereby commercially available BPX 65 diodes are manufactured for IR detection (Johnson, 2003). For X-ray detection, the glass window of the TO-18 casing of the diode was removed (Patran, 2002). Al filter of thickness of 10 microns was used to cover the diode since Al has the ability to filter the low energy or simply long wavelength radiations (Sprawls, 1993). The biasing circuit for diode is shown in Figure 1.

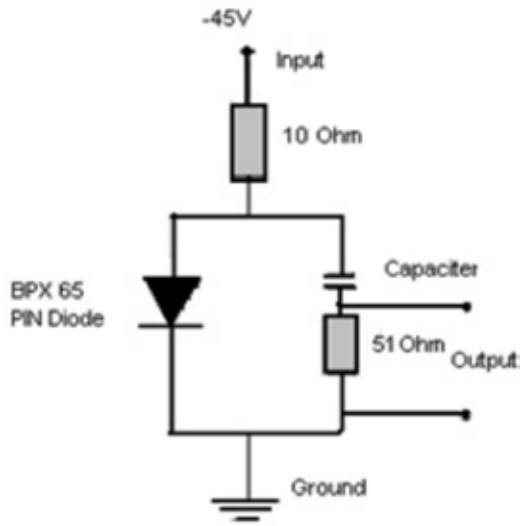


***Figure 1.*** *Biasing Circuit for Diode.*

The schematic diagram of experimental setup is shown in the Figure 2. The laser was focused on the target materials one by one, hence produced plasma cloud on target surface. X-rays were then generated from this cloud due to laser plasma interaction. A properly biased PIN photodiode (BPX 65) was used to detect soft X-rays where these signals were stored on 200 MHz oscilloscope. The equipment was arranged in the 8 ports of a stainless steel chamber. The experiment was performed under vacuum of approximately 1 mTorr where this vacuum level was achieved using a diffusion pump, which was supported by a rotary pump in the initial stage of evacuation process.

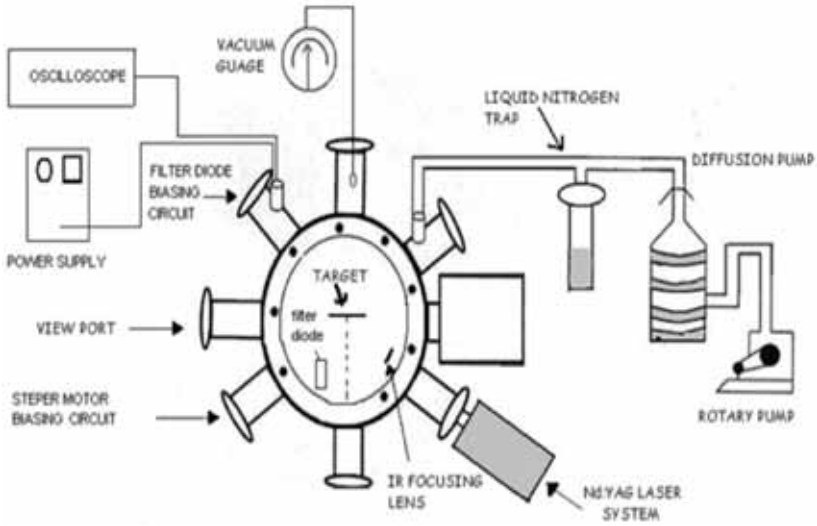


***Figure 2.*** *Schematic Illustration for Experimental Set-Up.*

## RESULT AND DISCUSSION

The graph between transmission factor and photon energy for Al filter with a thickness of 10 micron is shown in Figure 3. From the graph we can see that the transmission factor was 5 % at the photon energy of 1000 eV, and increased sharply up to 38 % at 1500 eV of photon energy. It then dropped sharply to zero transmission from 1500-2000 eV. The transmission increased again after that where it reached 50 % and 90 % of transmission at 4,500 and 9,000 eV respectively. Details of the transmission factor of photons with, respect to the photon energy are given in Table 1.

**Table 1.** Transmission coefficient of Aluminum filter.

| Photon Energy (eV) | Transmission (percentage) | Wavelength (nm) |
|---|---|---|
| 1000 | 5% | 0 – 1.242 |
| 1500 | 38% | 0.828 |
| 1500 – 2000 | No | 0.828 -0.621 |
| 4000 | 40% | 0.3105 |
| 4500 | 50% | 0.27 |
| 9000 | 90% | 0.138 |

Al density = 2.7 g/cm$^3$ Thickness = 10 microns

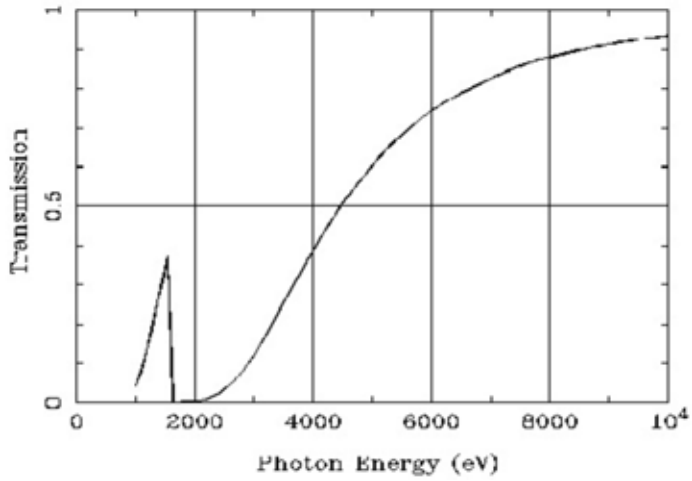


***Figure 3.*** *Filter Transmission Factor.*

Four different metals, namely, tungsten (W) (Table 2), silver (Ag) (Table 3), aluminium (Al) (Table 4) and copper (Co) (Table 5) were irradiated by intense laser pulses to study the time-resolved emission of X-rays from the plasma produced by these metals. These metal targets were attached to a mount and connected to a stepper motor which was capable of completing a round trip in four steps so that one metal target was irradiated at a time. This whole system was placed in a vacuum of approximately 1 mTorr, evacuated using a diffusion pump which was supported by a rotary pump. An Nd:YAG laser of wavelength 1064 μm, energy of 10 mJ and 12 ns pulse duration was used. The soft X-rays emitted from the Laser Produced Plasma in the metal targets were detected by PIN diode.

**Table 2.** Parameters for PIN Signals for Tungsten Target.

| Signals | Peak under observation | Peak start time $t_1$(ns) | Peak end time $t_2$(ns) | $\Delta t = t_2 - t_1$ (ns) | Peak Voltage (mV) | FWHM (ns) |
|---|---|---|---|---|---|---|
| 1st Signal | 1st | 8 | 16 | 8 | 120 | 6 |
| | 2nd | 24 | 39 | 15 | 324 | 7 |
| 2nd Signal | 1st | 0 | 11 | 11 | 120 | 6 |
| | 2nd | 17 | 35 | 18 | 320 | 9 |
| 3rd Signal | 1st | 5 | 15 | 10 | 140 | 6 |
| | 2nd | 21 | 35 | 14 | 340 | 9 |

**Table 3.** Parameters for PIN Signals for Silver Target.

| Signals | Peak under observation | Peak start time $t_1$ (ns) | Peak end time $t_2$ (ns) | $\Delta t = t_2 - t_1$ (ns) | Peak Voltage (mV) | FWHM (ns) |
|---|---|---|---|---|---|---|
| 1st Signal | 1st | 11 | 19 | 8 | 78 | 4 |
| | 2nd | 19 | 23 | 4 | 62 | 3 |
| | 3rd | 27 | 30 | 3 | 50 | 2 |
| | 4th | 33 | 44 | 11 | 316 | 7 |
| 2nd Signal | 1st | 16 | ____ | __ | 60 | 4 |
| | 2nd | _____ | 26 | _____ | 80 | 3 |
| | 3rd | 30 | 34 | 4 | 40 | 1 |
| | 4th | 37 | 47 | 10 | 29 | 9 |
| 3rd Signal | 1st | 16 | ____ | ____ | 4 | 80 |
| | 2nd | ____ | 30 | ____ | 2 | 78 |
| | 3rd | 32 | 36 | 4 | 2 | 40 |
| | 4th | 40 | 49 | 9 | 7 | 338 |

**Table 4.** Parameters for PIN Signals for Aluminium Target.

| Signals | Peak under observation | Peak start time $t_1$ (ns) | Peak end time $t_2$ (ns) | $\Delta t = t_2 - t_1$ (ns) | Peak Voltage (mV) | FWHM (ns) |
|---|---|---|---|---|---|---|
| 1st Signal | 1st | 21 | ____ | ____ | 80 | 4 |
| | 2nd | ____ | 34 | ____ | 80 | 3 |
| | 3rd | 36 | 41 | 5 | 60 | 2 |
| | 4th | 43 | 53 | 10 | 310 | 8 |
| 2nd Signal | 1st | 6 | ____ | ____ | 80 | 3 |
| | 2nd | ____ | 20 | ____ | 100 | 2 |
| | 3rd | 25 | 28 | 3 | 38 | 1 |
| | 4th | 32 | 43 | 11 | 322 | 6 |
| 3rd Signal | 1st | 4 | ____ | ____ | 98 | 4 |
| | 2nd | ____ | 16 | ____ | 78 | 4 |
| | 3rd | 17 | 22 | 5 | 77 | 2 |
| | 4th | 25 | 38 | 13 | 340 | 7 |

**Table 5.** Parameters for PIN Signal 1 for Copper Target.

| Signals | Peak under observation | Peak start time $t_1$ (ns) | Peak end time $t_2$ (ns) | $\Delta t = t_2 - t_1$ (ns) | Peak Voltage (mV) | FWHM (ns) |
|---|---|---|---|---|---|---|
| 1st Signal | 1st | 7 | 12 | 5 | 80 | 3 |
| | 2nd | 13 | 19 | 6 | 75 | 3 |
| | 3rd | 22 | 24 | 2 | 50 | 2 |
| | 4th | 29 | 39 | 10 | 320 | 7 |
| 2nd Signal | 1st | 4 | ____ | ____ | 65 | 4 |
| | 2nd | ____ | 16 | ____ | 70 | 3 |
| | 3rd | 18 | 22 | 4 | 60 | 2 |
| | 4th | 26 | 38 | 12 | 360 | 7 |
| 3rd Signal | 1st | 4 | ___ | ___ | 70 | 5 |
| | 2nd | ___ | 17 | ___ | 99 | 3 |
| | 3rd | 18 | 22 | 4 | 50 | 2 |
| | 4th | 27 | 38 | 11 | 342 | 7 |

## TIME-RESOLVED SOFT X-RAYS EMISSION

In order to find which material is a good source of soft X-ray we studied the time-resolved soft X-rays emission. These emissions were observed from properly biased Al masked PIN diode through a 250 MHz digital oscilloscope.

## TUNGSTEN

The starting time of Peak 1 in all 3 signals (Figures 4, 5 and 6) varied in obvious manner. However, the ending time of Peak 2 was almost the same, showing that the soft X-rays emission finished at the same moment in tungsten. The FWHM values were the same for Peak 1 in all three signals but a slight decrease was observed for FWHM for Peak 2 in Signal 1, compared to the other two signals. The voltage height was the same for the first two signals and there was an increase of 20 mV in the third signal. In summary, the time resolved variation in three signals from tungsten was observed to be small. Therefore, tungsten is not believed to be a good source of soft X-rays.

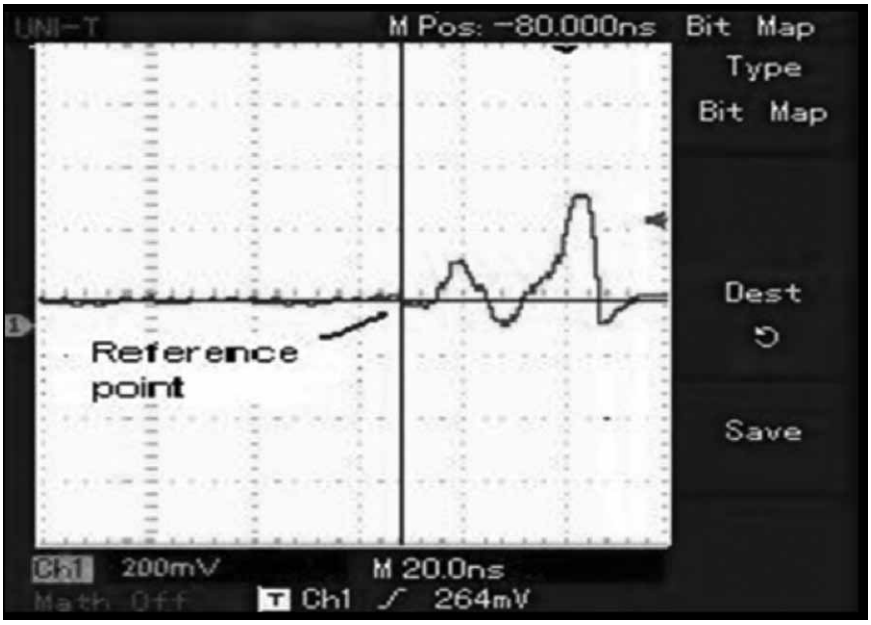


***Figure 4.*** *PIN Signal 1 observed for Tungsten Target.*

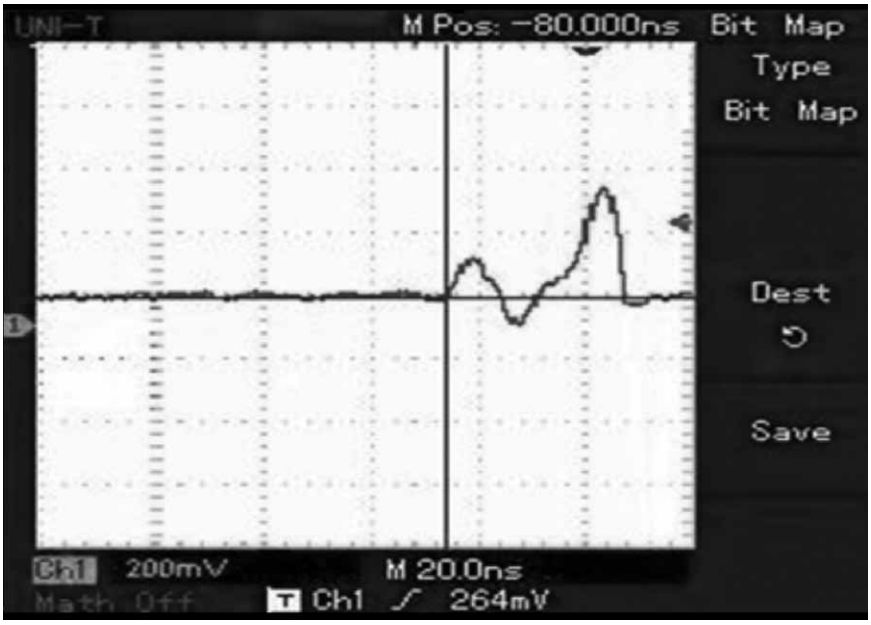


***Figure 5.*** *PIN Signal 2 observed for Tungsten Target.*

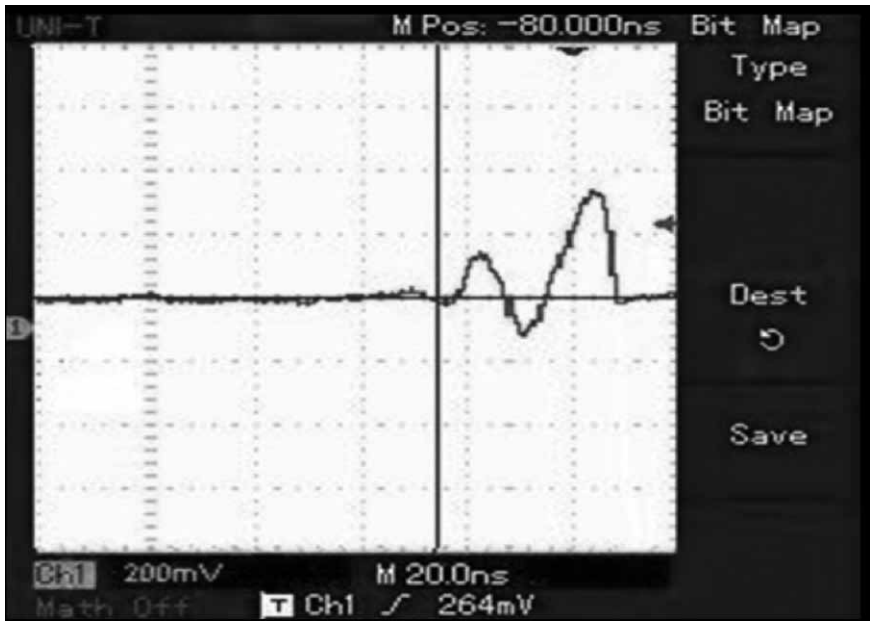


***Figure 6.*** *PIN Signal 3 observed for Tungsten Target.*

**SILVER**

The starting time of Peak 1 in all three signals was almost the same but Peak 4 ended at the same moment in the three signals. In signal 1, the first two peaks were distinct in nature, whereas the same peaks overlapped in Signal 2 and Signal 3 yet the combined time duration of these two peaks remained the same. After every shot, the behavior of voltage for all peaks was not the same. The FWHM was the same only for Peak 1 in all three signals. Time resolved variation for soft X-rays from silver is quite significant showing that it is a good source of soft X-rays.

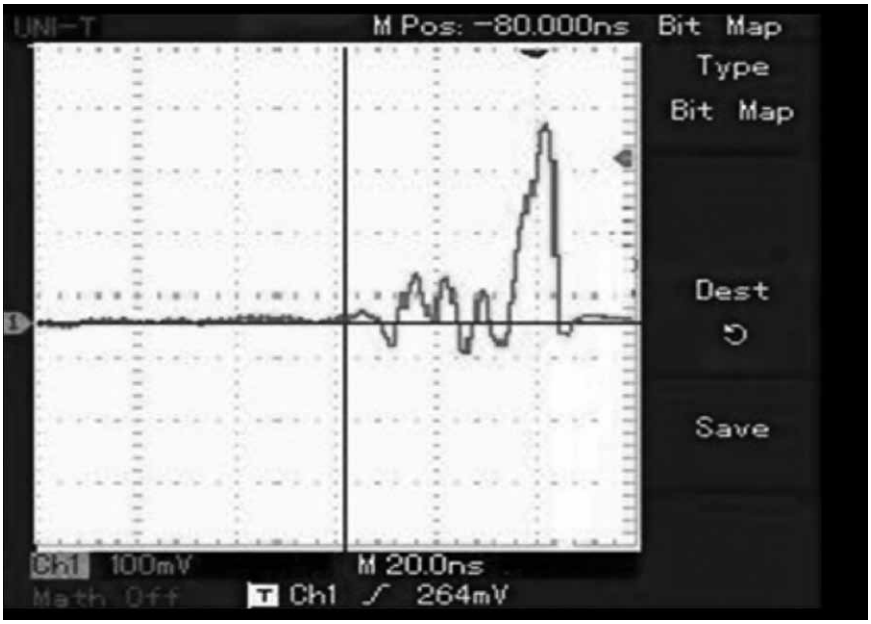


***Figure 7.*** *PIN Signal 1 observed for Silver Target.*

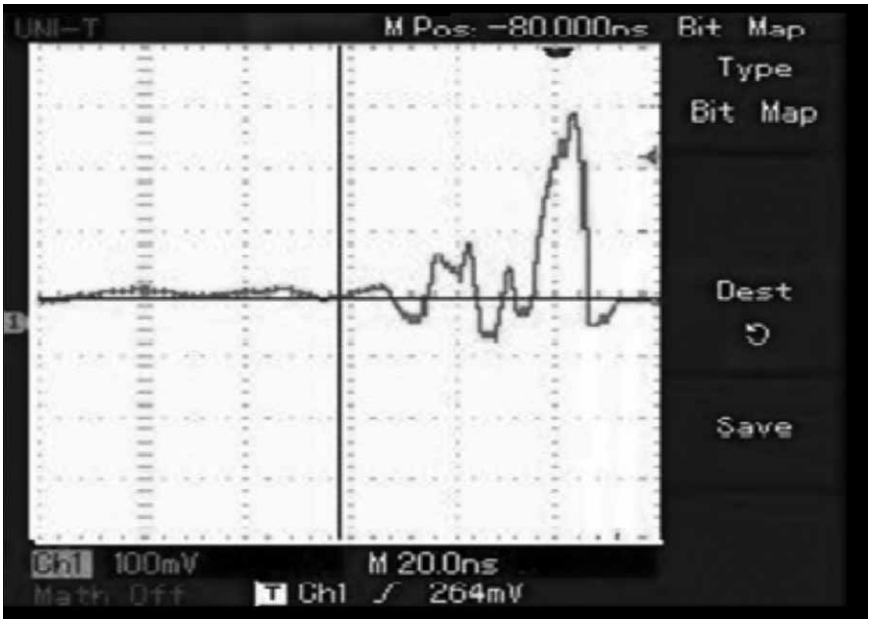


***Figure 8.*** *PIN Signal 2 observed for Silver Target.*

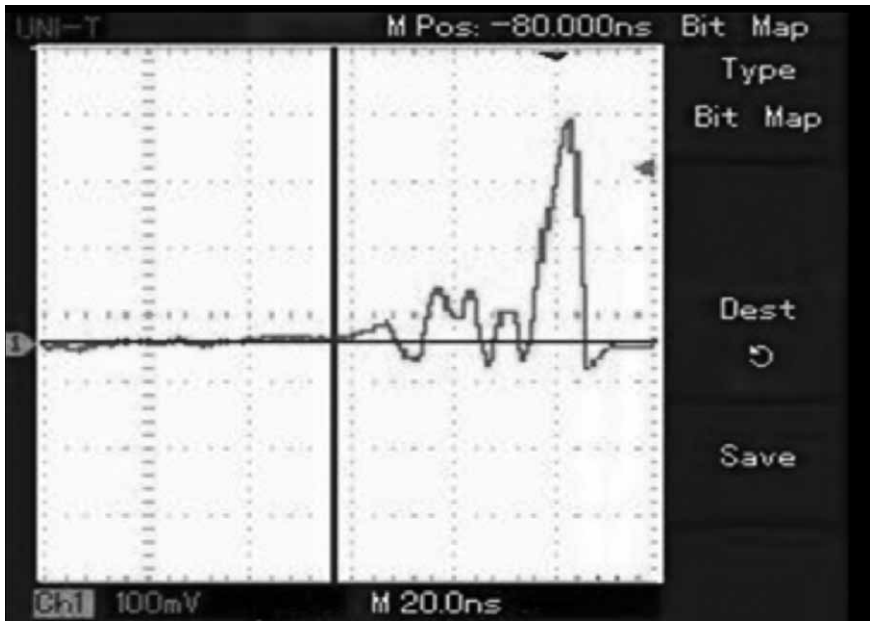


***Figure 9.*** *PIN Signal 3 observed for Silver Target.*

## ALUMINIUM

There was a significant variation in the starting time of Peak 1 and finishing time of Peak 4 in all three signals. However, the combined time duration remained almost the same in all signals. The overlapping of the first two peaks was observed in all signals. The maximum voltage of the first two peaks in Signal 1 was the same while it varied in other signals. The FWHM for all peaks in these signals had shown no significant correlation. The significant time-resolved variation showed that aluminium is also a good source of soft X-rays.

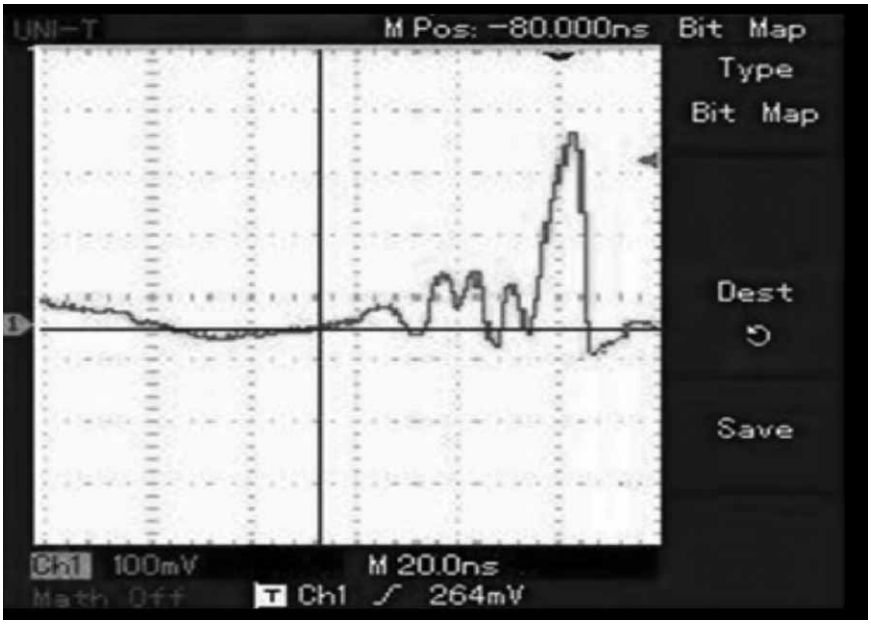


***Figure 10.*** *PIN Signal 1 observed for Aluminium Target.*

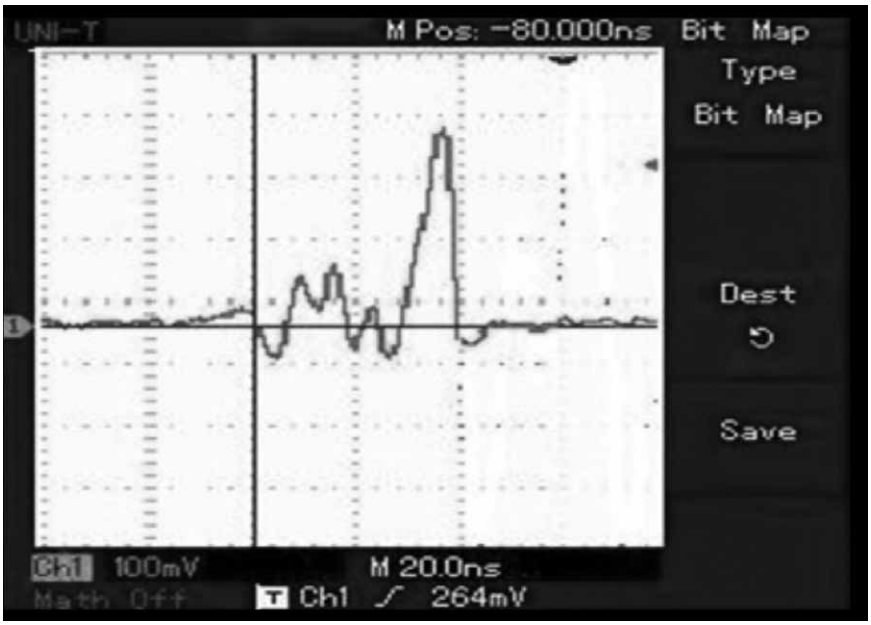


***Figure 11.*** *PIN Signal 2 observed for Aluminium Target.*

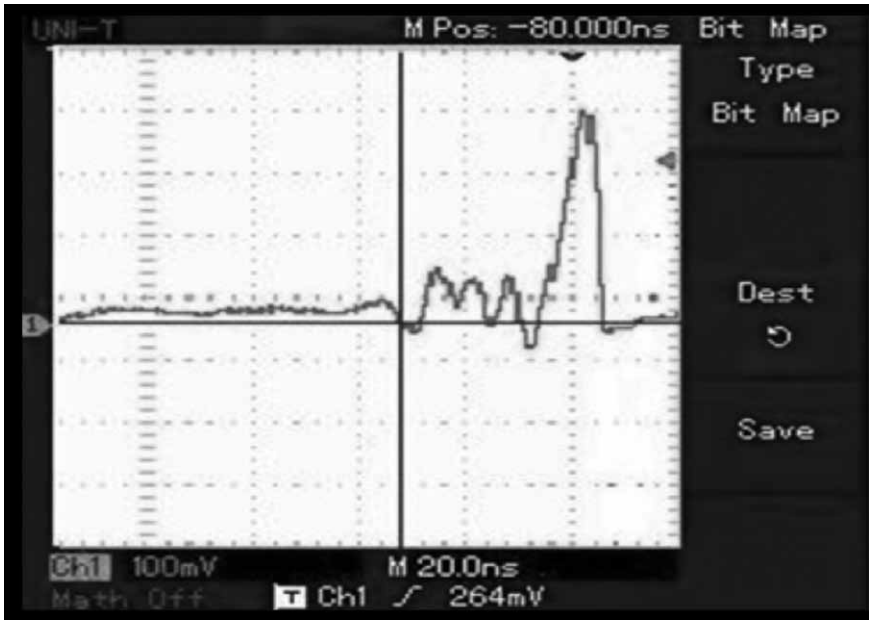


***Figure 12.*** *PIN Signal 3 observed for Aluminium Target.*

## COPPER

The starting time of Peak 1 and ending time of Peak 4 in Signal 1 was significantly different from those for other signals. In signal 1, first two peaks were distinct in nature, whereas the same peaks overlapped in Signal 2 and Signal 3 yet the combined time duration of these two peaks remained the same. The FWHM of all peaks was the same except for Peak 1. After every shot, the behavior of voltage for all peaks was not the same. Time resolved variation for soft X-rays from silver was quite significant, showing that it is a good source of soft X-rays.

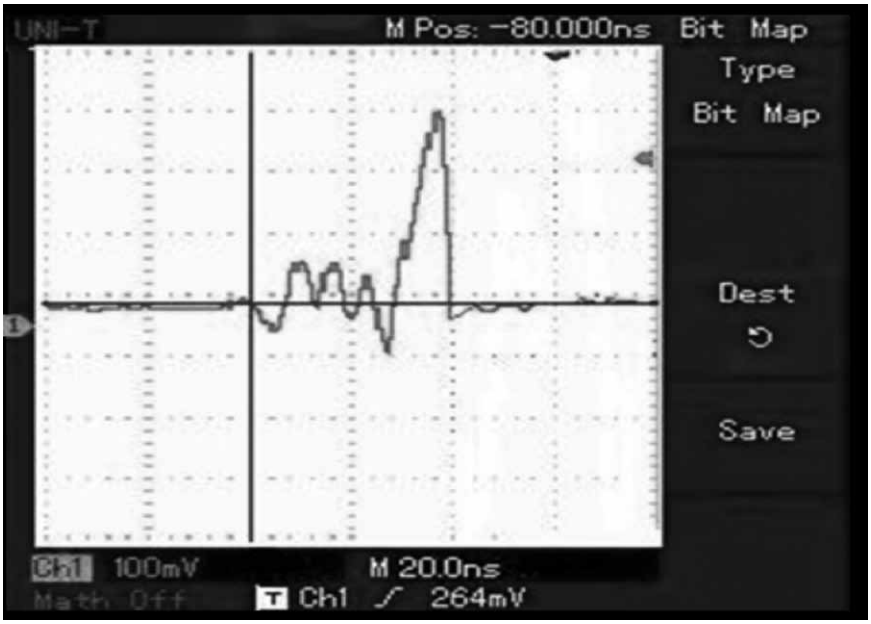


***Figure 13.*** *PIN Signal 1 observed for Copper Target.*

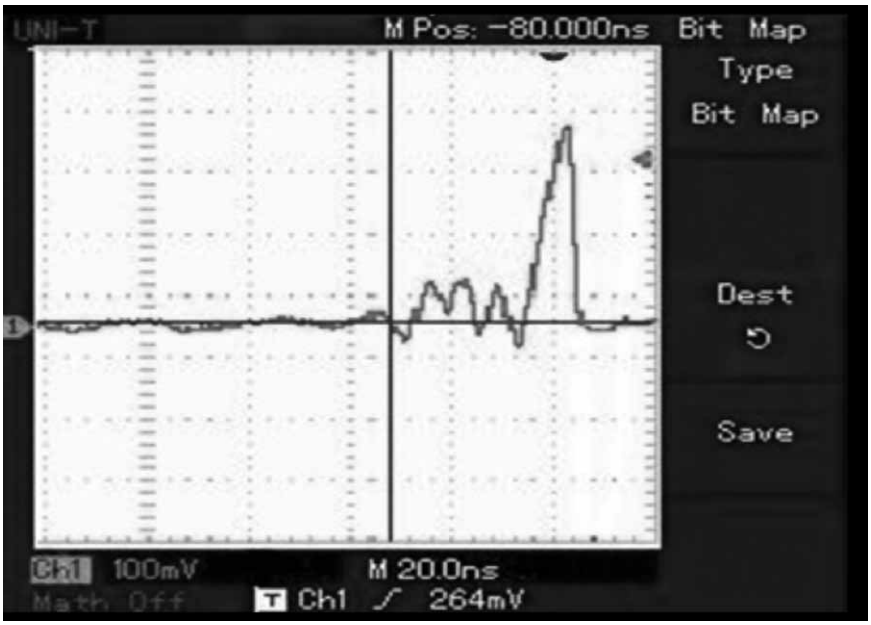


***Figure 14.*** *PIN Signal 2 observed for Copper Target.*

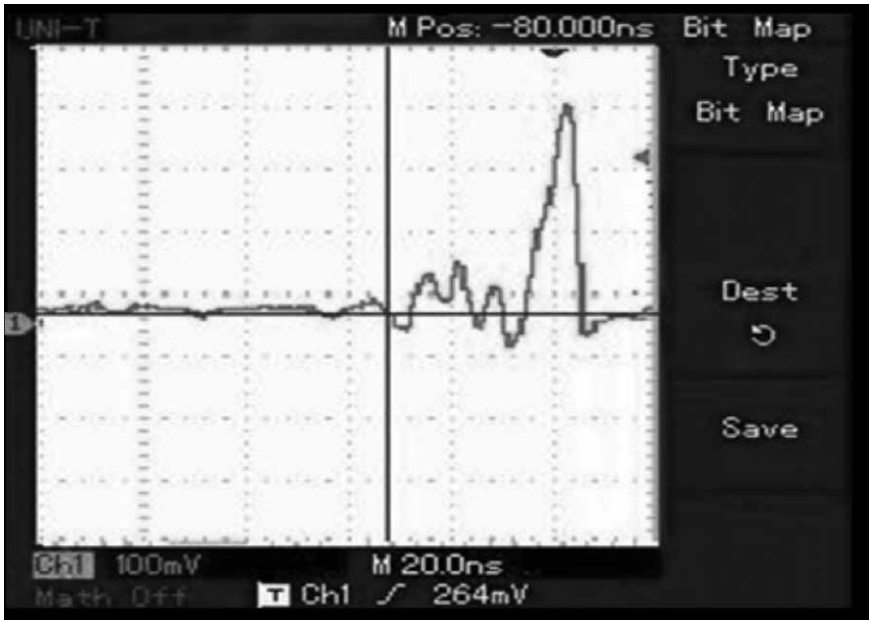


***Figure 15.*** *PIN Signal 3 observed for Copper Target.*

## CONCLUSION

The time resolved soft X-ray emission from Laser Produced Plasma of different materials had been studied successfully. The materials used were tungsten, silver, aluminium and copper. The Al masked PIN diode was used to detect soft X-rays emitted from the laser produced plasma of the target materials. The three soft X-ray signals for each metal had been observed. We observed that there was good time resolution for silver, aluminium and copper targets and poor time resolution for tungsten target. From the result obtained, it could be conclude that silver, aluminium and copper are the good sources of soft X-rays emission from Laser Produced Plasma, compared with tungsten. The results revealed that X-rays emission from the plasma depends strongly on the nature of atom. It also confirmed that tungsten is not suitable for producing soft X-rays from Laser Produced Plasma.

## REFERENCES:

Alaterre, P., Pépin H., Fabbro R., and Faral,B. (1986). Modeling of X-Ray Emission Created by Short Wavelength Laser Target Interaction. In: Laser Interaction and Related Plasma Phenomena, ed. Hora, H., Miley, G. H., Plenum Press, *New York*, pp 225-239.

Bushberg, J. T., Seibert, J. A., Leidholdt, E. M., and Boone, J.M. (2012). Interaction of Radiation with Matter In: the essential physics of medical imaging, ed. Mitchell, Lippincott Williams & Wilkins, USA, C. W., pp 33-59.

Carranza, J.E., and Hahn, D.W. (2002). Sampling statistics and considerations for single-shot analysis using laser-induced breakdown spectroscopy. *Spectrochimica Acta Part B.* **57**: pp 779–790.

Ditmire, T., Donnelly, T., Falcone, R. W., and Perry, M. D. (1995). Strong X-Ray Emission from High-Temperature Plasmas Produced by Intense Irradiation of Clusters. *Phys. Rev. Lett.* **75**: pp 3122.

Dutta, J., Bisoi, A., Pramanik, D., Ray, S., Saha, A., Tapader, S., and Sarkar, M. S. (2012). Characteristics of Si-PIN diode X Ray Detector with DSP electronics. In: Proceedings of the DAE Symp. on Nucl. Phys., India, **57**: pp 904- 905.

Giulietti, D., and Gizzi, L. A. (1998). X-ray emission from laser-produced plasmas. *La Rivista del Nuovo Cimento.* **21**: pp1.

Johnson, M. (2003). Photo Detection Basis: In Photodetection and Measurement: Maximizing Performance in Optical Systems, McGraw Hill Professional, *New York*, pp 1-18.

Kodama, R., Mochizuki, T., Tanaka, K. A., and Yamanaka, C. (1987). Enhancement of keV X-ray emission in laser produced plasmas by a weak prepulse laser. *Applied Physics Letter*. **50**: pp 720-722.

Kompitsas, M., Roubani-Kalantzopoulou, F., Bassiotis, I., Diamantopoulou, A., and Giannoudakos, A. (2000). Laser induced plasma spectroscopy (lips) as an efficient method for elemental analysis of environmental samples. In: Proceedings of EARSeL-SIG-Workshop LIDAR, Dresden, pp 130-138.

Liu, Y., Dong, Q., Peng, X., Jin, Z., and Zhang, J. (2009). Soft X-ray emission, angular distribution of hot electrons, and absorption studies of argon clusters in intense laser pulses.

McPherson, A., Luk, T. S., Thompson, B. D., Borisov, A. B., Shiryaev, O. B., Chen, X., Boyer, K., and Rhodes, C. K. (1994). Multiphoton induced X-ray emission from Kr clusters on M-shell (~100 Å) and L-shell (~6 Å) transitions. *Phys. Rev. Lett.* **72**: pp 1810-1813.

Parra, E., Alexeev, I., Fan, J., Kim, K. Y., McNaught, S. J., and Milchberg, H. M. (2000). X-ray and extreme ultraviolet emission induced by variable pulse-width irradiation of Ar and Kr clusters and droplets. *Phys. Rev.* **E 62**: pp R5931-R5934.

Patran, A. (2002). Electron and medium energy X-ray emission from a dense plasma focus. Ph.D thesis, National Institute of Education, Singapore.

Spencer, J. B., Alman, D. A., Ruzic, D. N., and Jurczyk, B. E. (2005). Dynamics of a laser produced plasma for soft X-ray production. In: Proceedings of SPIE The international society for optical engineering, USA, **5751**: pp 798-807.

Sprawls, P. (1993). Radiation penetration: In the physical principles of medical imaging 2nd ed. Aspen publishers, Gaithersburg, Md, pp 165-167.

*O. Bapokutty[1], Z. Sajuri[2] and J. Syarif[2]*

*[1] Department of Structure and Material, Faculty of Mechanical Engineering, Universiti Teknikal Malaysia Melaka, Hang Tuah Jaya, 76100 Durian Tunggal, Melaka, Malaysia.*

*[2] Department of Mechanical and Materials Engineering, Faculty of Engineering and Built Environment, Universiti Kebangsaan Malaysia, 43600, UKM Bangi, Selangor, Malaysia.*

***(omarbapokutty@utem.edu.my)***

## STRESS RELAXATION BEHAVIOUR AND MECHANISM OF HEAT TREATED INCONEL 718 IN HIGH TEMPERATURE ENVIRONMENTS

***RINGKASAN:*** *Kelakuan tegasan santaian bagi superaloi berasaskan nikel iaitu Inkonel 718 terawat haba telah dibuat kajian pada suhu tinggi. Rawatan larutan telah diperkenalkan kepada bahan diterima pada suhu 980 °C selama 1 jam sebelum dikenakan lindap-kejut dengan air, seterusnya bahan tersebut melalui proses penuaan berganda pada suhu 720 °C selama 8 jam dan pada suhu 621 °C selama 8 jam dan disejukkan dalam udara pada suhu bilik. Ujian tegasan santaian telah dilakukan dengan terikan 1 % pada suhu yang berbeza iaitu 550 °C, 650 °C dan 750 °C. Ujian dijalankan selama 72 jam. Ujian dihentikan pada 3 jam dan 48 jam bagi mengkaji evolusi mikrostruktur dan perubahan dalam sifat-sifat bahan melalui penggunaan Mikroskop Imbasan Elektron dan Pembiasaan Sinar-X. Keputusan menunjukkan tegasan bertambah tinggi dengan penurunan suhu. Sebaliknya, kadar tegasan santaian bertambah dengan pertambahan suhu. Pemerhatian mikrostruktur menunjukkan proses pemulihan berlaku. Ianya disokong oleh pengurangan ketumpatan kehelaan dengan pertambahan masa dan suhu, yang mana dipersetujui dengan keputusan kekuatan-mikro Vickers.*

**ABSTRACT:** The stress relaxation behaviour of heat treated nickel-base superalloy Inconel 718 at high temperature was investigated. Solution treatment was applied on the as-received material at 980 °C for 1 hour before water quenching followed by double aging treatments at 720 °C for 8 hours and 621 °C for 8 hours, then cooled in air. The stress relaxation test was conducted at 1 % strain at different test temperatures of 550 °C, 650 °C and 750 °C. The tests were carried out for a total of 72 hours. The tests were interrupted at 3 hours and 48 hours to investigate the evolution of microstructure and changes in material properties by using Scanning Electron Microscope (SEM) and X-Ray Diffractometer (XRD). The results showed that thermal dependent stress increased with decreasing temperature. In contrast, stress relaxation rate increased with increasing temperature. Microstructure observation by SEM showed that recovery process occurred. This was further

supported by the decrease in dislocation density with increase in time and temperature, which is in-line with the Vickers micro-hardness results.

Keywords: Heat treatment, stress relaxation, recovery, microstructure, Inconel 718

## INTRODUCTION

Inconel 718 is a nickel-based superalloy extensively used in fabrication of critical components for turbine because of its excellent mechanical properties at elevated temperatures and good corrosion resistance. Application of this alloy range from disc alloy in gas turbine engines to components used in nuclear and cryogenic structures, high-strength bolts and fasteners, and components in space craft, owing to its excellent fabricability and weldability (Kim *et al.*, 2008). In the turbine disc application, standard processing, high strength processing and direct age processing have been applied in order to achieve the desired properties (Nowotnik *et al*., 2008). Gas turbine blades are commonly made of Inconel 738LC alloy (Mazur *et al.*, 2005). Blade-disc fixing in turbine engine is highly loaded connections that allow only micrometer size relative movement between blade and disc. Initially, stresses were intentionally introduced at a desired level to hold the blade firmly. However, at high temperature environment, relaxation of such stresses can result in loss of tension in fitting and cause undesirable vibration (Pan and Xiong, 2010). Therefore, the aims of this study are to investigate the stress relaxation behaviour and mechanism of heat treated Inconel 718 in high temperature environments.

## MATERIALS AND METHODS

The material used in this study was nickel-based superalloy Inconel 718. The chemical composition of the material used is as follows: Ni 55.83 %, C 0.033 %, Fe 15.51 %, Cr 17.58 %, Cu 0.0293 %, Mo 3.522 %, Co 0.238 %, Mn 0.005 %, Al 1.032 %, Nb 5.189 %, Ti 1.103 % and Si 0.08 %. The geometry of the specimens used is presented in Figure 1 with a thickness of 3 mm. To increase the strength of Inconel 718 after sample preparation by Electrical Discharge Machining (EDM), standard heat treatment process was introduced to the samples (Ghosh et *al.*, 2008; Liu *et al.*, 2005; Kuo *et al.*, 2009; Xiao *et al.*, 2008). Samples were annealed at 980°C for 1 hour before quenching in water. Samples then underwent double aging treatment process at 720 °C for 8 hours and 621 °C for 8 hours. Finally, the samples were cooled in air to room temperature.

Stress relaxation tests were conducted at three different test temperatures of 550 °C, 650 °C and 750 °C with the same strain level of 1 %. The tests were carried

out for 3, 48 and 72 hours. Prior to the stress relaxation tests, tensile properties of heat treated Inconel 718 at elevated temperatures of 550 °C, 650 °C and 750 °C were identified.

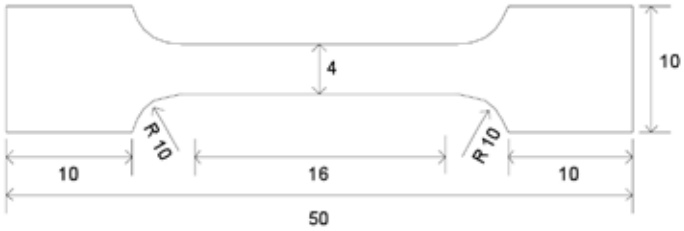


***Figure 1.*** *Test specimen dimension (in mm).*

Metallographic sections were prepared using standard mechanical polishing procedure. Samples were then etched using Kalling Reagent No. 2 and studied by means of Scanning Electron Microscopy (SEM). The micro-hardness of specimens was investigated using Vickers micro-hardness tester by using a 20 gram force (Hv0.020) to all samples that underwent relaxation tests. The dislocation density of specimens was evaluated by XRD to provide the evidence of recovery. The dislocation density $\rho$ is thus defined as:

$$\rho = (1.44 \times \varepsilon^2) / b^2$$

where b is the Burgers vector (0.25 nm) and $\varepsilon$ is strain broadening (Syarif *et al.*, 2007).

## RESULTS AND DISCUSSION

Figure 2(a) and Figure 2(b) show the stress-strain and stress-time (stress relaxation) curves of the heat treated Inconel 718 at different temperature levels, respectively. From Figure 2(a), the tensile properties at different temperatures are summarised in Table 1. Figure 2(b) showed that the thermal dependent stresses required to obtain 1 % strain were 1050, 1000 and 583 MPa at temperatures of 550 °C, 650 °C and 750 °C, respectively. These values were lower compared to the ultimate tensile strength. Figure 2(b) shows two distinguishable regions of stress relaxation rate; the accelerated region from the beginning up to 15 hours followed by the steadily and constantly reduced stress relaxation rate until the tests end. The slope of constantly reduced stress relaxation or calculated mean stress relaxation rates were 1.0531, 1.0713 and 1.6923 MPa/hour for 550 °C, 650 °C and 750 °C test conditions, respectively. After 72 hours, the measured internal stresses were 730, 443 and 69 MPa for 550 °C, 650 °C and 750 °C test conditions, respectively. These results are summarised in Table 2. These values were much lower compared to the

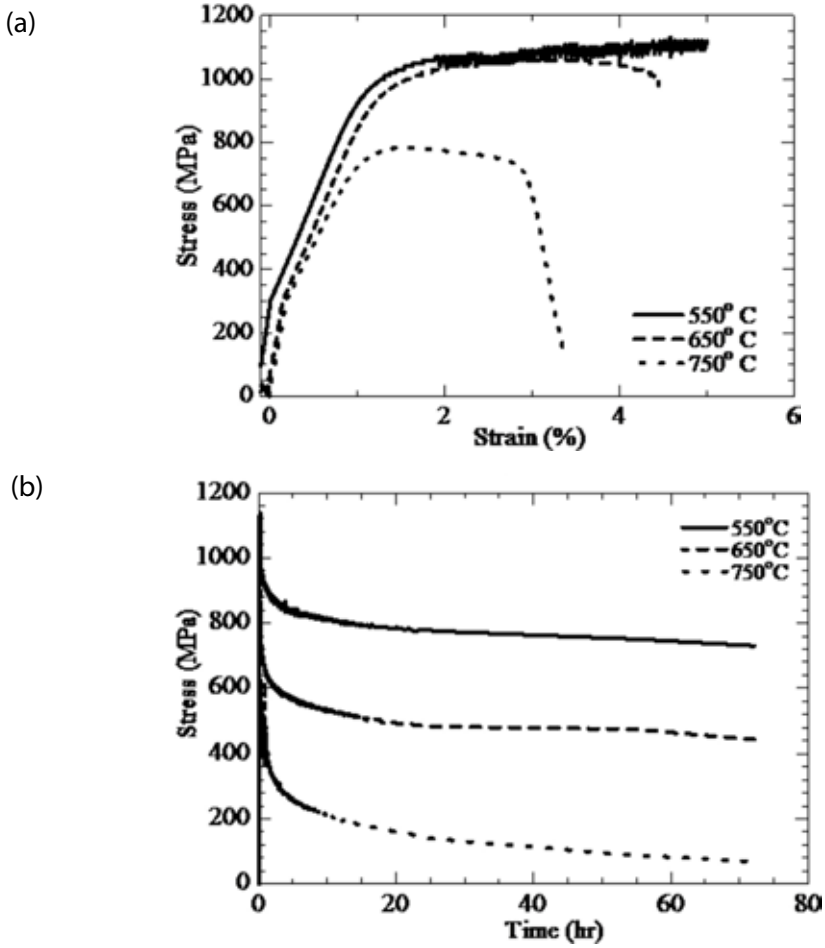


***Figure 2.*** *(a) Stress-strain and (b) stress relaxation curves.*

yield stress under the same temperature conditions. It was found that the stress drop (the difference between internal and thermal dependent stresses) increased with increasing temperature.

The SEM micrographs for heat treated Inconel 718 tested at different temperatures are shown in Figure 3. After 3 hours of stress relaxation test, the grain boundaries were still intact and can be clearly seen with very little deformation at grain boundary. As shown in Figure 2(b), accelerated phase occurs at the beginning of the test. After prolonging the test beyond 20 hours, the creep-controlled mechanism started to dominate the behaviour where recovery process started to occur until the end of the stress relaxation test. These mechanisms of recovery are shown at 48 hours in the micrograph in Figure 3 where rearrangement of microstructure and grain boundary occur which give impact of blurring in micrograph. At 72 hours, where tests ended, grain boundaries are visible and clearly seen especially at lower temperature.

**Table 1.** Mechanical properties of Inconel 718 at various temperatures.

| Temperature | $\sigma_{0.2}$ | $\sigma_{uts}$ | Elongation |
|---|---|---|---|
| (°C) | (MPa) | (MPa) | ε (%) |
| 550 | 999 | 1140 | 5.1 |
| 650 | 970 | 1060 | 4.4 |
| 750 | 767 | 783 | 3.5 |

**Table 2.** Thermal dependent, internal and calculated mean stresses relaxation rate

| Temperature (°C) | Thermal dependent (MPa) | Internal (MPa) | Stress drop (MPa) | Stress relaxation rate (MPa/hr) |
|---|---|---|---|---|
| | | | | |
| 550 | 1050 | 730 | 320 | 1.0531 |
| 650 | 1000 | 443 | 557 | 1.0713 |
| 750 | 583 | 69 | 514 | 1.6923 |

The average values of Vickers micro-hardness decreased with increasing relaxation time as shown in Figure 4 (a). This was believed to be due to the recovery at grain boundary. It was also observed that increase in temperature will further reduce the hardness. This phenomenon occurs because of rearrangement of microstructure and grain boundary which affects the hardness of the material. Higher temperature gives higher energy to the recovery process with more rearrangement of microstructure and grain boundary and reduced hardness of the materials. The hardness results are summarised in Table 3.

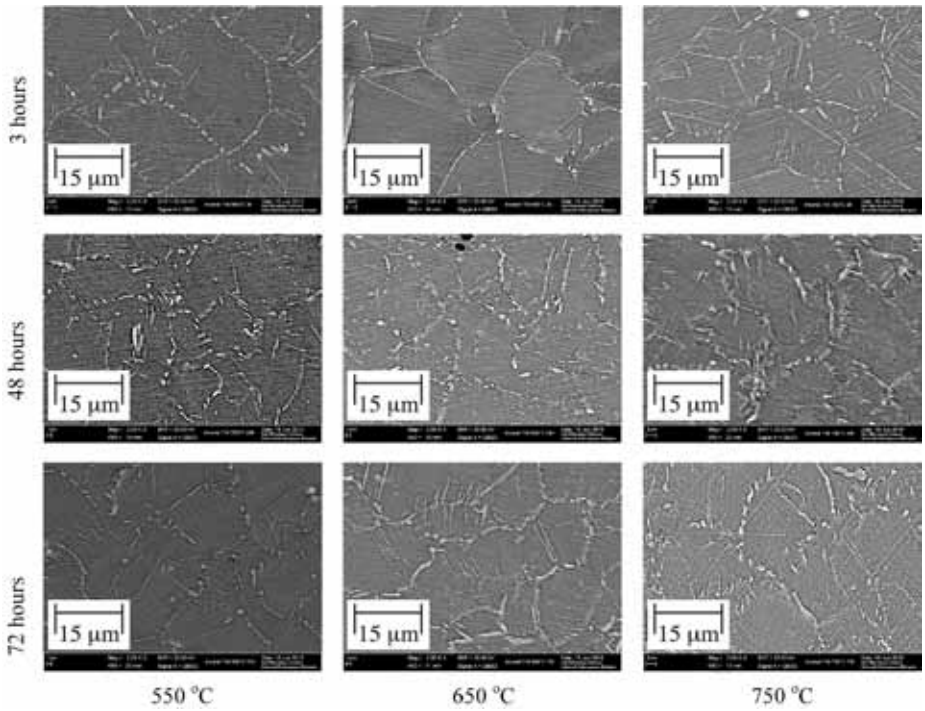


***Figure 3.*** *SEM micrographs after relaxation test for 3, 48 and 72 hours.*

Figure 4 (b) shows the decrease of dislocation density with increasing relaxation time and further decrease by increasing temperature. Detail results are summarised in Table 4. From Figure 4 (b), the recovery rate for each temperature condition was calculated and tabulated in Table 5. It was found that lower dislocation density gives lower Vickers micro-hardness and vice versa due to recovery process.

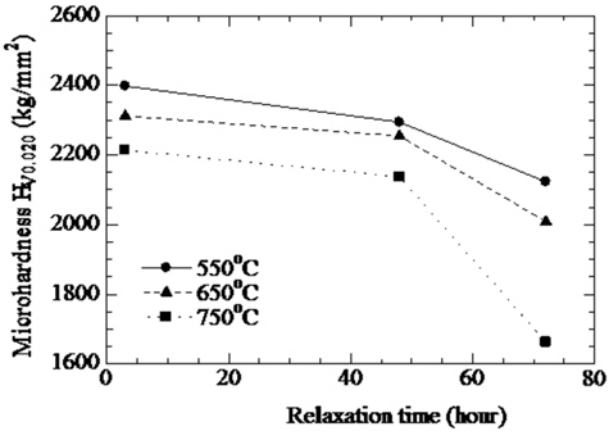


(a)

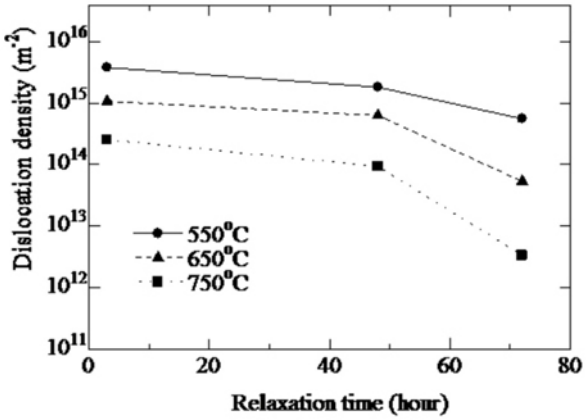


(b)

***Figure 4.*** *(a) Micro-hardness vs time and (b) dislocation density vs time.*

**Table 3.** Vickers micro-hardness at elevated temperature.

| Time(hour) | Temperature(°C) | | |
|---|---|---|---|
| | 550 | 650 | 750 |
| 3 | 2398 | 2294 | 2123 |
| 48 | 2311 | 2254 | 2008 |
| 72 | 2213 | 2137 | 1662 |

**Table 4.** Dislocation density.

| Time(hour) | Temperature(°C) | | |
|---|---|---|---|
| | 550 | 650 | 750 |
| 3 | 3.78E+15 | 1.07E+15 | 2.54E+14 |
| 48 | 1.81E+15 | 6.27E+14 | 9.73E+13 |
| 72 | 5.54E+14 | 5.31E+13 | 3.35E+12 |

**Table 5.** Recovery rate.

| Recovery rate (m-2/hr) | Time(hour) | Temperature(°C) | | |
|---|---|---|---|---|
| | | 550 | 650 | 750 |
| | Mar-48 | 4.38E+13 | 9.84E+12 | 3.56E+12 |
| | 48-72 | 5.23E+13 | 2.39E+13 | 3.77E+12 |

## CONCLUSION

In this study, stress relaxation behaviour of Inconel 718 has been studied at different temperatures. The difference in temperatures gives impact on stress relaxation rate, difference between internal and thermal dependent stresses, dislocation density and Vickers micro-hardness. Increasing the temperature will increase the stress relaxation rate of Inconel 718 at 1 % strain. Increasing temperature will also increase the differences between the internal and thermal dependent stresses. The dislocation density and Vickers micro-hardness decreased (evidence of recovery) with increasing relaxation time and further decreased by increasing temperatures.

## REFERENCES

Ghosh, S., Yadav, S. and Das. G. (2008). Study of standard heat treatment on mechanical properties of Inconel 718 using ball indentation technique. Materials Letters. **62(17-18)**: pp 2619-2622.

Kim, D-H., Kim, J-H., Sa, J-W., Lee, Y-S., Park, C-K. and Moon, S-Il. (2008). Stress rupture characteristics of Inconel 718 alloy for ramjet combustor. Materials Science and Engineering. **A 483–484**: pp 262–265.

Kuo, C.M., Yang, Y.T., Bor, H.Y., Wei, C.N. and Tai, C.C. (2009). Aging effects on the microstructure and creep behaviour of Inconel 718 superalloy. J. Materials Science and Engineering. **A 510-511**: pp 289-294.

Liu, L., Zhai, C., Lu, C., Ding, W., Hirose, A. and Kobayashi, K. F. (2005). Study of the effect of δ phase on hydrogen embrittlement of Inconel 718 by notch tests. Corrosion science. **47**: pp 355-367.

Mazur, Z., Luna-Ramirez, A., Juarez-Islas, J.A. and Campos-Amezcua, A. (2005). Failure analysis of a gas turbine blade made of Inconel 738LC alloy. Engineering Failure Analysis. **12**: pp 474–486.

Nowotnik, A., Sieniawski, J. and Mrowka-Nowotnik, G. (2008). Identification of dynamically precipitated phase in hot-working Inconel 718 alloy. J. of Achievements in Materials and Manufacturing Engineering. **31(2)**: pp 275-280.

Pan, Y. and Xiong, D. (2010). Stress relaxation behaviour of nano-hydroxyapatite reinforced poly(vinyl alcohol) gel composites as biomaterial. J. Mater. Sci.. Volume **45(20)**: pp 5495-5501.

Syarif, J., Nakashima, K., Tsuchiyama, T. and Takaki, S. (2007). Effect of solute copper on yield strength in dislocation-strengthened steels. The Iron and Steel Institute of Japan International. Vol. **47(2)**: pp 340-345.

Xiao, L., Chen, D.L. and Chaturvedi, M.C. (2008). Cyclic deformation mechanisms of precipitation-hardened Inconel 718 superalloy. Materials Science and Engineering. **A 483-484**: pp 369-372.

*M. Z. M. Zamzuri[1], N. F. W. M. Sidik[1], M. N. B. Derman[2], S. Norbahiyah[1] and M. Mat Salleh[1]*

*[1] Institute of Nano Electronic Engineering, Universiti Malaysia Perlis, 01000 Perlis, Malaysia*

*[2] School of Manufacturing Engineering, Universiti Malaysia Perlis, 02600 Perlis, Malaysia*

***(mzamzuri@unimap.edu.my)***

# IMPROVEMENT OF CORROSION RESISTANCE OF AZ91D MAGNESIUM ALLOY BY LANTHANUM-BASED CONVERSION COATING

***RINGKASAN:*** *Salut tukaran kimia dengan larutan garam logam nadir bumi dianggap sebagai satu alternatif kepada salut tukaran kromat untuk memperbaiki rintangan karatan aloi-aloi magnesium. Dalam kajian ini, salut tukaran dengan lanthanum dibentuk ke atas aloi magnesium AZ91D telah dicirikan dan kesan perawatan masa dibincangkan. Imej-imej "Scanning Electron Microscope" (SEM) menunjukkan spesimen yang dirawat dengan larutan lanthanum nitrat dan magnesium nitrat selama 30 minit telah membentuk satu lapisan oksida keseluruh permukaan aloi magnesium tersebut. Analisis EDS telah membuktikan bahawa lapisan tersebut terutamanya terdiri daripada unsur oksigen dan lanthanum. Ujian karatan menunjukkan salut tukaran dengan lanthanum mempunyai rintangan karatan yang lebih baik berbanding spesimen tanpa rawatan pada semua keadaan rawatan.*

**ABSTRACT:** Chemical conversion coating by rare earth metal salt solution was considered as an alternative to chromate conversion coating in order to improve the corrosion resistance of magnesium alloys. In this study, lanthanum-based conversion coatings formed on AZ91D magnesium alloy were characterized, and the effect of treatment period was discussed. SEM images showed that specimen treated with solution containing lanthanum nitrate and magnesium nitrate for 30 min has formed an oxide layer on the entire surface of magnesium alloy. EDS analysis has confirmed that the layer was mainly consisted of oxygen and lanthanum elements. Corrosion test indicated that lanthanum-based conversion coating has a better corrosion resistance than as-received specimen at all treatment conditions.

Keywords: Corrosion protection, magnesium alloy, conversion coating, rare earth element (REE)

## INTRODUCTION

Magnesium is widely distributed in the earth; it is the eighth elements in order of both terrestrial and cosmic abundance (Emley, 1966). Magnesium alloy has been used widely in electronics, electrical devices and automotive industries because of its superior properties such as low density, outstanding strength to weight ratio, excellent dimensional stability, and good machinability (Song *et al.*, 1999). However, their corrosion protections are limited because of their high chemical reactivity. Therefore it is necessary to do surface treatment properly onto the surface of the magnesium alloy to improve the corrosion resistance (Gray *et al.*, 2002).

Many surface treatment techniques have been proposed and mainly treatments include conversion coating, electro-plating/electroless and anodic coating (Yamamoto *et al.*, 2001). Conversion coatings are produced by chemical or electrochemical treatment of a metal surface to produce a superficial layer of substrate metal oxides, chromates, phosphates, or other compounds that are chemically bonded to the surface (Lowenheim, 1974). Different types of conversion coating include chromate, phosphate/permanganate and fluorozirconate treatments (Gray *et al.*, 2002). Conversion coating is one of the most cost effective and simplest processes for introducing a metallic coating to a magnesium substrate (Delong *et al.*, 1984).

Chemical conversion treatment is an easy method to grow a good corrosion resistance film on the surface of the magnesium alloy. Such film can also improve the adhesion ability between the coating and the substrate which makes it easy for the next process. The most widely used is chromate solution, DOW7, which is produced by Dow Chemical Company in Japan. The film has excellent corrosion resistance and adhesion ability (Ono *et al.*, 2001). However the disadvantage of this treatment process is the environment pollution due to the waste water containing hexavalent chromate ($Cr_6^+$) and the health-related concerns with people (Umehara *et al.*, 2001). Now, the great need is to develop new chrome-free chemical treatment methods to replace the current method. The phosphate, phosphate/permanganate (Kim *et al.*, 2004), and stannate-based (Gonzalez-Nunez *et al.*, 1999) processes are investigated. Some researchers reported that the corrosion resistance of magnesium was improved by the formation of a surface oxide film containing rare earth elements (REE) (Brunelli *et al.*, 2005).

In this paper, we produced an oxide film containing La on AZ91D magnesium alloy by conversion coating in nitrate solution, whereby the effect on the corrosion resistance against salt water was investigated. The influence of coating time period is also discussed.

## MATERIALS AND METHODS

The commercial AZ91D magnesium alloy was employed as specimen. Its chemical composition is given in Table 1. The specimens were embedded in resin form except for one surface (about 10 $mm^2$) in order to control the active area. The sample's surface without resin was polished with emery papers of grit #1000 to ensure that the same surface roughness is obtained for different tested specimens.

All conversion coating experiments were performed in solution containing 0.1 mM $La(NO_3)_3$, 0.1mM $Mg(NO_3)_2$ and 0.1 mM $La(NO_3)_3$ + 0.1mM $Mg(NO_3)_2$. The specimen was immersed at room temperature with different period of time treatment ranging from 10 - 60 min. After the treatment process, the specimens were thoroughly rinsed with distilled water and then air dried for 24 hours at 343 K in order to get them denitrated.

The anti-corrosive properties of the anodic films were examined against salt water. The corrosion rate of the specimen was measured in accordance with JIS H 0541(Japanese Standards Association, 2003). The specimen was immersed for 72 hours in NaCl solution of 0.5 $dm^3$. The NaCl concentration was 50g/$dm^3$, and the pH was adjusted at 10 - 11 by $Mg(OH)_2$. The specimen was rinsed with distilled water, where the corrosion product formed on the surface was removed with a plastic brush. The weight of specimen was measured, whereby the corrosion rate, R (mm/year) was calculated using the following equation;

$$R = \frac{8.76 \times 10^4 W}{ADt} \qquad (1)$$

Where W, A, D and t are weight change (g), active area ($cm^2$), density (g/$cm^3$) and immersion time (h), respectively.

The microstructure and surface morphology of the specimen was observed by Optical Microscope (OM) and Scanning Electron Microscope (SEM), coupled with Energy Dispersive Spectroscopy (EDS).

**Table 1.** Chemical analysis of AZ91D (wt. %).

| Alloy | Al | Mn | Zn | Si | Cu | Ni | Fe | Other | Mg |
|---|---|---|---|---|---|---|---|---|---|
| AZ91D | 8.5 - 9.5 | 0.17 - 0.4 | 0.45 - 0.9 | <0.05 | <0.008 | <0.001 | <0.004 | <0.001 | Bal. |

## RESULTS AND DISCUSSION

### Surface analysis

A thin coating layer was formed on the specimen by the conversion coating. Figure 1 shows the surface morphologies of the (a) untreated specimen and (b) specimen immersed in 0.1mM $La(NO_3)_3$ + Mg $(NO_3)_2$ solutions for 30 min. The lanthanum and magnesium treated specimens have shown a network resembling a micro-cracked surface coating. These cracks may be attributed to hydrogen being released through a chemical reaction process during the coating formation period. The tendency for the self-healing action increases with increasing lanthanum ion concentration. This could be explained by the increase of the coating thickness as shown in Figure 1(b). Mg, O and La elements were detected by EDS, both on the crevices and the oxide film as shown in Table 2(a). On the other hand, the polishing flaw could also be seen on the surface of the untreated specimen as shown in Figure 1(a); however O and La elements were not detected for the untreated specimen as shown in Table 2(b).

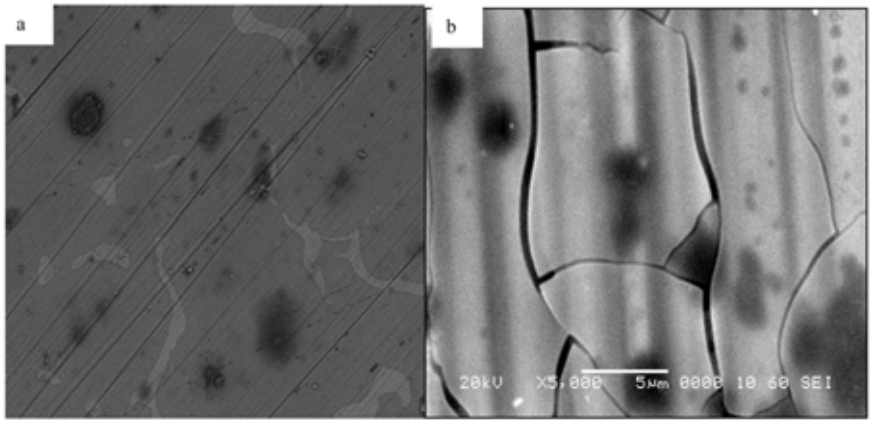


***Figure 1:*** *SEM images of (a) untreated and (b) specimen treated with $La(NO_3)_3$+$Mg(NO_3)_2$ electrolytes for 30 min.*

**Table 2.** EDS analysis of a) untreated and b) specimen treated with $La(NO_3)_3$+$Mg(NO_3)_2$ solution for 30 min

(a)

| Composition | O | Mg | Al | La |
|---|---|---|---|---|
| Mass (%) | 0 | 74.97 | 25.03 | 0 |

(b)

| Composition | O | Mg | Al | La |
|---|---|---|---|---|
| Mass (%) | 38.42 | 35.93 | 16.47 | 0.71 |

## Corrosion Behavior

The corrosion rate of the specimen with conversion coating by immersion in the $La(NO_3)_3$ solutions at different immersion time period is shown in Figure 2. The untreated specimen has shown the highest corrosion rate of 13 mm/year, compared to the corrosion rate of conversion coated specimen. The result indicated that the conversion coating formed on the surface of AZ91D alloy provides the best corrosion resistance when immersed in $La(NO_3)_3$ solution for 50 min.

Figure 3 shows the corrosion rates of specimen with conversion coating by immersion in $Mg(NO_3)_2$ solutions at different immersion time periods. It can be seen that the corrosion rate of the specimens treated with $Mg(NO_3)_2$ solution have given a good corrosion resistivity compared to the specimen without coating; whilst the specimen which was immersed in $Mg(NO_3)_2$ solutions for 40 min has shown slightly better corrosion resistance than others. It was reported that the corrosion resistance of magnesium metal was considerably better by these treatments (Brunelli et al., 2005), but only few works are reported for magnesium alloys in this study. Since the corrosion resistance of magnesium alloys are much better than magnesium metal, the conversion coating by immersion in electrolyte including either $La(NO_3)_3$ or $Mg(NO_3)_2$ is not good enough for the improvement of the corrosion resistance of magnesium alloy.

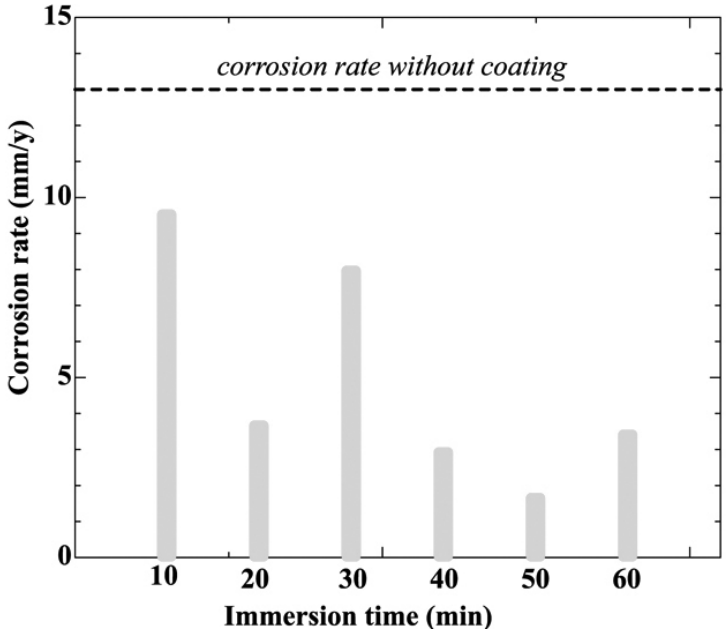


***Figure 2.*** *Corrosion rate of specimen with conversion coating by immersion in La $(NO_3)_3$ electrolyte at different immersion time period.*

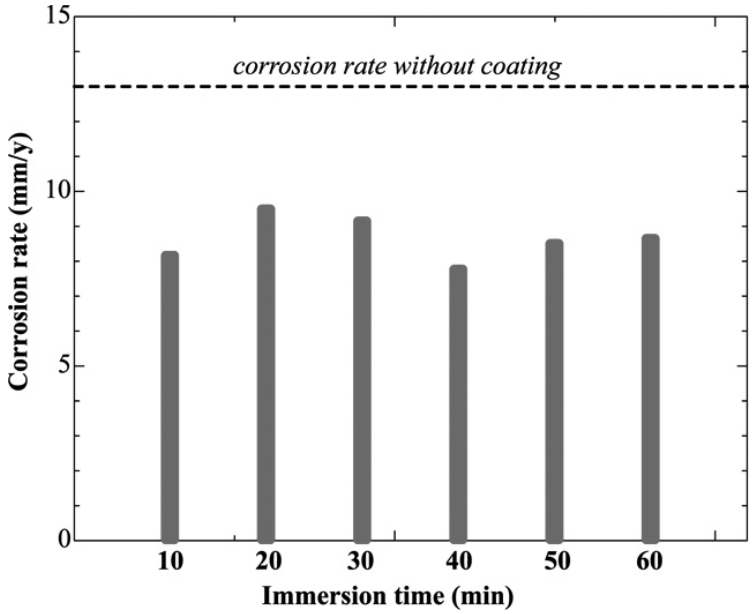


***Figure 3.*** *Corrosion rate of specimen with conversion coating by immersion in Mg $(NO_3)_2$ electrolyte at different immersion time period.*

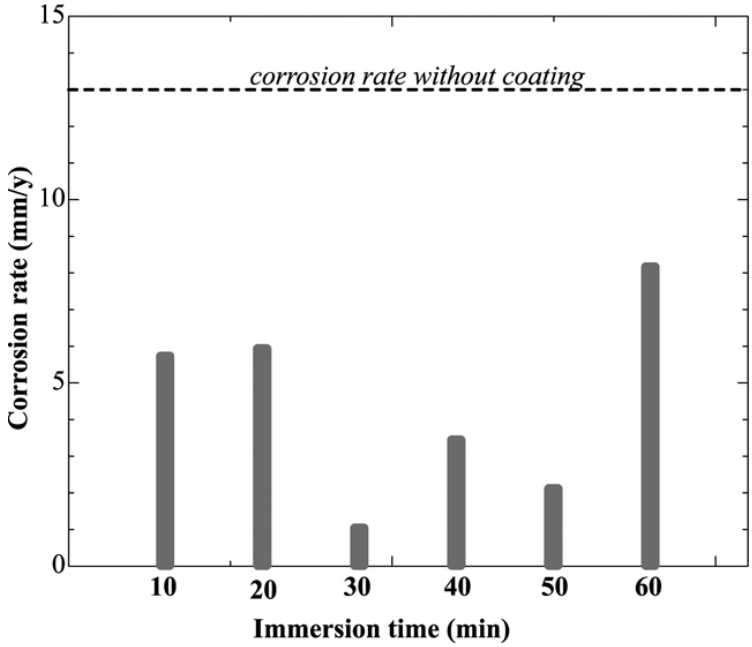


***Figure 4.*** *Corrosion rate of specimen with conversion coating by immersion in $La(NO_3)_3$ and $Mg(NO_3)_2$ electrolytes at different immersion time period.*

The corrosion resistance of AZ91D magnesium alloy was remarkably improved by conversion coating in both $La(NO_3)_3$ and $Mg(NO_3)_2$ electrolytes as shown in Figure 4. The results demonstrated that the specimen treated with conversion coating by immersion in $La(NO_3)_3 + Mg(NO_3)_2$ electrolytes for 30 min has given the highest corrosion resistance of 1.03 mm/year. From our previous work (Toshihide Takenaka *et al.*, 2008), the corrosion resistance of the chromate-based AZ91D magnesium alloy was approximately 2.4 mm/year. Therefore, our presented conversion coating has a potential to replace the chrome-based conversion coating treatment.

The captured SEM images also revealed that the conversion coating with both $La(NO_3)_3$ and $Mg(NO_3)_2$ for 30 min gave pitting free surface after being immersed in the NaCl for 72 hours as shown in Figure 5. This coating was found to be more compact with obviously less in the number of cracks and pores (Figure 5b). In contrast, large pores and cracks clearly appeared on the untreated specimen due to the pitting corrosion (Figure 5a).

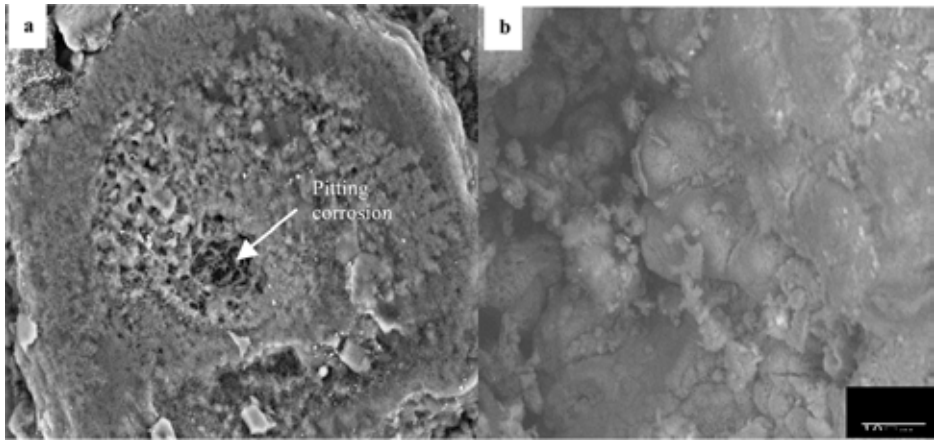


***Figure 5.*** *SEM images of a) untreated, and b) specimen immersed in $La(NO_3)_3 + Mg(NO_3)_2$ electrolytes for 30 min.*

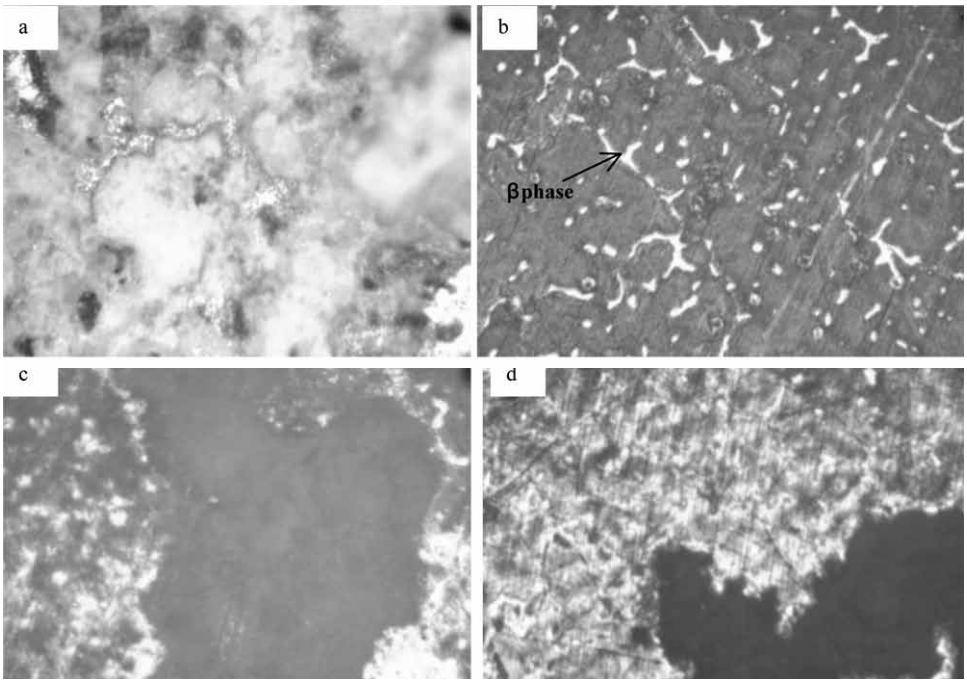


***Figure 6.*** *Optical micrograph images of specimens (a) untreated, (b) $La(NO_3)_3 + Mg(NO_3)_2$ (c) $La(NO_3)_3$ and (d) $Mg(NO_3)_2$ solutions after immersion in NaCl solution for 72 hours.*

Figure 6 shows the optical micrographs of (a) untreated specimen, (b) $La(NO_3)_3$ + $Mg(NO_3)_2$ (c) $La(NO_3)_3$ and (d) $Mg(NO_3)_2$ solutions after immersion in NaCl solution for 72 hours. It can be observed that the surface of lanthanum-treated specimen is more homogeneous with β phase distributed throughout the whole surface (Figure 6b). This indicated that, the combination of $La(NO_3)_3$ electrolyte and Mg $(NO_3)_2$ electrolyte could improve the corrosion resistance of AZ91D magnesium alloy significantly. However, the corrosion resistances of other specimens were inferior throughout the whole surface.

## CONCLUSION

A new chemical conversion coating was produced on AZ91D magnesium alloy by immersion in aqueous solutions containing $La(NO_3)_3$ and $Mg(NO_3)_2$ at ambient temperature for 10-60 min at constant concentration of aqueous solutions. SEM and EDS analyses showed that the lanthanum-based conversion coating exhibited chemical compositions that were uniform and the coating was enriched with La with some closed microcracks. The corrosion resistance of AZ91D magnesium alloy was significantly improved by the conversion coating in the solution containing both $La(NO_3)_3$ and $Mg(NO_3)_2$, especially for specimens immersed in 0.1mM $La(NO_3)_3$ + 0.1mM $Mg(NO_3)_2$ solutions for 30 minutes. The finding provides an interesting alternative to the undesirable $Cr_6^+$based coatings for magnesium alloys.

## REFERENCES

A. Yamamoto, A. Watanabe, K. Sugahara, S. Fukumoto, H. Tsubakino (2001). Deposition coating of magnesium alloys with pure magnesium. *J. Mater. Trans.* **42** : pp 1237–1242.

E.F. Emley (1966). Principles of Magnesium Technology, Pergamon Press Ltd., Headington Hill Hall, Oxford, pp 672.

F.A. Lowenheim (1974). Modern Electroplating, Wiley, New York, pp 381.

G.L. Song A.Atrens, M. Dargusch (1999). Influence of microstructure on the corrosion of diecast AZ91D. *J. Corr. Sci*. **41** : pp 249.

H. K. Delong, in: H. Lawrence, J. Durney (Eds) (1984). Electroplating Engineering Handbook, 4th ed., Van Nostrand Reinhold, Co, Wokingham Berkshire, pp 410.

H. Umehara, M. Takaya, Y. Kojima (2001). An investigation of the structure and corrosion resistance of permanganate conversion coatings on AZ91D magnesium alloy. *J. Mater. Trans.* **42** : pp 1691–1699.

J.E. Gray and B. Luan (2002). Protective coatings on magnesium and its alloys - a critical review. *J. Alloys Compd.* **336** : pp 88–113.

H.J. Kim, J. Zhang, R.H. Yoon, R. Gandour (2004). Development of environmentally friendly nonchrome conversion coating for electrogalvanized steel. *J. Surf. Coat. Technol.* **188** : pp 762–767.

Japanese Standards Association (2003). Method of alkaline salt solution testing for magnesium and magnesium alloys.

K. Brunelli, M. Dabala, I. Calliari and M. Magrini (2005). Effect of HCl pre-treatment on corrosion resistance of cerium-based conversion coatings on magnesium and magnesium alloys. *J. Corr. Sci*. **47** : pp 989-1000.

*Ropien Jokiman*

*Medical Technology Flagship*
*SIRIM Berhad*
*1, Persiaran Dato' Menteri,Section 2, P.O. Box 7035*
*40700 Shah Alam, Selangor*
*Malaysia*

***(ropien@sirim.my)***

## PHOSPHOLIPID BASED VESICULAR SYSTEM FOR TRANSDERMAL AND DERMAL DELIVERY

***RINGKASAN:*** *Vesikel berasaskan fosfolipid muncul sebagai sistem penghantaran dermal dan transdermal yang paling berpotensi disebabkan kelebihannya berbanding sistem-sistem penghantaran yang lain. Artikel ini mengulas mengenai jenis-jenis sistem vesikel berasaskan fosfolipid seperti liposomes, transferosomes dan ethosomes, dan mekanisma penelapan kulitnya. Ia juga menyediakan maklumat berkaitan kaedah penyediaan dan kegunaan sistem ini.*

**ABSTRACT:** Phospholipid based vesicular appears to be most promising transdermal and dermal delivery system due to their merits over other delivery systems. This article reviews the types of phopholipid based vesicular system such as liposomes, transferosomes and ethosomes and their mechanism of skin permeation . It also provides an information on the method of preparation and application of the system.

Keywords: Phopholipid based vesicular, transdermal and dermal delivery, liposomes, transferosomes, ethosomes

## INTRODUCTION

The skin is the largest organ in the human body and covers a total surface area of approximately 1.8 $m^2$ and provides the contact between the human body and its external environment. It has various functions such as protective barrier from external environment, maintenance of body posture and regulation of temperature. The skin itself has three main layers ; epidermis, dermis, and hypodermis as shown in Figure 1 (El Maghraby *et al.*, 2008 and Williams, 2003). The epidermis which is the outermost layer of the skin, covers the dermis that is the active part of the skin, holding the hair muscles, blood supply, sebaceous glands, and nerve receptors. The deepest layer of the skin is the subcutaneous tissue or hypodermis. The hypodermis acts as a heat insulator, a shock absorber, and an energy storage region. This layer is a network of fat cells arranged in lobules and linked to the dermis by interconnecting collagen and elastin fibers. The stratum corneum (SC), despite its thickness of only 10 to 20 µm, forms a formidable barrier for the solutes and moisture and provides a very effective barrier for penetration. The structure of the stratum corneum is often compared with a brick wall, with the corneocytes as the bricks surrounded by the mortar of the intercellular lipid lamellae (Elias, 1983). It has been generally accepted that the highly organized crystalline lipid lamellae plays an essential role in the barrier properties of the stratum corneum (Williams and Elias, 1987). Dermal and transdermal drug delivery systems have been aimed to disrupt and weaken the highly organized intercellular lipids in an attempt to enhance drug transport across the intact skin or to increase the driving force for permeation of drugs across this skin barrier (Barry, 2001).

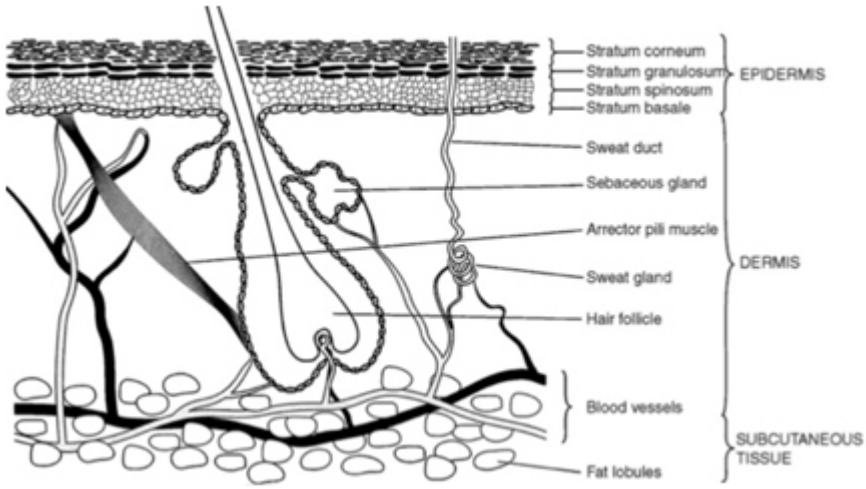


***Figure 1.*** *A diagrammatical representation of a cross-section through human skin showing the different cell layers and appendages ( El Maghraby et al., 2008 and Williams, 2003).*

Dermal drug delivery is the topical application of drugs to the skin in the treatment of skin diseases. The goal of dermal delivery is to maximise drug retention in the skin, while minimising drug absorption into the systemic circulation therefore also reducing the systemic side effects. Transdermal drug delivery uses the skin as an alternative route for the delivery of systemically acting drugs. The goal in transdermal systems is to maximise drug absorption in the systemic circulation. The rate and extent of drug penetration into different layers of skin and into systemic circulation are governed by the drug properties and formulation characteristics. This drug delivery route can have several advantages compared with oral drug administration. First of all, it circumvents the variables that could influence gastro-intestinal absorption such as pH, food intake and gastro-intestinal motility. Secondly, it circumvents the hepatic metabolism and is therefore suitable for drugs with a low bioavailability. Thirdly, it can give a constant, controlled drug input decreasing the variation in drug plasma level, thus reducing the side effects particularly on drugs with a narrow therapeutic window (Honeywell-Nguyen and Bouwstra, 2005). The permeation of the molecules through the skin has several routes: intracellular (across the corneocytes), intercellular lipids, and appendageal (through sweat glands or hair follicles) as shown in Figure 2 (Barry, 1991). The intercellular lipids are the major transport pathways for most drugs, in which the molecule has to pass through successive hydrophilic and hydrophobic domains in the lipid bilayers. On the other hand, the skin appendages serve as a shunt pathway for drug molecules. Since the appendages occupy a very low surface area, this mean of permeation is less significant under normal conditions ( Hadgraft, 2001).

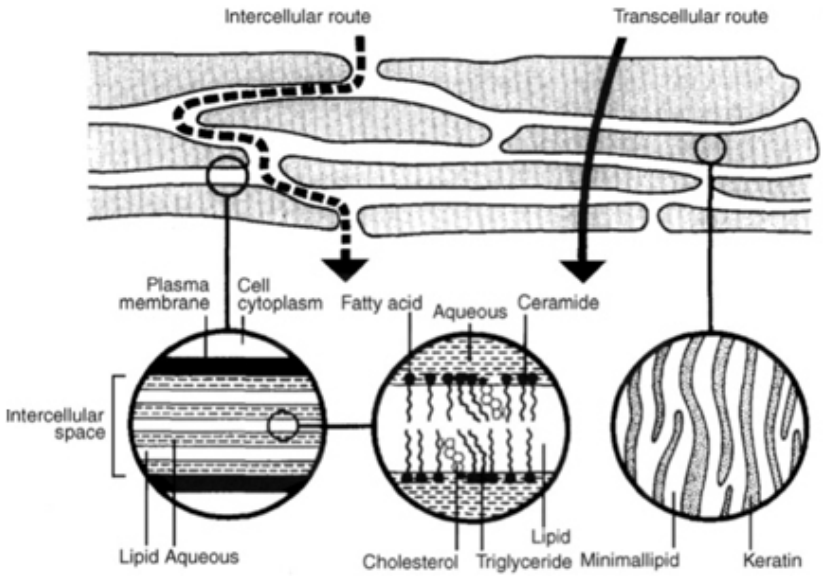


***Figure 2.*** *Major routes of skin penetration (Barry, 1991).*

A large variety of nanocarriers are used as drug delivery systems. All of them accomplish the substantial task of carrying drugs to the target in a controlled manner. In recent years the popularity of phospholipid based vesicular as a dermal and transdermal drug delivery system has increased because of many advantages associated with it. The advantages of phospholipid based vesicular in comparison to other delivery systems (Verma and Pathak, 2010) are as follows:

1. The compatibility of phospholipid with membrane of human either internal membrane as well as skin.
2. These systems show enhanced permeation of drug through skin for transdermal and dermal delivery.
3. These are platforms for the delivery of large and diverse drug groups.
4. Their composition is safe and the components are approved for pharmaceutical and cosmetic use.
5. The toxicology profiles of the phospholipids are well documented in the scientific literature.

Phospholipids are amphiphilic, possesing both hydrophilic (water soluble) and hydrophobic (lipid soluble) groups. The hydrophobic tail is composed of two fatty acid chains containing 10-24 carbon atoms and 0-6 double bond in each chain. The polar end of the molecule is mainly phosphoric acid bound to water-soluble molecule. Some commonly used phospholipids are dioleoyl-phosphatidyl-choline (DOPC), dioleoyl-phosphatidyl-ethanolimane (DOPE), distearoyl-phosphatidyl-choline (DSPC) and distearoyl-phosphatidyl-ethanolimane (DSPE)(Verma et al., 2010 ).

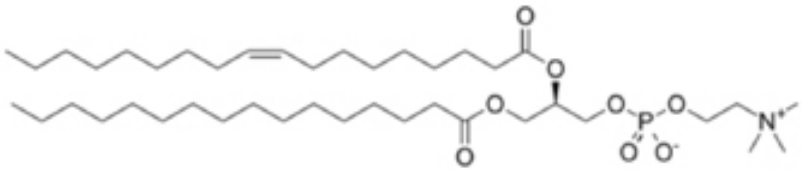

***Figure 3.*** *Phosphatidylcholine containing oleyl and palmitoyl side chains (Verma et al.,2010 )*

Among all these phospholipids, phosphatidyl-choline (Figure 3) is very important in drug delivery technology.

## PHOSPHOLIPID BASED VESICULAR

Phospholipid based vesicular system can be classified into two categories: Rigid vesicles liposomes and elastic or ultra deformable vesicles – transferosomes and ethosomes.

## Liposomes

Liposomes were first described by British hematologist Alec D Bangham (Bangham and Horne, 1964). Liposomes are thermodynamically stable, spontaneously formed, submicroscopic vesicular structures of amphiphilic lipids arranged in one or more concentric bilayers with an entrapped aqueous core. The lipids are natural or synthetic phosphilipids, which include phosphatidyl-choline (lecithin), phosphatidyl-ethanolimane, phosphatidyl-glycerol, phosphatidyl-serine, and phosphatidyl-ionositol (Venuganti and Perumal, 2009).

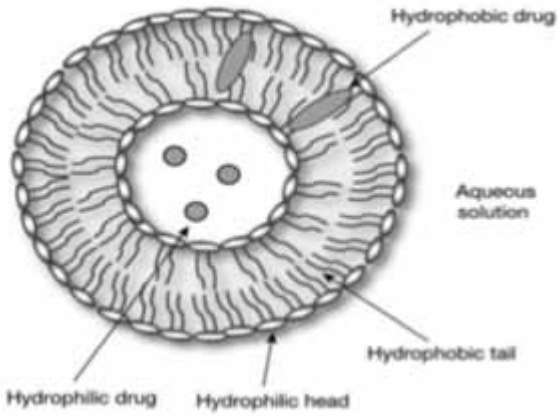


***Figure 4.*** *Liposomes contain a lipid bilayer (Lembo and Cavalli, 2010)*

On mixing with an aqueous medium, the phosphate groups of the phospholipids orient themselves to the hydrophilic environment spontaneously forming unilamellar or multilamellar bilayer vesicles. Cholesterol is usually included to improve the stability of the vesicles, impart fluidity to the bilayer membrane, and prevent the leakage of vesicle contents. Hydrophilic drugs are incoporated in the aqueous core, whereas hydrophobic drugs are entrapped within the bilayer as shown in Figure 4.

Liposomes are classified based on the size of vesicles or number of lipid bilayers. There are small unilamellar visicles (SUV), multilamellar vesicles (MLV) and large unilamellar vesicles (LUV). The diameter for SUV range from 20 nm to 100 nm, MLV is more than 500 nm, and LUV a few hundred nanometers as shown in Figure 5 (Parthiban *et al.*, 2012; Yang *et al.*, 2011).

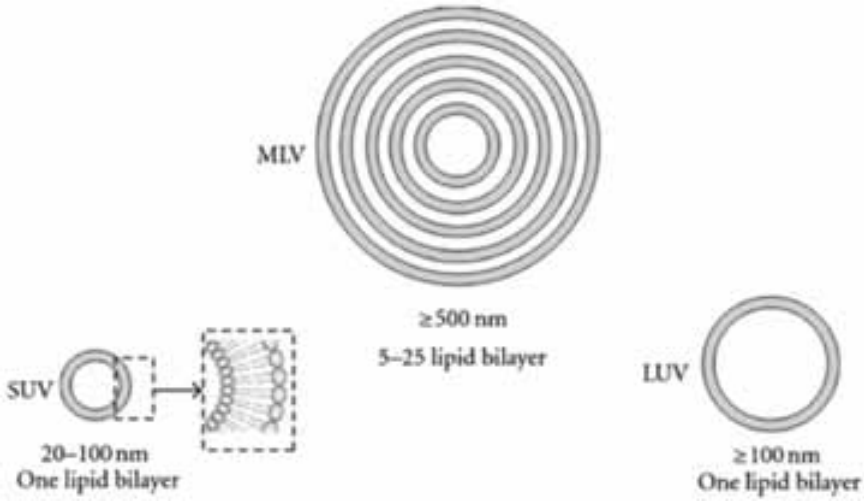


***Figure 5.*** *Liposomes classification based on size and number of lamellar (Parthiban et al., 2012; Yang et al., 2011)*

**Method of Liposomes Preparation**

The basic underlying principle for the formation of liposomes, regardless of the preparation methodology, is the hydrophilic/hydrophobic interaction between lipid-lipid and lipid-water molecules. Input of energy (e.g. in the form of sonication, homogenisation, shaking, heating, etc.) results in the arrangement of the lipid molecules, in the form of bilayered vesicles, to achieve a thermodynamic equilibrium in the aqueous phase as shown in Figure 6 (Mozafari, 2005; Mozafari *et al.*, 2004).

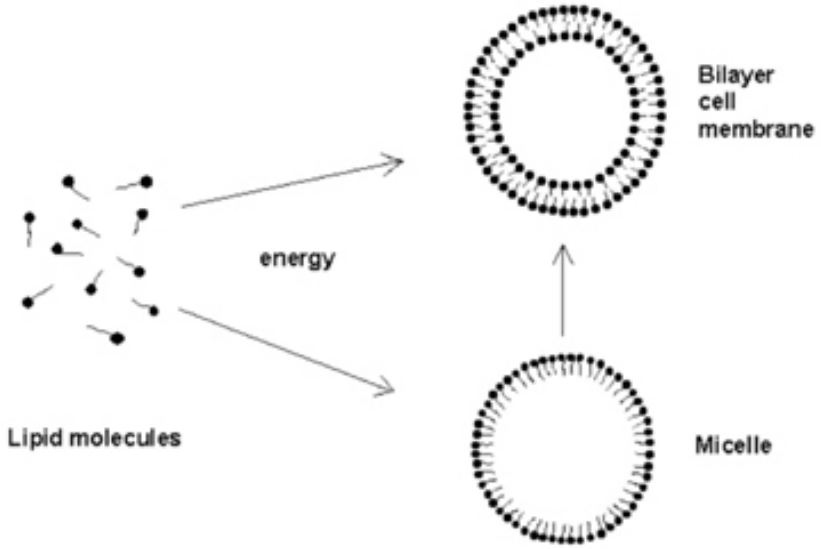


***Figure 6.*** *A possible mechanism of the formation of liposomes from the lipid by some energy input (Mozafari, 2005; Mozafari et al., 2004)*

The different methods used to prepare liposomes are described below:

(i) Thin-film hydration

Lipid mixture is dissolved in a suitable solvent such as methanol or chloroform. The organic solvent is removed under reduced pressure and lyophilised to remove any traces of solvent. The thin lipid film is redispersed in aqueous medium to form MLV . SUV can be prepared by sonication of MLV by using a probe or bath sonicator as shown in Figure 7 (Mozafari, 2005). Small vesicle sizes can also be achieved by passing MLV through a polycarbonate filter under high pressure (extrusion) as shown in Figure 8 (Vemuri and Rhodes, 1995).

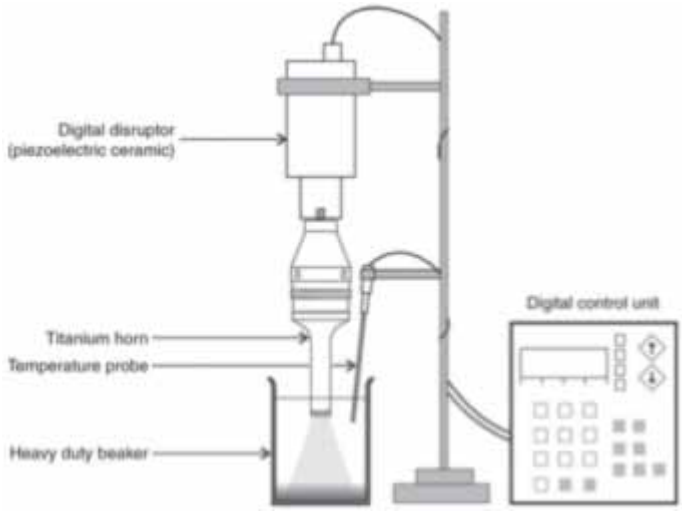


***Figure 7.*** *Schematic representation of a probe-type sonicator (Mozafari, 2005).*

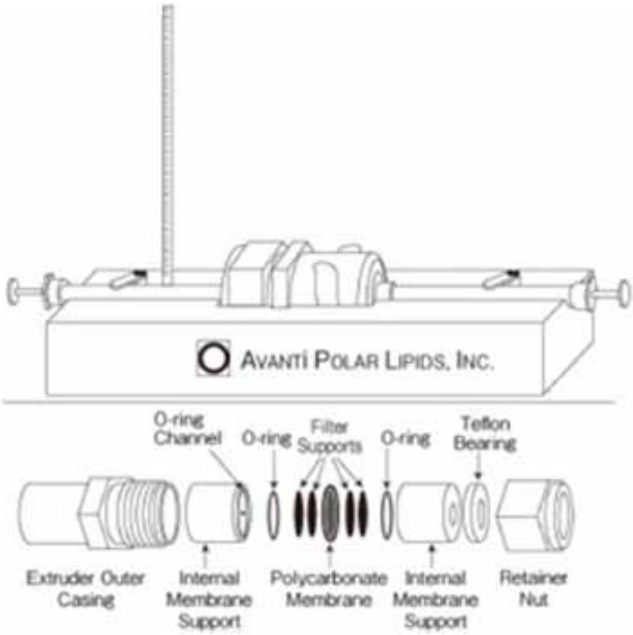


***Figure 8.*** *Schematic representation of a small hand-held extruder (Vemuri and Rhodes, 1995).*

(ii) Microfluidisation

A method of liposomes preparation without using potentially toxic solvents is the microfluidisation technique using microfluidiser as shown in Figure 9 (Vemuri *et al.*, 1990).

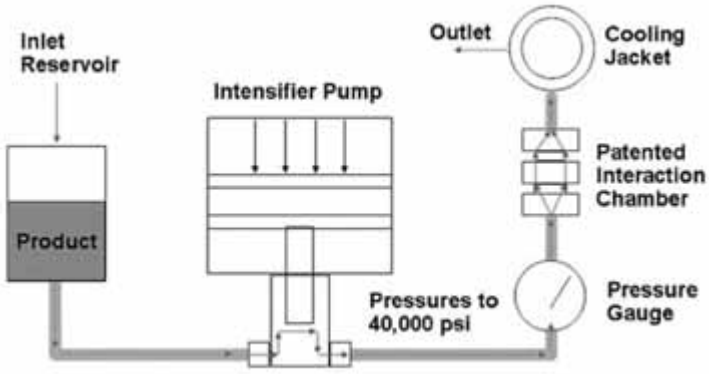


***Figure 9.*** *Schematic representation of a microfluidiser apparatus (Vemuri et al., 1990).*

Microfluidisation is based on the principle of dividing a pressure stream into two parts, passing each part through a fine orifice, and directing the flows at each other inside the chamber of microfluidiser (Geciova *et al.*, 2002; Jafari *et al.*, 2006). Within the interaction chamber, cavitation, along with shear and impact, reduce particle

sizes of the liposomes. The advantages of microfluidisation are; a large volume of liposomes can be formed in a continuous and reproducible manner, the average size of the liposomes can be adjusted, very high capture effciencies (>75%) can be obtained, and the solutes to be encapsulated are not exposed to sonication, detergents or organic solvents (Mozafari, 2010).

(iii) Heating Method

This a new method for liposomes preparation without the use of potentially toxic solvents. Liposomes can be prepared by using a single apparatus with very low shear forces (Mozafari *et al.*, 2002; Mozafari, 2005; Colas *et al.*, 2007 and Mortazavi *et al.*, 2007) . This method is economical and capable of producing liposomes with superior monodispersity and storage stability, using a simple protocol. Another important feature of the heating method is that it can be adapted from small to industrial scale. The heating method involves hydration of the ingredients of the carrier system, followed by heating and stirring the ingredients and the active compound to be encapsulated, in the presence of a polyol, such as glycerol (Mozafari *et al.*, 2008).

**Application of Liposomes**

The first paper to report on the effectiveness of liposomes for skin delivery was published in the early 1980s (Mezei and Gulasekharam, 1982).The result from the study showed that the liposomes delivered four to five fold higher steroid concentration in the skin layers, compared to topical application of a simple lotion. Since then, there has been an exponential growth in the use of liposomes as topical delivery vehicles (Fang *et al.*, 2006). On the other hand, conflicting results continued to be published concerning the effectiveness of liposomes as transdermal delivery vehicles. Now it is clear that liposomes only enhanced the drug disposal in the skin, suggesting that liposomes are only useful for topical dermal delivery (Elsayed *et al.*, 2007). Liposomes are widely used in topical products for their moisturising and smoothening effect on the skin (Weiner *et al.*, 1994). Furthermore, they can be used to deliver skin protectants, antioxidants, and skin-whitening agents. Some examples of active ingredient for topical application delivered using liposomes system is shown in Table 1.

**Table 1.** Representative list of active ingredients delivered by using liposomes.

| Active ingredient | Use | Reference |
|---|---|---|
| Tretinoin | Inflammatory diseases | Sinico et al., 2005 |
| Sodium copper cholorophyllin | Repair of skin tissue | Dorogi et al., 2010 |
| Ferulic acid and phloretin | Skin rejuvenation | Sanmiguel and Zamora, 2010 |
| Tocopheryl phosphate | Anti skin ageing | Dumas et al., 2009. |

**Transferosomes**

The term "transferosomes" and the underlying concept were intoduced in 1991 by Gregor Cevc (Cevc, 1991). Transferosomes is a term registered as a trademark by the German company IDEA AG, and used by it to refer to its proprietary drug delivery technology. These deformable vesicles are novel types of liquid-state vesicles consisting of phospholipid and edge activator as shown in Figure 10 (Ravi *et al.*, 2012). An edge activator is often a single chain surfactant that destabilises the lipid bilayer of the vesicles and increases the deformability of the bilayer by lowering its interfacial tension.

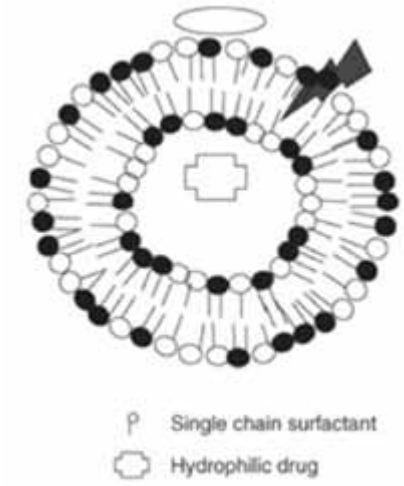


***Figure 10.*** *Transferosomes (Ravi et al., 2012).*

Transferosomes range in size from 200 to 300 nm. Due to their high deformability, they are believed to squeeze through skin pores (20-40 nm), which are one-tenth of their size and reach deeper layers in the skin ( Cevc and Blume, 1992). The flexibility of transferosomes membrane minimises the risk of complete vesicle rupture in the skin and allows tranferosomes to follow the natural water gradient across the epidermis, when applied under non-occlusive condition as shown in Figure 11 (Ogunsola *et al.*, 2012). Transferosomes can penetrate the intact stratum corneum spontaneously either through intracellular route or transcellular route as shown in Figure 2 (Schatzlein and Cevc, 1995).

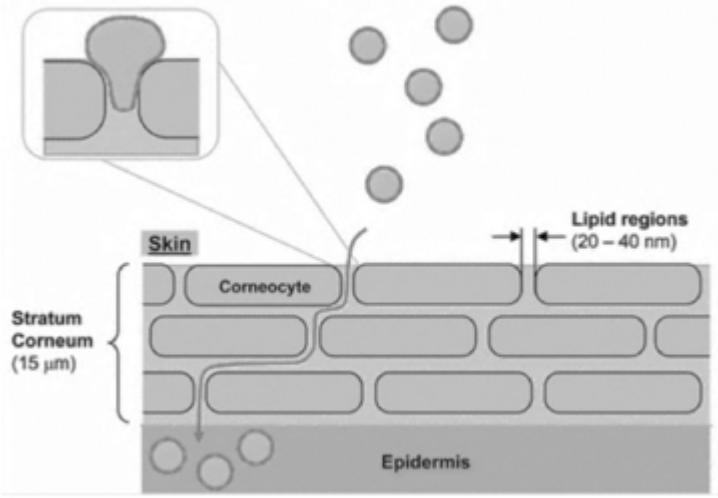


***Figure 11.*** *The mechanism of skin penetration of transferosomes (Ogunsola et al., 2012).*

**Method of transferosomes preparation**

Phospholipids, surfactant and the drug are dissolved in alcohol. The organic solvent is then removed by rotary evaporation and final traces of solvent are removed under vacuum. The deposited lipid film is hydrated with the appropriate buffer by rotation. The resulting vesicles, multilamellar lipid visicles (MLV), which are swollen at room temperature are then sonicated at room temperature. Sonication may be replaced by extrusion, low shear mixing or high shear mixing at room temperature (Jadupati *et al.*, 2012; Elsayed *et al*, 2007).

**Application of Transferosomes**

Transferosomes have been widely explored for dermal and transdermal application. Transferosomes have been widely used as carrier for the transport of proteins and peptides. Proteins and peptides are large biogenic molecules which are very difficult to transport into the body; when given orally they are completely degraded in the gastrointestinal tract. Paul *et al.* (1998) investigated the feasibility of non-invasive immunisation with a large membrane associated macromolecule, gap junction protein (GJP). The success of cell-mediated immune with response to the epicutaneous or subcutaneous administration of GJP in various colloidal formulation was studied. The result of the study showed that a non-invasive, transdermal immunisation with GJP-loaded transferosomes elicits 0.16 ± 0.06 and 0.37 ± 0.08 relative units of the specific IgG2a in the presence and absence of lipid A, respectively. Corresponding injections under the skin result in 0.18 ± 0.07 and 0.38 ± 0.02 relative units. It is shown that GJP is transported across the intact murine skin and processed immunologically, and the bioavaibility obtained from transferosomes is somewhat similar to that resulting from subcutaneous injection of the same protein formulation.

Delivery of insulin by transferosomes is the successful means of non invasive therapeutic use of such large molecular weight drugs on the skin. Cevc (Cevc, 2003) studied on vesicles containing insulin and tested them on NMRI (Nuclear Magnetic Resonance Imaging) mice and humans. Epicutaneous administration produced results similar to a subcutaneous injection in mice. Transferosome-associated insulin (Transfersulin® ) was able to reduce the blood glucose levels by 20-30 % in mice within 2-4 hours. Human data also showed very similar results but with a delay of 45-145 min from comparable subcutaneous doses. The representative list of drugs delivered using transferosomes is shown in Table 2.

**Table 2.** Representative list of drugs delivered by using transferosomes.

| Drug | Use | Reference |
|---|---|---|
| Interferons, for example leukocytic derived interferone-α (INF- α) | Treatment of infections (antiviral, antiproliferative and some immunomodulatory effects) | Hafer et al., 1999 |
| Epidermis growth factor (EGF) | Diabetic foot amputation prevention | Escalona et al., 2009 |
| Nonsteroidal anti-inflammatory drugs (NSAIDs) | Anti-inflammatory | Cevc and Vierl, 2004 |
| Tetracaine, lignocain | Topical analgesic | Planas et al., 1992 |

## Ethosomes

Ethosomes as shown in Figure 12 (Parashar *et al.*, 2013) are lipid vesicles containing phospholipids, alcohol (ethanol and isopropyl alcohol) in relatively high concentration and water, and they were first reported by Touitou *et al.* (Touitou *et al.*, 1997). The ethanol concentration in ethosomes usually ranges from 20 % to 45 %, and it imparts high flexibility and malleability to the vesicles. Ethosomes can entrap drug molecule with various physicochemical characteristics i.e. hydrophilic, lipophilic, or amphipilic. The size range of ethosomes may vary from tens of nanometer to microns (Bhalaria *et al.*, 2009; Verma and Fahr, 2004).

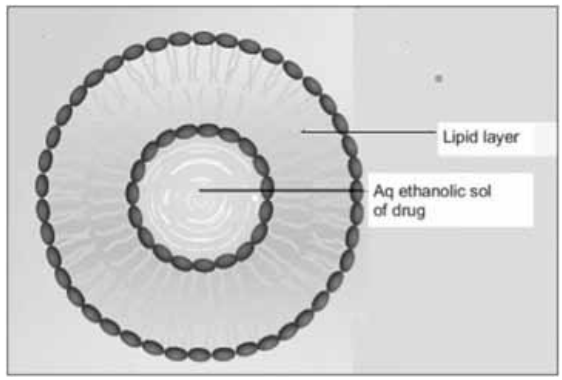


***Figure 12.*** *Ethosomes (Parashar et al., 2013).*

Very high encapsulation efficiencies of lipophilic drugs can be achieved due to the enhanced solubility from the presence of ethanol (Touitou *et al.*, 2000). Unlike transferosomes, ethosomes can enhance drug delivery through skin under both non-occluding and occluding conditions (Elsayed *et al.*, 2006).

The enhanced delivery of actives using ethosomes over liposomes can be ascribed to an interaction between ethosomes and skin lipids. A possible mechanism for this interaction has been proposed as shown in Figure 13 (Verma and Pathak, 2010), it is thought that the first part of the mechanism is due to the ethanol effect, where ethanol acts as a penetration enhancer through the skin. Ethanol interacts with the lipid molecules in the polar head group region resulting in a reduction in the transition temperature of the lipids in the stratum corneum, increasing their fluidity and decreasing the density of the lipid multilayer. This is followed by the 'ethosome effect,' which includes lipid penetration and permeation by the opening of new pathways, due to the malleability and fusion of ethosomes with skin lipids, resulting in the release of the drug into the deep layers of the skin. Ethanol may also provide vesicles with soft flexible characteristics, which allow them to penetrate more easily into the deeper layers of the skin. The release of the drug in the deep layers of the skin and its transdermal absorption could then be the result of a fusion of ethosomes, with skin lipids and drug release at various points along the penetration pathway (Elsayed *et al.*, 2006).

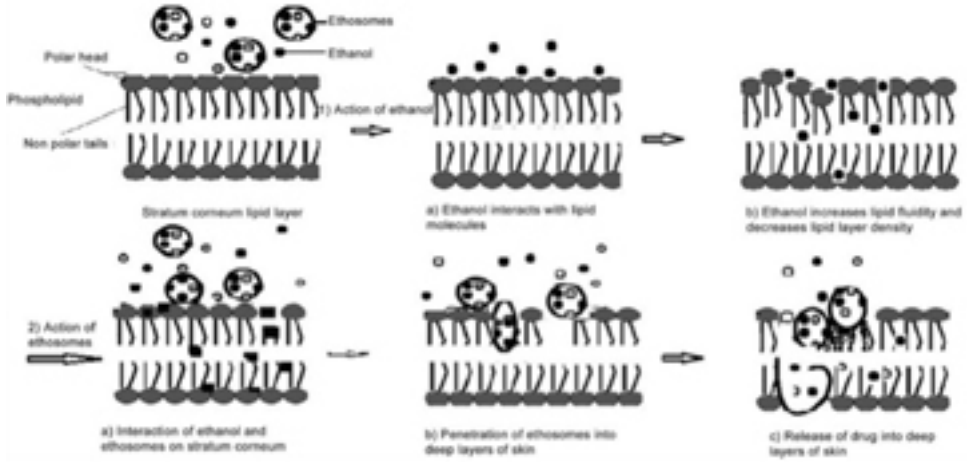


***Figure 13.*** *Proposed mechanism of penetration of ethosomal drug delivery system (Verma and Pathak, 2010).*

**Method of Ethosomes preparation**

Ethosomes can be prepared by two very simple and convenient methods, hot method and cold method.

(i) Cold Method

This is the most common and widely utilised method for the preparation of ethosomes.The phospolipid, drug and other lipid materials are dissolved in ethanol in a covered vessel at room temperature with vigorous stirring. The mixture is heated up to 30 °C in a water bath. In a separate vessel, the water is heated to 30 °C and added to the above mixture and then stirred for five minutes in a covered vessel. The vesicle size of ethosomal formulation can be decreased using sonication or extrusion method. Finally the formulation must be properly stored under refrigeration (Nikalje and Tiwari, 2012; Dinesh *et al.*, 2009).

(ii) Hot Method

The drug is dissolved in a mixture of ethanol and propylene glycol at 40 °C. In a separate vessel phospholipid is dispersed in water at 40 °C. Once both mixtures reach 40 °C, the organic phase is added to the aqueous phase. After mixing for five minutes the preparation is sonicated at 4 °C for three cycles of five minutes, with a rest of five minutes between each cycle, using Probe Sonicator. The formulation is then homogenised at 15,000 psi pressure, in three cycles, using high pressure homogeniser to get nano-sized ethosomes (Bhalaria *et al.*, 2009).

**Application of Ethosomes**

Ethosomes are able to penetrate the deeper layers of the skin and hence appear to be vesicles of choice for transdermal drug delivery of hydrophilic and impermeable drug through skin. One of the application of ethosomes is as a vesicle for topical delivery of antibiotics. Conventional oral therapy causes several allergic reactions along with several side effects. Conventional external preparations possess low permeabilty to deep skin layers and subdermal tissue. The antibiotic (erythromycin) loaded ethosomal formulation have been prepared for dermal and intracellular delivery (Godin *et al.*, 2005). A model for deep dermal *Staphylococcus aureus* infection in mice was developed. The efficiency of ethosomal erythromycin applied to the skin-infected site was compared with intraperitoneal erythromycin administration and with local application of hydroethanolic erythromycin solution. The in vivo experiments demonstrated a very efficient healing of *Staphylococcus aureus*-induced deep dermal infections when the mice were treated with ethosomal erythromycin. Bacterial counts and histological evaluation of the skin treated with ethosomal antibiotic revealed no bacterial growth and normal skin structure. On the contrary, no subdermal healing was observed in infected animals treated with topical hydroethanolic erythromycin solution. The results of this study showed that the ethosomal formulation of antibiotic could be highly efficient and would overcome the problems associated with conventional therapy.

Dubey, *et al.* (2007) prepared methotrexate (MTX) ethosomes used for the treatment of psoriasis. They also compared the extent of penetration of ethosomes and liposomes loaded with rhodamine red (RR) by CLS microscopy. They found

that ethosomes penetrated to a depth of 170 µm with fluorescence intensity (FI) of 160 AU, whereas liposomes penetrated only up to 80 µm with FI of 40 AU. On the other hand the flux of MTX ethosomes was found to be 57.2 ± 4.34 µg/cm$^2$ /hour whereas the flux for hydroethanolic solution and liposomes was found to be 22.43 ± 0.24 µg/cm 2 /hour and 14.6 ± 1.65 µg/cm$^2$ /hour, respectively. Table 3 is a short compilation of ethosomes application as a carrier for topical and transdermal delivery of a variety of drugs.

**Table 3.** Representative list of drugs delivered by using ethosomes

| Drug | Use | Reference |
|---|---|---|
| Colchicine | Anti gout activity | Sing et al., 2008 |
| Bullatacin | Reduce skin irritation | Tan et al., 2012 |
| Vitamin A palmitate, vitamin E, vitamin C | Anti oxidant | Koli and Lin, 2009 |
| Terbinafme salts | Anti fungal (for treatment of onychomycosis) | Touitou, 2010 |

## FUTURE PERSPECTIVE

Consumers nowadays are more focused on their health and appearance. As a result, there has been an increasing demand in topical anti-ageing formulation with active ingredients. Novel and innovative delivery systems are transforming the new product development in the cosmetic field because of consumer perceivable benefits and optimised sensory attributes. Liposomes are the most widely known topical delivery systems. A special characteristic of liposomes is the ability to adapt to water soluble and non-water soluble active ingredients in the liposomes membrane. Liposomes are used in a variety of skin care rejuvenation products because of their ability to encapsulate active ingredients and deliver them deep into the cells. Several excellent phytochemicals and herbal extracts have been successfully delivered via liposomes and showed some distinct advantages over conventional cosmetic products. Thus, it can be predicted that liposomes will be continously used as an efficient delivery system of active ingredients in topical products and will improve the cosmetic market even more, although a lot of research and human studies in this field is required to obtain real life data.

Transdermal route is a promising alternative to drug delivery for systemic effect. Transferosomes and ethosomes have iniatiated a new area in vesicular research for transdermal drug delivery which can provide better skin permeation than liposomes. Hence, enhanced delivery of drug molecules through the skin by means of transferosomes opens new challenges and opportunities for the development of novel improved therapies. Thus, it could be concluded that the transferosomes can

overcome all the problems associated with transdermal delivery as transferosomes itself are specially optimised vesicles having the capability of responding to external stress by rapid and energetically inexpensive shape transformations. The high tolerability and efficiency of these vesicular systems open vast potential therapeutic uses. These nanocarriers might offer advanced local and systemic new therapies with agents that are unable to efficiently penetrate the stratum corneum via passive diffusion. IDEA AG breakthrough, proprietary Transfersome® technology enables the targeted and non-invasive delivery of drugs (including large molecules such as proteins) through the skin, with particular focus on pain relief and dermatology. The Company's Transfersome® carriers are topically applied on the skin and can be engineered to achieve high drug concentration at or near the site of application, increasing drug potency and diminishing side effects. The non-steroidal anti-inflammatory drug (NSAID), ketoprofen, in a transferosomes formulation gained marketing approval by the Swiss regulatory agency (SwissMedic). Further therapeutic products based on the transferosome technology, according to IDEA AG, are in clinical development.

Ethosomes has shown promising result and potential for delivery of various agents more effectively. Ethosomes offers a good opportunity for non – invasive delivery of small, medium and large size drug molecules. Ethosomes can be a promising tool for dermal/transdermal delivery of various agents and an alternate formulation for problematic drugs. Further research in this area will allow better control over drug release in vivo, allowing the physician to make the therapy more effective. Therefore, it should not be long before corresponding drug formulation finds its way into clinics to be tested for widespread usage.Thus, it can be logically concluded that ethosomal formulations possess a promising future in effective dermal/transdermal delivery of bioactive agents. More formulations based on ethosomes is expected be launched in the market in the coming years, including formulations for the treatment of alopecia, deep skin infection, hormone deficiencies, inflammation and atopic dermatitis.

## CONCLUSION

A number of transdermal and dermal delivery system for drugs are emerging today. The phospholipid based delivery systems are important because of intense advantages associated with them. The delivery systems described above have proved their ability and efficacy to deliver the drugs to the desired location. Liposomes are only suitable for dermal system but not suitable for transdermal delivery because they cannot reach the deeper layer of the skin as they are trapped in the superior layer of stratum corneum. Transdermal route is a promising alternative to drug delivery for systemic effect. Transferosomes and ethosomes have initiated a new area in vesicular research for transdermal drug delivey which can provide better skin permeation than liposomes.

## REFERENCES

Bangham, A.D., Horne, R. W. (1964). Negative staining of phospholipids and their structural modification by surface-active agents as observed in the electron microscope. *J. Mol.Bio*. **8** : pp 660–668.

Barry, B.W. (1991). Lipid protein partitioning theory of skin penetration enhancement. *J. Control. Release.* **15** : pp 237–248.

Barry, B.W. (2001). Novel mechanisms and devices to enable successful transdermal drug delivery. *Eur. J. Pharm. Sci.* **14** : pp 101-114.

Bhalaria, M.K., Naik, S. and Misra A.N. (2009). Ethosomes: A novel delivery system for antifungal drugs in the treatment of topical fungal diseases. *Indian Journal of Experimental Biology.* **47** : pp 368-375.

Cevc, G. (1991). Isothermal lipid phase. *Transitions chemistry and physics of lipids.* **57** : pp 293-299.

Cevc, G. (2003). Transdermal drug delivery of insulin with ultradeformable carriers. *Clin Pharmacokinet.* **42** : pp 461-474.

Cevc, G. and Blume, G. (1992). Lipid vesicles penetrate into intact skin owing to the transdermal osmotic gradients and hydration force. *Biochim Biophys Acta.* **1104** : pp 226-232.

Cevc, G. and Vierl, U. (2004). Aggregate with increased deformability comprising at least three amphipats for improved transport through semi-permeable barriers and for the non-invasive drug application in vivo especially through the skin. WO Patent: 2004032900A1.

Colas, J.C., Shi, W.L., Rao, V.S.N.M., Omri, A., Mozafari, M.R. and Singh, H. (2007). Microscopical investigations of nisin-loaded nanoliposomes prepared by Mozafari method and their bacterial targeting. *Micron.* **38** : pp 841-847.

Dinesh, D., Amit, A.R., Maria, S., (2009). Drug vesicle based approaches of penetration enhancement. *Int. J. Phar. Sci.* **1(1)** : pp 24-45.

Dorogi, P.L., Vasily, D.B. and McCook, J.P. (2010). Skin treatment composition containing copper pigment complex. U.S. Patent: 20100247591A1.

Dubey, V., Mishra, D., Dutta, T., Nahar, M., Saraf, D.K. and Jain, N.K. (2007). Dermal and transdermal delivery of an anti-psioriatic agent via ethanolic liposomes. *J. Control Release.* **123(2)** : pp 148-154.

Dumas, M., Noblesse, E., Alard, V., Quiles, D. and Perrier, E. (2009). Use of tocopheryl phosphate as an agent for preventing or slowing down the appearance of the effects of skin ageing. U.S. Patent: 20090104258A1.

El Maghraby, G.M., Barry, B.W. and Williams, A.C. (2008). Liposomes and skin: From drug delivery to model membranes. *Eur. J. Pharm. Sci.* **34** : pp 203-222.

Elias, P.M. (1983). Epidermal lipids, barrier function, and desquamation. *J. Invest. Dermatol.* **80** : pp 44-49.

Elsayed, M.M.A., Abdallah, O.Y., Naggar, V.F., (2006). Deformable liposomes and ethosomes. Mechanism of enhanced skin delivery. *Int. J. Pharm.* **322** : pp 60-66.

Elsayed, M.M.A., Abdallah, O.Y., Naggar, V.F., (2006). Lipid vesicles for skin delivery of drugs. Reviewing three decades of research. *Int. J. Pharm.* **332** : pp 1-6.

Elsayed, M.M.A., Abdallah, O.Y., Naggar, V.F., (2007). Deformable liposomes and ethosomes as carrier for skin delivery of ketotifen. *Pharmazie.* **62** : pp 133-137.

Escalona, E.P., Meireles, R.P., Acosta, J.A.B. and Redriquez, B.Y.B. (2009). Use of a topical composition containing epidermal growth factor (EGF) for the diabetic foot amputation prevention. U.S. Patent: 20090074850A1.

Fang, J., Hong, C., Chiu, W. and Wang, Y. (2001). Effect of liposomes and niosomes on skin permeation of enoxacin. *Int. J. Pharm.* **219** : pp 61-72.

Geciova, J., Bury, D. and Jelen, P. (2002). Methods for disruption of microbial cells for potential use in the dairy industry- a review. *Int. Dairy J.* **12** : pp541-553.

Godin, B., Touitou, E., Rubinstein, E., Athamna, E. And Athamna, M. (2005). A new approach for treatment of deep skin infections by an ethosomal antibiotic preparation : an in vivi study. *J. Antimicrob Chemother.* **55**: pp 989-994.

Hadgraft, J. (2001). Passive enhancement strategies in topical and transdermal drug delivery. *Int. J. Pharm.* **184(1)** : pp 1-6.

Hafer, C., Goble, R., Deering, P., Lehmer, A. and Breut, J. (1999). Formulation of interleukin-2 and interferon-α containing ultradeformable carriers for potential transdermal application. *Anticancer Res.* **19(2c)** : pp 1505-1512.

Honeywell-Nguyen, P.L. and Bouwstra, J.A. (2005). Vesicles as a tool for transdermal and dermal delivery. *Drug Discovery Today.* **2** : pp 67-74.

Jadupati, M., Amites, G and Kumar, N.A. (2012). Transferosomes: An opportunity carrier for transdermal drug delivery system. *Int. Research J. Pharm.* **3(3)** : pp 35-38.

Jafari, S.M., He, Y.H. and Bhandari, B. (2006). Nanoemulsion production by sonication and microfluidization – a comparison. *Int. J. Food Prop.* **9** : pp 475-485.

Koli, J.R. and Lin, S. (2009). Development of antioxidant ethosomes for topical delivery utilizing the synergistic properties of vit A palmitate, vit E and vit C. *AAPS Pharm. Sci. Tec.* **11** : pp 1-8.

Lembo, D. and Cavalli, R. (2010). Nanoparticulate delivery systems for antviral drugs. *Antiviral Chem. & Chemotheraphy.* **21**: pp 53-70.

Mezei, M. And Gulasekharam, V. (1982). Liposomes: A selective drug delivery system for the topical route of administration: Gel dosage form. *J. Pharm. Pharmacol.* **34** : pp 473-474.

Mortazavi, S.M., Mohammadabadi, M.R., Khosravi-Darani, K. and Mozafari, M.R. (2007). Preparation of liposomal gene theraphy vectors by a scalable method without using volatile solvents or detergents. *J. Biotechnol.* **129** : pp-604-613.

Mozafari, M.R. (2005). Liposomes: An overview manufacturing techniques . *Cell Mol. Biol. Lett.* **10** : pp 711 – 719.

Mozafari, M.R. (2010). Nanoliposomes: Preparation and analysis. In: Liposomes, method in molecular biology, ed. Weissig, V. Humana Press, New York pp 29-50.

Mozafari, M.R., Reed, C.J., Rostron, C., Kocum, C. and Piskin, E. (2002). Construction of stable anionic liposome-plasmid particles using the heating method: a preliminary investigation. *Cell Mol. Biol. Lett.* **7(3)**: pp 923-927.

Mozafari, M.R., Reed, C.J. and Rostron, C. (2004). Formation of the initial cell membranes under primordial earth conditions. *Cell Mol. Biol. Lett.* **9 (Suppl. 2)**: pp 97-99.

Mozafari, M.R., Johnson, C., Hatziantoniou, S. and Demetzos, C. (2008). Nanoliposomes and their applications in food nanotechnology. *J. Liposome Research.* **18**: pp 309-327.

Nikalje, A.P. and Tiwari, S. (2012). Ethosomes: A novel tool for transdermal drug delivery. *IJPRS*. **2(1)**: pp 1-20.

Ogunsola, O.A., Kraeling, M.E., Zhong, S., Pochan, D.J., Bronaugh, R.L. and Raghavan, S.R. (2002). Structural analysis of flexible liposomes formulations: new insights into skin-penetrating ability of soft nanostructures. *Soft Matter.* **8**: pp 10226-10232.

Parashar, T., Soniya, Sachan, R., et al (2013). Ethosomes: A recent vesicle of transdermal drug delivery system. I*nt. J. Res. Dev. Pharm. L. Sci.* **2 (2)**: pp 285-292.

Parthiban C. P., Jeroen C. H. L., Pieter J. D., Marcel K. and Janine N. P. (2012). Nanomaterials for the local and targeted delivery of osteoarthritis drugs. *Journal of Nanomaterials*. **2012**: pp 1-13.

Paul, A., Cevec, G. and Bachhavat, B.K. (1998). Transdermal immunisation with an integral membrane component, gap junction protein, by means of ultradeformable drug carriers, transferosomes. *Vaccineur.* **16**: pp 188-195.

Planas, M.E., Gonzalez, P., Rodriguez, S., Sanchez, G. and Cevc, G. (1992). Non invasive percutaneous induction of topical analgesia by a new type of drug carrier, and prolongation of local pain insensitivity by anesthetic liposomes. *Anesthia Analog*: pp 615-621.

Ravi, K., Singh, M., Bala, R., Seth, N. and Rana, A.C. (2012). Transferosomes: A novel approach for transdermal drug delivery. *Inter. Research J Pharm.* **3(1)**: pp 20-24.

Sanmiguel, G.S. and Zamora, J.M. (2010). Systems and method for skin rejuvenation. Eur. Patent: 2241303A2.

Schatzlein, A. and Cevc, G. (1995). Skin penetration by phospholipids vesicles, transferosomes as visualized by means of the confocal scanning laser microscopy, in charazterization, metabolism, and novel biological application. Champaign. AOCS Press. pp 191-209.

Singh, H.P., Utreja, P., Tiwary, A.K. and Jain, S. (2008). Elastic liposomal formulations for sustained delivery of colchicine: In vitro characterization and In vivo evaluation of anti gout activity. *AAPS Pharm. Sci. Tec.* **11**: pp 54-64.

Sinico, C., Manconi, M., Peppi, M., et al. (2005). Liposomes as carriers for dermal delivery of tretinon: In vitro evaluation of drug permeation and vesicle-skin intercation. *J. Control. Release.* **103**: pp 123-136.

Tan, J., Jiang, L., Chang, T. and Zhou, Z. (2012). Bullatacin ethosome gel and preparation method thereof. *CN Patent*: 102552147(A).

Touitou, E. (2010). Stable compositions for nail onychomycosis treatment. WO Patent: 2010086727.

Touitou, E., Alkabes, M., and Dayan, N. (1997). Ethosomes: Novel lipid vesicular system for enhanced delivery. *Pharm. Res.* **S14**: pp 305–306.

Touitou, E., Dayan, N., Bergelson, L., et al. (2000). Ethosomes: Novel vesicular carriers: Characterization and delivery propeties. *J. Control. Release.* **65**: pp 403-418.

Vemuri, S., Yu, C.D., Wangsatorntanakun, V. And Roodsdorp, N. (1990). Large-scale production of liposomes by a microfluidizer. *Drug Dev. Ind. Pharm.* **16**: 2243-2256.

Vemuri, S. And Rhodes C.T. (1995). Preparation and characterisation of liposomes as therapeutic delivery systems: A review. *Pharma Acta Helv.* **70**: pp 95-111.

Venuganti, V.V. and Perumal, O.P. (2009). Nanosystems for dermal and transdermal drug delivery. In: Drug delivery nanoparticles formulation and characterization, ed. Pathak, Y. and Thassu, D., Informa Helthcare, New York, pp 126-154.

Verma, D.D. and Fahr, A. (2004). Synergistic penetration effect of ethanol and phospholipids on the topical delivery of cyclosporin A. *J. Control Release.* **97**: pp 55-66.

Verma, P. and Pathak, K. (2010). Therapeutic and cosmeceutical potential of ethosomes: An overview. *Journal of Advanced Pharmaceutical Technology & Research.* **1(3)**: pp 274-282.

Verma, P., Ram, A., Jha, A.K., Mishra, A. and Thakur, A. (2010). Phosphatidylcholine: A revolution in drug delivery technology. *Int. J. Pharm. Sci. & Research.* **1(2)**: pp 1-9.

Weiner, N., Lieb, L., Niemiec, S., (1994). Liposomes: A novel topical delivery system for pharmaceutical and cosmetic application. *J. Drug Target.* **2**: pp 405-410.

Williams, A.C. (2003). Transdermal and topical drug delivery; from theory to clinical practice. Pharmaceutical Press, London.

Williams, M.L. and Elias, P.M. (1987). The extracellular matrix of stratum corneum: role of lipids in normal and pathological function. *Crit. Rev. Ther. Drug Carrier Syst.* **3**: pp 95-122.

Yang, F., Jin, C. and Jiang, Y. (2011). Liposome based delivery systems in pancreatic cancer treatment: from bench to bedside. *Cancer Treatment Reviews.* **37(8)**: pp 633–642.

*Tan Yong Nee,*
*Chen Sau Soon,*
*Izham Bakar,*
*Zulkarnain Abdullah,*
*Mosses a/k Jaraw*

*SIRIM Berhad*
*No.1, Persiaran Dato' Menteri,*
*40700 Seksyen 2, Shah Alam, Selangor*

***(yntan@sirim.my)***

## SOLAR PHOTOCATALYTIC DECONTAMINATION AND DISINFECTION OF WATER

***RINGKASAN:*** *Fotopemangkinan menggunakan $TiO_2$ untuk menyahtosikkan air yang tercemar merupakan kajian yang paling luas dijalankan dan dibangunkan pada hari ini untuk aplikasi yang praktikal dalam rawatan air pencemaran. Rawatan fotopemangkinan berguna untuk merawat bahan-bahan merbahaya seperti fenol, sisa pertanian, racun perosak dan lain-lain. Objektif kajian ini adalah untuk menunjukkan kebolehan proses fotopemangkinan dalam menyahtosik air yang dicemari oleh racun perosak. Prestasi kemusnahan fotopemangkinan racun perosak tercemar air bawah tanah telah dikaji pada skala perintis dengan menggunakan fotomangkin $TiO_2$. Kajian ini menunjukkan bahawa 80 % dan 54 % penguraian telah dicapai selepas 24 jam melalui sinaran UV dan solar.*

**ABSTRACT:** Photocatalysis using $TiO_2$ for detoxification of contaminated water is most extensively been studied and developed today as of its practical applications to treat water contaminants. Photocatalytic treatment can be useful for addressing hazardous contaminants such as phenols, agricultural wastes, pesticides and etc. The objective of this study was to demonstrate whether detoxification of pesticide contaminated water by $TiO_2$ photocatalysis process is possible. The performance of photocatalytic degradation of pesticide contaminated groundwater has been studied at pilot scale with the $TiO_2$ photocatalyst. The study showed that 80 % and 54 % mineralization has been attained after 24 hours of UV and solar radiation, respectively.

Keywords: Photocatalytic treatment, UV, solar, $TiO_2$

## INTRODUCTION

Photocatalytic technology is one of the most promising methods applied to treat the environmental pollutants. Photocatalytic technology evolves around the irradiation of photocatalysts to create powerful oxidation reactions that will, among the many applications, degrade organic pollutants to carbon dioxide, and also to disinfect microbial.

Photocatalytic treatment of contaminated water is clearly the most successful photochemical application of solar photons. Particularly, heterogeneous titanium dioxide ($TiO_2$) photocatalysis is the process for which the solar technology is the most extensively studied and developed to treat water contaminants (Blanco & Malato, 2010). The photocatalytic process can be applied to hazardous non-biodegradable contaminants, with difficult conventional treatment, in the range of several hundred mg/L of maximum organic concentration. It also extends to complex mixtures of organic contaminants. Thus, the photocatalytic technology can be considered useful for addressing hazardous contaminants such as phenols, agrochemical wastes, halogenated hydrocarbons, biocide compounds from pharmaceutical industry, wood preserving waste and etc.

Purification of contaminated groundwater is a challenging task. (Lim *et al.*, 2010). For some recalcitrant contaminants, the conventional treatment technologies are either slow or do not decompose the contaminant in-situ. Photocatalysis is an environmentally friendly process in which the photocatalyst such as titanium dioxide is a non-toxic material and the reaction degrades a wide range of organic compounds to carbon dioxide, water and mineral acids (Hoffmann *et al.*, 1995). $TiO_2$ has proved to be the most suitable and is the most widely used for treatment process as it is relatively inexpensive, easy to produce and highly stable (Matsuoka & Masakazu, 2009).

Since Malaysia (located at 3.1 °N and 101.7 °E) is in the tropical region, it enjoys a conducive climate with abundance natural resource of sunlight. Sunlight has been proposed as having promising role in improving the water quality. However, solar treatment process is lengthy and its efficiency is very much affected by daily and diurnal change. Therefore, to increase the treatment efficiency and promote the practicality of using solar in treatment process, the use of the $TiO_2$ photocatalyst has been suggested in this study.

This paper describes how photocatalysis treatment could become a significant sector of the water treatment technologies for pesticide contaminated water. It evaluates the photocatalysis process that makes use of natural sunlight and UV radiation in a pilot plant with $TiO_2$ as the catalyst.

## MATERIALS AND METHODS

### Analytical Method

The total organic carbon measurement was performed using an on-line Total Organic Carbon analyser (Siever 900). Pesticides analyses were performed using Liquid Chromatography – Mass Selective-Mass Selective Detector (Applied Biosystems 3200Q Trap with Phenomenex Synergi 4u Fusion-RP 80A 50 x 2 mm). The mobile-phase composition was acetonitrile and water with 0.1 % formic acid and 5 mM ammonium formate.

### Pilot Plant Design

Figure 1 shows a diagram of the integrated photocatalytic treatment plant that was used for the study. The pilot plant was constructed next to an underground well in a vegetable farming at Cameron Highlands where pesticide contamination was confirmed. The pilot plant was made up of the preliminary treatment system and the photocatalytic treatment system. The preliminary treatment system is used to remove coarse solids and other large materials often found in raw water. Removal of these materials is necessary to enhance the operation and maintenance of the subsequent treatment unit namely the photoreactor.

The photoreactor consists of five glass tubes with a total irradiated area of 0.53 $m^2$ connected in series and mounted on a fixed platform that can be tilted at 90°. The $TiO_2$ photocatalysts were packed into the glass tubes with 7400 $gTiO_2/m^2$. The $TiO_2$ photocatalyst used in this study was supplied by Photocatalyst Material Inc, Japan. Water flowed at 6.8 L/min directly from one tube to another tube. The photoreactor was operated in a recycle mode and the photoreactor is connected by a recirculation pipe with a 1 $m^3$ stainless steel tank. The water coming from the preliminary treatment was pumped into the tank with approximate volume of 250 litre. The photocatalytic treatment started when the water was pumped to the photoreactor. The water recycled between the tank and the photoreactor. The degradation and mineralization of pesticide were monitored as Total Organic Carbon (TOC). The solar UV intensity was measured using Kipp Zonen UV radiometer.

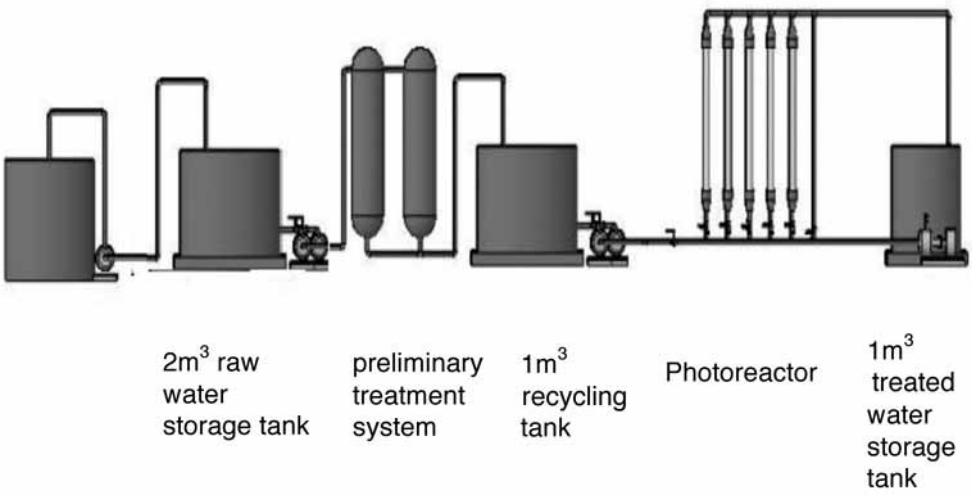


***Figure 1.*** *A schematic diagram of the pilot plant.*

## RESULTS AND DISCUSSION

Figure 2 shows the results of the photocatalytic reduction of TOC in the presence of solar and UV radiation. From the results, it is clear that solar and UV radiation are able to degrade the organic contaminants in the water. As the initial TOC concentration of the groundwater source was varied in which it depends on the farming activity of the day, no comparison can be done. However, in Figure 3, it is observed that after 14 hours of UV radiation, the degradation percentage of TOC was about 60 % and the degradation percentage of TOC is about 80 % after 24 hours of UV exposure. The degradation rate of 38 % is attained after 14 hours irradiation under sunlight exposure. However, only 54 % of degradation is observed under 24 hours solar radiation.

Figure 4 shows the total organic reduction by photocatalytic reaction as a function of accumulated solar energy in the presence of solar and UV radiation, respectively. The reaction rate is a sum of parameters which include several organic products inclusive of pesticides listed in Table 1. It is clear that the solar radiation requires high accumulated energy for mineralization of TOC. A smaller reduction of TOC of 47 % is observed under the solar radiation as compared to 74 % in the case of UV radiation by accumulating energy of 270 KJ/L which corresponds to 20 hours exposure as shown in Figure 3. This is a rather inefficient process in mineralization under solar radiation, although the process has an advantage of using natural sunlight as environmentally friendly technology. Further improvement is needed for practical applications of industrial and environmental interests.

Table 1 indicates the pesticide compounds that contribute to the TOC content. Results of Table 1 show that the pesticides are degraded under UV photocatalysis and solar photocatalysis. A few pesticide compounds such as aldicarb, methomyl, terbufos and thiphanate methyl are completely mineralized after 37 hours of UV exposure. Thiofanox sulfone and thiphanate methyl can be mineralized under 16 hours of solar illumination. Under these circumstances, it is demonstrated that photocatalytic treatment using $TiO_2$ as catalyst can mineralize pesticide residue in water. The complete mineralization of pesticides may require a prolong UV/ sunlight exposure which is dependent on the stoichiometry reactions of each pesticide compound.

The stoichiometry reactions of the pesticide compounds are as follows (Fernandez-Alba *et al.*, 2002; Malato *et al.*, 2001, 2003; Marinas *et al.*, 2001:

$C_7H_{14}N_2O_2S + 13.5O_2 \rightarrow 7CO_2 + 5H_2O + H_2SO_4 + 2HNO_3$ ……..aldicarb

$C_7H_{14}N_2O_4S + 12.5\ O_2 \rightarrow 7CO_2 + 5H_2O + H_2SO_4 + 2HNO_3$ …….aldicarb sulfone

$C_7H_{14}N_2O_3S + 13\ O_2 \rightarrow 7CO_2 + 5H_2O + H_2SO_4 + 2HNO_3$ ……..aldicarb sulfoxide

$C_5H_{10}O_2N_2S + 10.5O_2 \rightarrow 2HNO_3 + H_2SO_4 + 5CO_2 + 3H_2O$……....methomyl

$C_8H_{14}N_4OS + 17.5O_2 \rightarrow 8CO_2 + 5H_2O + H_2SO_4 + 4HNO_3$ …….metribuzin

$C_{10}H_{14}N_2 + 16O_2 \rightarrow 10CO_2 + 6H_2O + H_2SO_4 + 2HNO_3$ …… nicotine

$C_{10}H_{11}N_5O + 18.5O_2 \rightarrow 10CO_2 + 3H_2O + 5HNO_3$ …….. pymetrozin

$C_9H_{21}O_2PS_3 + 19O_2 \rightarrow 9CO_2 + 6H_2O + H_3PO_4 + 3H_2SO_4$ ……terbufos

$C_9H_{18}N_2O_4S + 15.5O_2 \rightarrow 9CO_2 + 7H_2O + 2HNO_3 + H_2SO_4$ …….. thiofanox sulfone

$C_{12}H_{14}N_4O_4S_2 + 21.5O_2 \rightarrow 12CO_2 + 3H_2O + 4HNO_3 + 2H_2SO_4$ ...thiphanate methyl

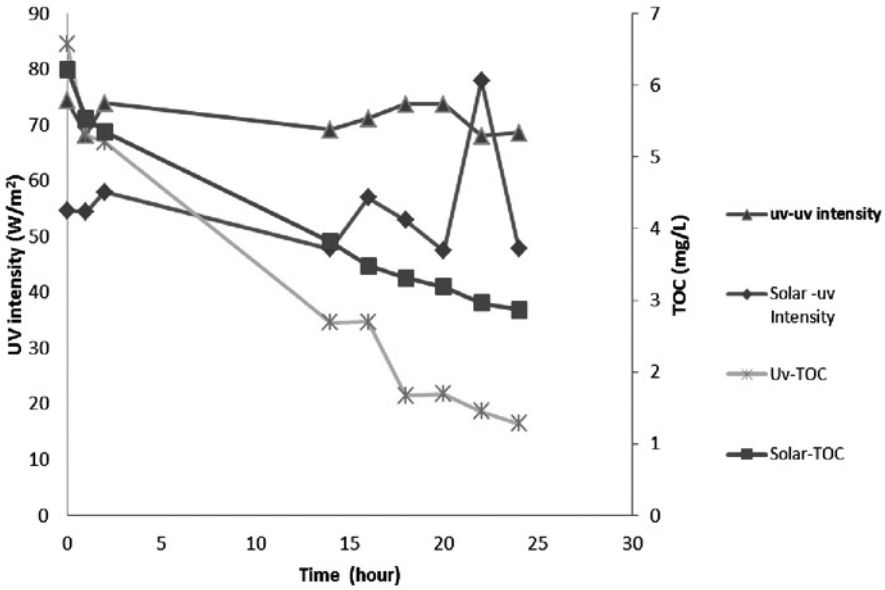


**Figure 2.** Total Organic Carbon reduction under solar and UV radiation

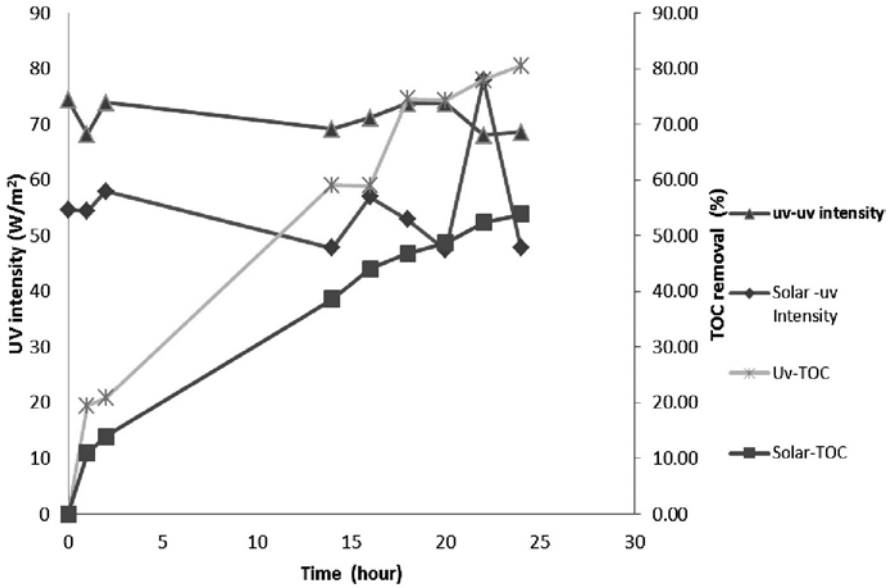


**Figure 3.** Total Organic Carbon removal efficiency under solar and UV radiation

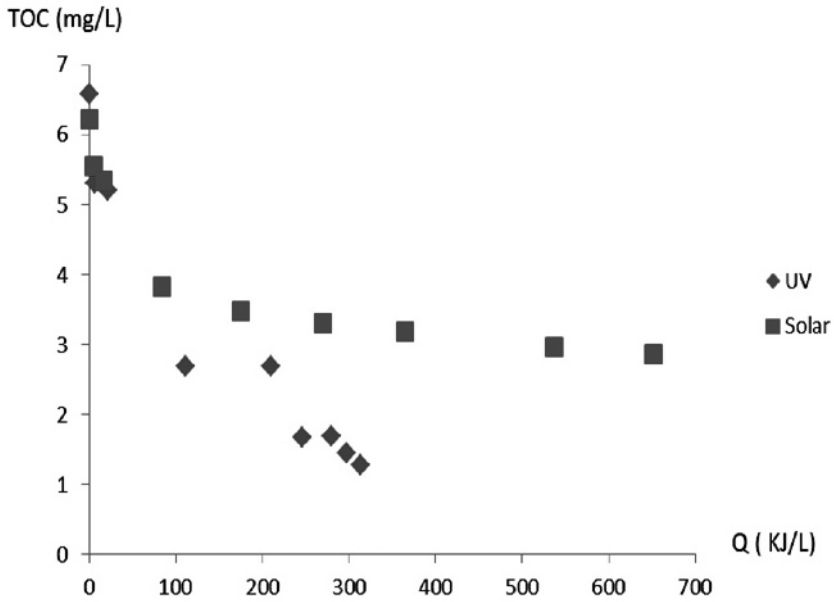


**Figure 4.** Total organic reduction by photocatalytic reaction as a function of accumulated solar energy in the presence of solar and UV radiation calculated according to Malato *et al.*, 2003.

**Table 1.** Results of pesticide concentration under photocatalytic treatments after 37 hours of UV radiation and 16 hours of solar radiation

| Parameter | UV (µg/L) | | solar (µg/L) | |
|---|---|---|---|---|
| | before | after 37 hours exposure | before | after 16 hours exposure |
| Aldicarb | 0.0695 | ND | 0.663 | 0.162 |
| Aldicarb Sulfone | 0.813 | 0.462 | ND | ND |
| Aldicarb Sulfoxide | 11.5 | 2 | 2.56 | 0.138 |
| Methomyl | 0.103 | ND | ND | ND |
| Metribuzin | 0.457 | 0.0687 | 0.0608 | 0.0102 |
| Nicotine | 0.23 | 0.168 | 0.161 | 0.121 |
| Pymetrozin | 0.27 | 0.209 | ND | ND |
| Terbufos | 1.56 | ND | 0.925 | 0.69 |
| Thiofanox Sulfone | 125 | 0.924 | 52.8 | ND |
| Thiphanate Methyl | 0.112 | ND | 0.0287 | ND |

## CONCLUSION

The detoxification of water containing pesticides had been demonstrated by photocatalytic treatment without total mineralization. The results showed that the photocatalytic treatment can mineralize the pesticide contaminants in groundwater.

## ACKNOWLEDGEMENTS

The authors wish to thank MOSTI for financial support under the Technofund Project (TF 0109D009).

## REFERENCES

Blanco Galvez, J. and Malato Rodriguez, S. (2010). Solar Photochemistry; Solar Energy Conversion and Photoenergy Systems. **Vol. II** : pp 67 -95.

Fernandez- Alba, A.R., Hernando, D., Aguera,A., Caceres, J., Malato, S. (2002) Toxicity assays : a way for evaluating AOPs efficiency. *Water Res.* **36**, 4255-4262.

Hoffmann M.R., Scot T. Martin, Wonyong Choi and Deflef W. Bahnemann (1995) Environmental Applications of Semiconductor Photocatalysis; *Chem. Rev.* **95**: pp 69-96.

Lim, L.L.P, .Lynch, R.J. (2010). A proposed Photocatalytic Reactor Design for In Situ Groundwater Applications; Applied Catalysis A : General. **378**: pp 202-210.

Malato, S., Caceres, J., Aguera, A., Mezcua, M., Hernando, D., Vial, J., Fernandez-Alba, A.R., (2001). Degradation of imidacloprid in Water by Photo-Fenton and $TiO_2$ Photocatalysis at a Solar Pilot Plant: A Comparative Study; *Environmental Science & Technology.* **35**, pp 4359-4366.

Malato, S., Caceres, J., Fernandez-Alba, A.R., Piedra, L., Hernando , Ma, D., Aguera, A., Vial, G, (2003). Photocatalytic Treatment of Diuron by Solar Photocatalysis : Evaluation of Main Intermediates and Toxicity; *Environmental Science & Technology.* **37**, pp 2516-2524.

Marinas, A., Guillard, C., Marinas, J.M., Fernandez-Alba, A., Aguera, A., Herrmann, J.M., (2001). Photocatalytic Degradation of Pesticides-Acaricide Formetanate in Aqueous Suspension of $TiO_2$. Applied Catalyst B : *Environmental.* **34**, pp 241 -252.

Matsuoka M. and Masakazu A. (2009).Applications of Environmentally Friendly $TiO_2$ Photocatalysts in Green Chemistry: Environmental Purification and Clean Energy Production Under Solar Light Irradiation; Handbook of Green Chemistry Vol. 2: *Heterogeneous Catalysis*. pp 59 -80.

Sixto Malato, Julian Blanco, Alfonso Vidal, Diego Alarcon, Manuel I. Maldonado, Julia Caceres, Wolfgang Gernjak (2003). Applied Studies in Solar Photocatalytic Detoxification : An Overview ; S*olar Energy.* **75**: pp 329-336.